Probing the Interfacial Peptides/Proteins by Using Sum Frequency Generation Spectroscopy with Hamiltonian Approach Data Analysis Method

by

Tieyi Lu

A dissertation submitted in partial fulfillment
of the requirements for the degree of
Doctor of Philosophy
(Chemistry)
in the University of Michigan
2022

Doctoral Committee:

Professor Zhan Chen, Chair
Professor Jinsang Kim
Professor Stephen Maldonado
Professor Roseanne J Sension

Tieyi Lu

lutieyi@umich.edu

ORCID iD: 0000-0003-0135-7653

© Tieyi Lu 2022

Dedication

To my family

Acknowledgements

Firstly, I would like to thank my Ph.D. advisor Prof. Zhan Chen. During the past five years, I have received a tremendous amount of help and support from Prof. Chen. From his guidance and mentoring, I learned the essential skills and knowledge to become an independent researcher and gained an optimistic attitude when facing difficult challenges in life and academic research. Prof. Chen was very supportive when I had some "crazy" ideas, and he would always discuss them with me and provide me with the necessary support and resources. Prof. Chen's enthusiasm has always inspired me along my Ph.D. pathway, and I wish I could become someone like him who can light up the darkness for other people in the future.

Secondly, I want to thank my labmates, who helped me greatly in the past five years. When I started to learn SFG technique as an undergrad in Chen Group, Dr. Minyu Xiao was the first mentor who taught me how to operate the laser system and analyze the data. He was also a great English teacher when I was struggling with my TOEFL and GSI-OET exams. Dr. Xingquan Zou, Dr. Nathan Ulrich, Dr. Yaoxin Li, Dr. Joshua Jasensky, and Dr. Ganganath Perera instructed me on using the data analysis methods and provided many technical supports for my experiments. Dr. Bolin Li taught me how to use the femtosecond-SFG and the important maintenance skills for SFG laser systems. I also want to thank John Andre, Ralph Crisci, and Wen Guo for the help and the insightful discussions over the past five years.

Thirdly, I would like to express my gratitude to my collaborators. Dr. Jifeng Zhang and Dr. Fu Li collaborated with us on the antibody projects, taught me the important antibody knowledge, and provided the antibody samples. Dr. Shuai Wei conducted the simulation to obtain the

structures of two antibodies so I could finish the orientation analysis. I learned the basic knowledge about molecular dynamics simulation from Dr. Tao Wei from Howard University and successfully conducted several simulations with his great help.

Fourthly, I want to thank Prof. Roseanne Sension, Prof. Stephen Maldonado, and Prof. Jinsang Kim for being my committee members. I appreciate their help, support, and suggestions during the past five years.

Finally, I would like to thank my family and friends. Pursuing the Ph.D. degree is not an easy task, and I could never make this far without your continuous support in this long journey. I will never forget the moments of happiness that we spent together.

Table of Contents

Dedication ii

Acknowledgements iii

List of Tables ix

List of Figures xi

Abstract xviii

Chapter 1 Introduction 1

1.1 Motivation 1

1.2 Application of Sum Frequency Generation in Biological Study 2

1.3 Introduction of Sum Frequency Generation 3

1.4 SFG Data Analysis Methodology on α-helix and β-sheet Structures 6

1.5 SFG-Hamiltonian Analysis Method 9

1.6 SFG Instrumentation 10

1.7 Research Objective and Contents in This Thesis 11

1.8 References 13

Chapter 2 Development of Hamiltonian Analysis Method 22

2.1 Introduction 22

2.2 Theory of the Hamiltonian Local Mode Approximation 23

2.3 Matching Experimental Data with Calculated Spectra 28

2.4 Applications of the Hamiltonian Analysis Method 30

2.5 References 32

Chapter 3 Probing Protein Aggregation at Buried Interfaces: Distinguishing Adsorbed Protein Monomer, Dimer, and Monomer-Dimer Mixture in Situ 35

3.1 Introduction 35

3.2 Experimental Details 38

3.2.1 Sum Frequency Generation (SFG) Vibrational Spectroscopy 38

3.2.2 Samples and materials 39

3.2.3 Silica-coated CaF_2 prisms 39

3.2.4 Preparation of Silicone Oil Thin Film 40

3.2.5 Circular Dichroism 40

3.2.6 Native-PAGE Experiments 41

3.3 Results and Discussions 41

3.3.1 SFG Experiment Result 41

3.3.2 Hamiltonian Data Analysis and Protein Orientation Determination Method 43

3.3.3 Orientation and Structure Analysis by Hamiltonian Method 45

3.3.4 Circular Dichroism Spectroscopic Study Result 53

3.3.5 Solvent Accessible Surface Area Analysis 54

3.3.6 Native-PAGE Experiment Results 57

3.4 Conclusions 60

3.5 References 62

Chapter 4 Monitoring Orientation and Conformation Changes of Fibrinogen during the Adsorption Process at the Buried Interface in Situ in Real Time 74

4.1 Introduction 74

4.2 Experimental Details 76

4.2.1 Material and Sample Preparation 76

4.2.2 Instrumentation 76

4.2.3 Hamiltonian Method for SFG Spectral Analysis 77

4.3 Result and Discussion 78
4.3.1 SFG Experiment Result 78
4.3.2 Conformation and Orientation Analysis by Hamiltonian 79
4.3.3 Surface Coverage Analysis Result 88
4.4 Conclusion 92
4.5 References 93
Chapter 5 Investigation of Antibody Adsorption Behavior Onto Silicone Oil Surface 99
5.1 Introduction 99
5.2 Methods and Materials 102
5.2.1 Materials 102
5.2.2 Silica-coated CaF_2 prisms 103
5.2.3 Preparation of silicone oil thin film 103
5.2.4 Preparation of antibody and surfactant mixture solutions 103
5.2.5 SFG experiment setup 103
5.3 Results and Discussion 104
5.3.1 Lowest possible effective concentration of PS80 to prevent antibody adsorption 104
5.3.2 Adsorption kinetics of BsAb onto Silicone Oil 106
5.3.3 Orientation analysis of BsAb by Hamiltonian method 107
5.3.4 Orientation analysis of mAb by Hamiltonian method 113
5.3.5 Solvent Accessible Surface Analysis of Adsorbed Antibody Structure 118
5.4 Summary 123
5.5 References 124
Chapter 6 Probing the Molecular Behavior of Barnacle Cement Peptide during the Fouling Process on Polystyrene using SFG and Molecular Dynamics Simulation 129
6.1 Introduction 129
6.2 Experimental Details 131

6.3 Barnacle Cement Peptide Structure Prediction and MD Simulation 132
6.4 Results and Discussions 133
6.4.1 SFG Results of BCP2C on PS 133
6.4.2 I-TASSER Prediction and CD Results of BCP Solutions 135
6.4.3 MD Simulation of BCP2C on PS Surface 137
6.4.4 Hamiltonian Analysis of BCP2C after 1 μs MD Simulation 138
6.4.5 Secondary Structure Evolution Plot of BCP2C during the MD Simulation 143
6.4.6 SFG Results of BCP1 147
6.4.7 Structure Prediction and MD Simulation of BCP1 148
6.4.8 Hamiltonian Analysis of BCP1 on PS 150
6.4.9 Secondary Structure Evolution Plot of BCP1 during the MD Simulation 152
6.5 Conclusion 154
6.6 References 156
Chapter 7 Summary and Outlook 159

List of Tables

Table 3.1 Fitting parameters of the SFG spectra of BSA on silicone oil shown in Figure 3.2(b).43

Table 3.2 Fitting parameters of the SFG spectra of BSA on silicone oil after the DTT treatment and the BSA-DTT mixture shown in Figure 3.6..... 48

Table 3.3 The sum of the difference square of the SFG spectra with best matching quality for each dimer-monomer ratio. The calculated SFG spectra based on the BSA dimer-monomer ratio of 60:40 has the lowest value of the square difference (or the best matching quality)..... 53

Table 3.4 Solvent accessible surface area (SASA) calculation results of positively charged, negatively charged, and hydrophobic amino acids in the adsorption and the rest parts of BSA dimer and monomer. 57

Table 3.5 Average solvent accessible surface area results of positively charged, negatively charged, and hydrophobic amino acids in the adsorption and other parts of BSA dimer and monomer. 57

Table 3.6 Quantitative analysis results of the PAGE experiments. The first two rows are intensities of the BSA monomer and dimer bands in the gel. The third row is the ratios of the intensities from dimer vs. monomer. 59

Table 4.1 Fitting parameters of the SFG spectra of fibrinogen on silicone oil at t = 900 s, 1200 s, 1500 s, and 1800 s shown in Figure 4.1..... 83

Table 4.2 Highest matching scores of calculated spectra based on different fibrinogen structures with the reconstructed resonant SFG spectra collected at different times during the fibrinogen adsorption process..... 84

Table 4.3 Effective second order nonlinear optical susceptibility $\chi_{eff}^{(2)}$ and calculated $\beta_H^{(2)}$ values at different times during the adsorption. The coverage percentages of fibrinogen on silicone oil calculated by assuming 100% coverage at t=1800s and deconvoluting the orientation effect..... 90

Table 4.4 Relative surface coverage percentages of the adsorbed fibrinogen on silicone oil at t = 300 s and 600 s of the adsorption..... 91

Table 5.1 Half-life time of SFG signal increase of BsAb with and without PS80 in the solution. 107

Table 5.2 Fitting parameters of the SFG spectra (shown in Figure 5.3 and Figure 5.8) of BsAb and mAb on silicone oil without and with 0.002% PS80 in the protein solution. 108

Table 5.3 Hydrophobic SASA calculation results of the Fab and Fc fragments in mAb and BsAb. The results are calculated by VMD with "-restrict" option, thus the amino acids that are buried inside the protein are excluded in the calculation. 119

Table 5.4 Positive and negative SASA calculation result of the Fab and Fc fragments in mAb and BsAb. 121

Table 6.1 Fitting parameters of the SFG spectra of BCP2C on PS shown in Figure 6.2. 135

Table 6.2 Highest matching scores of different BCP2C final structures with the reconstructed SFG spectra collected from adsorbed BCP2C on PS after 1 h and 48 h. 141

Table 6.3 Fitting parameters of the SFG spectra of BCP1 on PS shown in Figure 6.14. 147

Table 6.4 Highest matching scores between the calculated and reconstructed experimental SFG spectra obtained based on the four final BCP1 simulation structures and the spectra collected after 1 h adsorption. 150

List of Figures

Figure 1.1 (a) SFG signal generation, and (b) SFG energy level diagram. 4

Figure 2.1 Diagram showing the direction and location of the IR amide I transition dipole of a peptide unit..... 24

Figure 2.2 The principal axes of the Raman polarizability in the molecular frame of the amide I stretch mode. 25

Figure 2.3 SFG amide I spectrum of a protein can be calculated based on the calculated frequencies and χ_{Lab} values of all the amide I normal modes. 27

Figure 2.4 Flow chart showing the Hamiltonian data analysis method used to deduce protein orientation from experimentally collected SFG spectra. μ, α, and β are the IR transition dipole, Raman polarizability and SFG hyperpolarizability respectively. 31

Figure 3.1 Schematic of the SFG sample geometry used in this experiment. 39

Figure 3.2 (a) Time-dependent SFG ssp signal intensity observed at ~1650 cm^{-1} during the BSA adsorption process onto silicone oil (b) SFG ssp and ppp spectra of adsorbed BSA collected from the silicone oil/BSA solution interface. The spectra are offset. Dots are experimental data and the lines are fitted spectra. 41

Figure 3.3 Comparison between simulated and experimental SFG spectra. (a) Red: reconstructed resonant SFG zzz spectrum from the experiment data. Blue: Calculated zzz SFG spectrum based on BSA dimer. (b) Red: reconstructed resonant SFG yyz spectrum from the experiment data. Blue: Calculated yyz SFG spectrum based on BSA dimer. (c) Red: reconstructed resonant SFG zzz spectrum from the experiment data. Blue: Calculated zzz SFG spectrum based on BSA monomer. The ssp and ppp spectra can be converted to yyz and zzz spectra after considering the Fresnel coefficients. 43

Figure 3.4 Reference orientations (Tilt=0, Twist=0) of (a) BSA dimer and (b) BSA monomer. 44

Figure 3.5 (a) Heat map showing the matching quality between the reconstructed resonant SFG spectra and calculated orientation dependent SFG spectra based on BSA monomer. (b) Heat map showing the matching quality between the reconstructed resonant SFG spectra and calculated orientation dependent SFG spectra based on BSA dimer. (c) Most likely orientation of BSA dimer on silicone oil. Each heat map shows two most likely orientations, with different absolute orientations (up and down). Since BSA dimer has two identical monomers, it is not necessary to differentiate the two orientations. 46

Figure 3.6 SFG ppp (a) and ssp (b) spectra of BSA with DTT treatment. The SFG spectra collected from BSA before the DTT treatment, BSA after the DTT treatment, and BSA pre-mixed with the DTT are displayed in black, red, and blue color, respectively. 47

Figure 3.7 Matching qualities between the experimental data and calculated spectra based on BSA monomer structure for BSA after the DTT treatment: (a) Heat map showing the matching quality between the reconstructed resonant SFG spectra of BSA after the DTT treatment and calculated SFG spectra using the BSA monomer structure. The blue spectra in (b) and (c) show the calculated SFG yyz (b) and zzz (c) spectra of BSA after the DTT treatment with the best matching quality with the reconstructed resonant SFG spectra (shown in red). The matching qualities of the spectra are much worse than those shown in Figure 3.8 below based on BSA dimer-monomer mixture. The SFG spectra shown in (d) are replotted fitted experimentally collected SFG spectra. The spectra shown in (e) are calculated SFG yyz (blue) and zzz (red) spectra with the best matching quality. The matching qualities of the spectral features can be seen from (b) and (c), while the matching quality for the ssp and ppp intensity ratio can be seen from (d) and (e). 50

Figure 3.8 Matching qualities between the experimental data and calculated spectra based on BSA dimer-monomer mixture of a 60:40 ratio for BSA after the DTT treatment: (a) Heat map showing the matching quality between the reconstructed resonant SFG spectra of BSA after the DTT treatment and calculated SFG spectra using the BSA dimer-monomer mixture ratio of 60:40. The BSA dimer was assumed to have the same orientation as deduced previously while the orientation angles are the BSA monomer orientations. The blue spectra in (b) and (c) show the calculated SFG yyz (b) and zzz (c) spectra of BSA after the DTT treatment with the best matching quality with the reconstructed resonant SFG spectra (shown in red). The SFG spectra shown in (d) are replotted fitted experimentally collected SFG spectra. The spectra shown in (e) are calculated SFG yyz (blue) and zzz (red) spectra with the best matching quality. The matching qualities of the spectral features can be seen from (b) and (c), while the matching quality for the ssp and ppp intensity ratio can be seen from (d) and (e). 51

Figure 3.9 Schematic showing the interfacial reaction between DTT and BSA dimer on the silicone oil surface and the deduced orientations of BSA monomer and BSA dimer on the silicone oil surface after the DTT treatment. 52

Figure 3.10 CD spectra of BSA on silicone oil before and after the DTT treatment. 54

Figure 3.11 Solvent accessible surface area (SASA) analysis of E/K ratio of the adsorption site and other parts of a BSA dimer and a BSA monomer. 55

Figure 3.12 Native PAGE results of BSA solution before (1) and after (2) silicone oil surface contact, and DTT treated BSA solution before (3) and after (4) silicone oil surface contact. 58

Figure 4.1 SFG (a) ssp and (b) ppp spectra collected from the silicone oil/fibrinogen solution interface to follow the fibrinogen adsorption process onto the silicone oil surface. The exposure time for each spectrum is 30 s. The fibrinogen solution was placed into contact with silicone oil at t = 0 s. 78

Figure 4.2 The structures of fibrinogen that were used for the Hamiltonian method in this study. (a) Fibrinogen original structure (pdb: 3ghg). Half of the protein structure (chain A, chain B, and chain C) was rotated by (a) 30 degrees, (b) 45 degrees, (c) 60 degrees, (d) 90 degrees to approximate the possible bent conformations of fibrinogen..... 81

Figure 4.3 (a) The final matching score heat map showing the matching quality between the reconstructed resonant SFG experimental spectra (at t = 900 s) and the calculated orientation dependent SFG spectra based on the Fibrinogen-30° structure (shown in Figure 4.2b). (b) and (c) are the two most probable orientations of the adsorbed fibrinogen molecules on silicone oil..... 81

Figure 4.4 Comparison between reconstructed experimental data and calculated spectra based on the Fibrinogen-30° structure with the highest matching score. The blue spectra in (a) and (b) show the calculated SFG yyz (a) and zzz (b) spectra of adsorbed fibrinogen after 900 s adsorption with the highest matching score with the reconstructed experimental resonant SFG spectra (shown in orange). The unnormalized SFG spectra of (c) experimental data and (d) calculated spectra are plotted for evaluating the matching quality of the ssp and ppp spectral intensity ratio. 82

Figure 4.5 (a) The final matching score heat map showing the matching quality between the reconstructed resonant SFG experimental spectra (at **t = 1200 s**) and the calculated orientation dependent SFG spectra based on the **Fibrinogen-30°** structure. The blue spectra in (b) and (c) show the calculated SFG yyz (b) and zzz (c) spectra of adsorbed fibrinogen after 1200 s adsorption with the highest matching score with the reconstructed experimental resonant SFG spectra (shown in orange). The unnormalized SFG spectra of (d) experimental data and (e) calculated spectra are plotted for evaluating the matching quality of the ssp and ppp spectral intensity ratio. 85

Figure 4.6 (a) The final matching score heat map showing the matching quality between the reconstructed resonant SFG experimental spectra (at **t = 1500 s**) and the calculated orientation dependent SFG spectra based on the **Fibrinogen-45°** structure. The blue spectra in (b) and (c) show the calculated SFG yyz (b) and zzz (c) spectra of adsorbed fibrinogen after 1500 s adsorption with the highest matching score with the reconstructed experimental resonant SFG spectra (shown in orange). The unnormalized SFG spectra of (d) experimental data and (e) calculated spectra are plotted for evaluating the matching quality of the ssp and ppp spectral intensity ratio. 86

Figure 4.7 (a) The final matching score heat map showing the matching quality between the reconstructed resonant SFG experimental spectra (at **t = 1800 s**) and the calculated orientation dependent SFG spectra based on the **Fibrinogen-45°** structure. The blue spectra in (b) and (c) show the calculated SFG yyz (b) and zzz (c) spectra of adsorbed fibrinogen after 1800 s adsorption with the highest matching score with the reconstructed experimental resonant SFG spectra (shown in orange). The unnormalized SFG spectra of (d) experimental data and (e) calculated spectra are plotted for evaluating the matching quality of the ssp and ppp spectral intensity ratio. 87

Figure 4.8 The most probable orientations of fibrinogen on silicone oil at different times during the adsorption process..... 87

Figure 4.9 Surface coverage percentages of adsorbed fibrinogen on the silicone oil surface during the adsorption process. 91

Figure 5.1 SFG sample geometry for monitoring the adsorption of antibodies on silicone oil. This sample geometry is the same as that used to study BSA adsorption, as shown in Figure 3.1…. 101

Figure 5.2 Structures of the monoclonal antibody (mAb) and the bispecific antibody (BsAb) used for Hamiltonian analysis. 102

Figure 5.3 Time-dependent SFG ssp spectra collected from interfaces between silicone oil and BsAb without or with PS80 of different concentrations after the silicone oil surface was placed into contact with the solution: (a) no PS80, (b) 0.002 wt% PS80, (c) 0.02 wt% PS80, (d) 0.2 wt% PS80, (e) 2 wt% PS80 during the adsorption process. (f) SFG ssp spectra collected from the interfaces between silicone oil and BsAb solutions after the silicone oil was placed in contact with each solution for 10 mins. (g) Time-dependent SFG signal (calculated by peak integral) of amide I mode for BsAb without (black dots) or with 0.002 wt% PS80 (red dots). The lines are the fitted results. Each first spectrum shown at time zero in Figures (a) to (e) was collected from silicone oil/buffer solution (without BsAb) for comparison. Other spectra shown in these figures at 90 seconds or later were collected after the silicone oil was placed in contact with BsAb solutions without or with PS80. Each of these spectra is an averaged spectrum of three consecutively collected spectra (each collected with 30 seconds). The SFG signal shown in (g) is the signal from each 30-second spectrum. 106

Figure 5.4 SFG spectra and the fitting results of (a) BsAb, and (b) BsAb with 0.002% PS80 mixture solution in contact with silicone oil for 10 mins. Dots are experimental data, and lines are fitting results. 107

Figure 5.5 Matching qualities between the experimental data and calculated spectra of BsAb on silicone oil without PS80: (a) Heat map showing the matching quality between the reconstructed resonant SFG spectra of BsAb and the calculated spectra. The blue spectra in (b) and (c) show the calculated SFG yyz (b) and zzz (c) spectra of BsAb with the best matching quality with the reconstructed resonant SFG spectra (shown in red). The SFG spectra shown in (d) are replotted fitted experimentally collected SFG spectra. The spectra shown in (e) are calculated SFG yyz (blue) and zzz (red) spectra with the best matching quality. The matching qualities of the spectral features can be seen from (b) and (c), while the matching quality for the ssp/ppp intensity ratio can be seen from (d) and (e). 109

Figure 5.6 Matching qualities between the experimental data and calculated spectra of BsAb on silicone oil with PS80: (a) Heat map showing the matching quality between the reconstructed resonant SFG spectra of BsAb and the calculated spectra. The blue spectra in (b) and (c) show the calculated SFG yyz (b) and zzz (c) spectra of BsAb with the best matching quality with the reconstructed resonant SFG spectra (shown in red). The SFG spectra shown in (d) are replotted fitted experimental spectra. The spectra shown in (e) are calculated SFG yyz (blue) and zzz (red) spectra with the best matching quality. The matching qualities of the spectral features can be seen from (b) and (c), while the matching quality for the ssp/ppp intensity ratio can be seen from (d) and (e)..... 112

Figure 5.7 The deduced most likely orientations of BsAb on silicone oil (a) without PS80 in solution, (b) with 0.002 wt% PS80 in solution in “front view” and (c) with 0.002 wt% PS80 in solution in “side view”. 113

Figure 5.8 SFG spectra and fitting results of interfaces between solutions of (a) mAb, (b) mAb with 0.002% PS80, (c) mAb with 0.02% PS80 and silicone oil. Dots are experimental data, and lines are fitting results. 113

Figure 5.9 Matching qualities between the experimental data and calculated spectra of mAb on silicone oil without PS80: (a) Heat map showing the matching quality between the reconstructed resonant SFG spectra of mAb and the calculated SFG spectra. The blue spectra in (b) and (c) show the calculated SFG yyz (b) and zzz (c) spectra of mAb with the best matching quality with the reconstructed resonant SFG spectra (shown in red). The SFG spectra shown in (d) are replotted fitted experimental spectra. The spectra shown in (e) are calculated SFG yyz (blue) and zzz (red) spectra with the best matching quality. The matching qualities of the spectral features can be seen from (b) and (c), while the matching quality for the ssp/ppp intensity ratio can be seen from (d) and (e). 115

Figure 5.10 Matching qualities between the experimental data and calculated spectra of mAb on silicone oil with PS80: (a) Heat map showing the matching quality between the reconstructed resonant SFG spectra of mAb and the calculated SFG spectra. The blue spectra in (b) and (c) show the calculated SFG yyz (b) and zzz (c) spectra of mAb with the best matching quality with the reconstructed resonant SFG spectra (shown in red). The SFG spectra shown in (d) are replotted fitted experimental spectra. The spectra shown in (e) are calculated SFG yyz (blue) and zzz (red) spectra with the best matching quality. The matching qualities of the spectral features can be seen from (b) and (c), while the matching quality for the ssp/ppp intensity ratio can be seen from (d) and (e). 116

Figure 5.11 The deduced most likely orientations of mAb on silicone oil in contact with mAb solution (a) without PS80, (b) with 0.002 wt% PS80 in “front view” and (c) with 0.002 wt% PS80 viewed from a different angle in “side view”. 117

Figure 5.12 Hydrophobic SASA percentage calculation result of Fab and Fc fragments of (a) mAb and (b) BsAb. 119

Figure 6.1 The initial configuration of combined simulation system between BCP2C (green) with water and polystyrene (yellow). The chloride counter ions are shown in balls with grey color. 133

Figure 6.2 SFG spectra collected from the BCP2C/PS interface after (a) 1-hour and (b) 48-hour adsorption. The experimental data and fitted curves are denoted by open points and solid lines, respectively. 134

Figure 6.3 Amino acid sequences of BCP1 and BCP2C. BCP1 only has one simple segment, and BCP2C has one simple segment and one charged segment.[9] 135

Figure 6.4 Top 5 final models predicted by I-TASSER using BCP2C sequence. 135

Figure 6.5 CD spectrum of a 1.0 mg/ml BCP2C solution. 136

Figure 6.6 Flow chart showing the process of relaxing the predicted BCP2C structure in solution. 137

Figure 6.7 Snapshots of MD simulation box showing the adsorption of BCP2C (green) onto the PS surface (yellow) at (a) T=200 K after 10 ns, (b) T=298.15 K after 10 ns, (c) T=298.15 K after 20 ns, and (d) T=298.15 K after 140 ns. The periodic boundary is shown as blue rectangle in (a). Molecules in (b)(c)(d) are corrected by the periodic boundary for better visualization. 138

Figure 6.8 Flow chart showing the Hamiltonian analysis method used to deduce the orientation of adsorbed peptide on PS. The input structure was extracted from the MD simulation result. 139

Figure 6.9 The initial simulatiuon system with four peptides and the PS layer (left) as well as the structures of the four BCP2C peptides at simulation time of 969 ns while interacting with the PS layer (right). Peptides are rendered in different colors based on the secondary structure. At the beginning of the simulation at 298.15K (left), four BCP2C peptides were not attached to the PS surface and only showed α-helical structure. After 969 ns, all the BCP2C molecules lied down on the PS surface, and β-sheet structure formation was observed. 140

Figure 6.10 Closer look of the structures of the four BCP2C peptides at the simulation time of 969 ns. 140

Figure 6.11 (a) The final matching score heat map showing the matching quality between the reconstructed resonant SFG experimental spectra (adsorption time = 1 h) and the calculated orientation dependent SFG spectra based on the **BCP2C-4** structure. The blue spectra in (b) and (c) show the calculated SFG yyz (b) and zzz (c) spectra of adsorbed BCP2C after one-hour adsorption with the highest matching score with the reconstructed experimental resonant SFG spectra (shown in orange). The unnormalized SFG spectra of (d) experimental data and (e) calculated spectra are plotted for evaluating the matching quality of the ssp and ppp intensity ratio. 142

Figure 6.12 Two most probable orientations of BCP2C on PS after one-hour adsorption. 143

Figure 6.13 Secondary structure evolution plot of BCP2C/PS system during the simulation from 0 to 969 ns. The results of the four BCP2C peptides are plotted together. Different colors represent different secondary structures. Significant β-sheet formation was observed during 480 to 840 ns for BCP2C-1, BCP2C-2, and BCP2C-4. 146

Figure 6.14 (a) Ssp and (b) ppp SFG spectra collected from the BCP1/PS interface after 1-hour adsorption. 147

Figure 6.15 Top 5 final models predicted by I-TASSER using BCP1 sequence. 148

Figure 6.16 The initial simulatiuon configuration of four peptides and the PS layer (left) as well as the structures of the foiur peptides and the PS layer at the end of the simulation (right). Peptides are rendered in different colors based on the secondary structures. 149

Figure 6.17 The extracted structures of four BCP1 peptides on the PS from the MD simulation at the end of the simulatiuon with t = 1.017 μs. 150

Figure 6.18 (a) The final matching score heat map showing the matching quality between the reconstructed resonant SFG experimental spectra (adsorption time = 1 h) and the calculated orientation dependent SFG spectra based on the **BCP1-2** structure. The blue spectra in (b) and (c) show the calculated SFG yyz (b) and zzz (c) spectra of adsorbed BCP2C after one-hour adsorption with the highest matching score with the reconstructed experimental resonant SFG spectra (shown in orange). The unnormalized SFG spectra of (d) experimental data and (e) calculated spectra are plotted for evaluating the matching quality of the ssp and ppp intensity ratio. 151

Figure 6.19 Two possible orientations of BCP1 on PS: (a) Tilt = 50, Twist = 230 degree, (b) Front and side view of Tilt = 130, Twist = 50 degree.s 152

Figure 6.20 Secondary structure evolution plot of BCP1/PS system during the simulation from 0 to 1017 ns. Different colors represent different secondary structures. 153

Abstract

Interfacial protein behavior has been extensively studied due to its tremendous impact on many biological applications and related research fields, such as biosensors, protein-resistant anti-fouling coatings, protein-drug formulations, biomedical implants, etc. However, it is still challenging to probe the interfacial protein behavior at buried solid/liquid interface in situ in real time. Many traditional analytical tools that are surface-sensitive require high vacuum to operate, which cannot be applied to study solid/liquid interfaces. Sum Frequency Generation (SFG) vibrational spectroscopy has been developed into a powerful tool to characterize the interfacial protein molecules due to its sub-monolayer surface sensitivity and in situ detecting capability without the need for high vacuum. Besides, some detailed structural information (e.g., the orientation or tilt and twist angles) of the interfacial protein molecules can also be elucidated by interpreting SFG spectra, which is difficult to access with other analytical tools.

This thesis research focuses on the development and application of a systematic method to deduce interfacial peptide and protein structures using SFG spectroscopy. Particularly, this research adopted Hamiltonian local mode approximation method to calculate SFG spectra as a function of the interfacial peptide/protein orientation based on the input peptide/protein conformation. This newly developed method that combines SFG technique and Hamiltonian analysis method can evaluate the orientation and conformation of interfacial proteins by comparing the matching scores between calculated orientation dependent SFG spectra of different input conformations and experimental SFG spectra. Such a method was successfully applied to study molecular structures of a variety of peptides/proteins at buried interfaces in situ. This method

makes it possible to monitor the time-dependent behavior of proteins during adsorption, understand the protein aggregation mechanism on surfaces, investigate the anti-fouling process, and optimize antibody drug formulation, etc. This method broadens the application of SFG technique in the biological research field and adds a new toolset for studying the detailed molecular structural information of biomolecules at the solid/liquid interface.

The thesis is presented as follows: Chapter 1 briefly introduces the background of the thesis research and the SFG technique. Chapter 2 discusses the details of the Hamiltonian approach developed for SFG spectra calculation and methods for protein structural determination using SFG. Chapters 3, 4, and 5 presents the applications of the Hamiltonian analysis method combined with SFG data on solving the molecular interfacial structures of adsorbed proteins including bovine serum protein, fibrinogen, and antibody drugs respectively. Chapter 6 elucidates the interfacial structures of barnacle peptides to understand biofouling mechanisms using SFG experiments, molecular dynamics simulations, and Hamiltonian spectral calculations. Chapter 7 summarizes the main findings in this thesis research and proposes some future directions. This research develops a widely applicable approach to use SFG to characterize molecular structures of peptides and proteins at buried interfaces in situ.

Chapter 1 Introduction

1.1 Motivation

Protein adsorption is a very common phenomenon that can happen on surfaces or at interfaces, which can adversely impact on many applications, such as biomedical implants, antibody-protein drugs, biosensors, and anti-fouling coatings, etc.[1-7] For example, protein adsorption onto the surface of a biomedical implant is the first event when the implant is placed into contact with tissue or blood inside a human being.[1] Unfavorable protein-implant surface interactions may cause protein denaturation and/or aggregation and lead to harmful biological responses such as blood coagulation, unnecessary immunological response, etc.[8-9] Recently, antibody drugs have been developed to treat various diseases. Silicone oil is a widely used lubricant in the pharmaceutical industry, which is usually applied on various surfaces (such as the inner surface of a pre-filled syringe or vial stopper) for antibody drug storage and administration. However, it was reported that the interaction between silicone oil and protein molecules can induce protein adsorption on the surface and cause protein aggregation, affecting the efficacy of protein drugs and resulting in unforeseen problems in the practical use of antibody drugs.[3, 5, 10-13] Moreover, the adsorption of adhesive proteins from marine organisms onto the ship hull is the first step of the biofouling process, while biofouling can cause many problems like slow ship speed, extra fuel consumption, and additional expense for ship cleaning.[14] Therefore, it is important to investigate the protein adsorption onto various surfaces to understand protein-surface interaction mechanisms for the rational design of surfaces to prevent protein from adsorption and/or ensuring adsorbed protein adopting a reasonable structure which would not cause a negative effect.

Protein adsorption has been a long active research focus for several decades. Many analytical techniques have been developed to characterize the adsorption behaviors and the molecular structures of many different proteins, such as X-ray diffraction,[15] NMR,[16] ATR-FTIR,[17] cryo-EM,[18] QCM,[19] ellipsometry,[20] neutron reflection,[21] AFM,[22] leading to essential knowledge about the adsorption mechanism of proteins. However, many of these techniques either lack surface/interface selectivity, require high vacuum/low temperature to operate, or cannot provide molecular level structural information.

1.2 Application of Sum Frequency Generation in Biological Study

In recent years, Sum Frequency Generation (SFG) vibrational spectroscopy has been developed into a unique and powerful tool for investigating surfaces and interfaces. It has been successfully applied to detect various functional groups, probe interfacial chemical reactions, elucidate orientations of molecules, and monitor the dynamics of molecules at various interfaces in situ, including buried interfaces such as solid/solid and solid/liquid interfaces.[23-29] It has also been successfully applied to study the interfacial protein structure in situ and in real time.[30-36]

SFG is a second order nonlinear optical spectroscopic technique. Because of the selection rule of a second-order nonlinear optical process, SFG signal can only be generated in a medium without inversion symmetry. In most cases, the bulk of a solid material or solution can be treated as central symmetric medium, while a surface or interface does not possess inversion symmetry, which makes SFG a highly surface-sensitive technique with a sub-monolayer surface sensitivity.

In the published linear vibrational spectroscopic studies, amide I signals have been widely used to study peptide and protein structures.[17, 37] SFG amide I signals from proteins/peptides can be selectively detected at buried solid/liquid interfaces in situ. The interfacial protein orientation can be deduced from the SFG amide I signal collected using different polarization combinations

of the input beams and the output SFG beam. Previous studies from our group demonstrated the feasibility and power of applying SFG to investigate interfacial behaviors of various proteins/peptides on many different surfaces, such as chemically immobilized enzymes on self-assembled monolayers (SAM) and polymers, physically adsorbed proteins on polymers, silicone oils, and 2D materials, membrane proteins associated with model cell membranes, antimicrobial peptides on polymers, and peptides in lipid bilayers, etc.[4, 34-35, 38-48]

1.3 Introduction of Sum Frequency Generation

The details of the nonlinear optical effect and the theory of SFG have been extensively discussed elsewhere[27-29, 49-52], and the SFG basics will only be introduced briefly in this chapter. In terms of the light interaction with a medium, the generalized polarization **P** of the medium can be given by:

$$\boldsymbol{P} = \varepsilon_0\left(\chi^{(1)}\boldsymbol{E} + \chi^{(2)}\boldsymbol{E}^2 + \chi^{(3)}\boldsymbol{E}^3 + \ \cdots\right) \quad (1)$$

where ε_0 is the vacuum permittivity, **E** is the electric field of the input light beam, and $\chi^{(1)}$, $\chi^{(2)}$, and $\chi^{(3)}$ are the first-, the second-, and the third-order nonlinear susceptibilities of the medium, respectively. $\chi^{(1)}$ is also called the linear susceptibility and is considerably larger than those higher-order (nonlinear) terms. In order to observe the nonlinear responses of a medium when interacting with light, pulsed lasers are often used to achieve this goal by applying an electromagnetic field comparable with the field experienced by the electrons of a molecule.

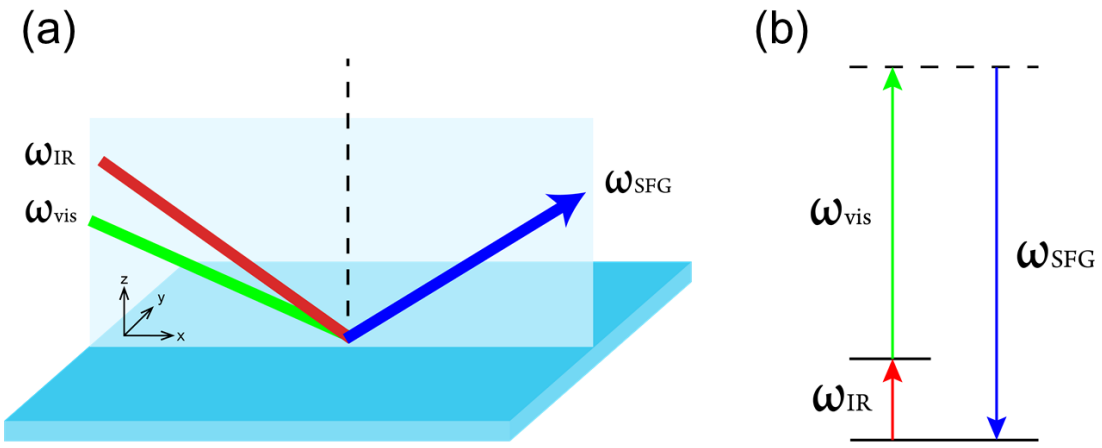


Figure 1.1 (a) SFG signal generation, and (b) SFG energy level diagram.

SFG is a second-order nonlinear optical spectroscopic technique, and it mainly detects the second-order nonlinear optical susceptibility $\chi^{(2)}$. In the experiment setup of SFG, two laser beams are overlapped spatially and temporally at the sample interface, one of which is a wavelength-fixed visible beam while the other is a frequency-tunable infrared beam. The energy diagram of an SFG process is shown in Figure 1.1 In an SFG process, the IR absorption of the vibrational modes of molecules happens first then followed by an anti-Stokes Raman scattering process. Under the electric-dipole approximation, the magnetization and the electric quadrupole polarization are ignored and thus the second-order nonlinear optical susceptibility $\chi^{(2)}$ dominates the SFG signal intensity. Since $\chi^{(2)}$ is a third-rank polar tensor, the sign needs to be changed after the inversion operation:

$$-\chi^{(2)}(r) = \chi^{(2)}(-r) \tag{2}$$

For a medium with inversion symmetry, the sign remains the same after the inversion operation:

$$\chi^{(2)}(r) = \chi^{(2)}(-r) \tag{3}$$

The only solution for Equation (2) and (3) is $\chi^{(2)}(r) = 0$, which means no SFG signal will be generated from a medium with inversion symmetry. The bulk of most solid materials and liquid solutions can be considered centrosymmetric due to the randomly oriented molecules, thus no SFG signals can be produced. The inversion symmetry is broken on surfaces or at the interfaces of materials; therefore, Equation (3) does not hold and $\chi^{(2)}$ becomes nonzero, therefore SFG signal can be generated. This selection rule is the foundation of the intrinsic surface/interface sensitivity of SFG technique. The intensity of SFG signal is given by the following equation:

$$I(\omega) = \frac{8\pi^3\omega^2\, sec^2\,\beta}{c^3 n(\omega) n(\omega_{IR}) n(\omega_{VIS})} \left|\chi^{(2)}_{eff}\right|^2 I_1(\omega_{IR}) I_2(\omega_{VIS}) \tag{4}$$

where ω, ω_{IR}, and ω_{VIS} are the frequencies of output sum frequency beam, input IR beam, and input visible beam, respectively, β is the reflection angle of the sum frequency beam, n is the refractive index of the medium at corresponding frequency, and $\chi^{(2)}_{eff}$ is the effective second-order nonlinear optical susceptibility. When the frequency of the input IR beam ω_{IR} is close to the resonance of the vibrational state of molecules, $\chi^{(2)}_{eff}$ can then be expressed as:

$$\chi^{(2)}_{eff} = \chi^{(2)}_{NR} + \sum_q \frac{A_q}{\omega_{IR} - \omega_q + i\Gamma_q} \tag{5}$$

where $\chi^{(2)}_{NR}$ denotes the nonresonant background contribution, A_q, ω_q, and Γ_q are the amplitude, resonant frequency, and damping term of the qth vibrational mode of molecules, respectively. These parameters can be obtained by fitting the experimental SFG spectra with the Lorentzian function.

One common approach to deduce the orientation of molecules on surfaces or at interfaces from SFG data is to calculate the ratio of the effective second-order nonlinear optical susceptibility components obtained from different polarization-combination measurements. Two commonly

used polarization combinations in our research are ssp (s-polarized SFG output, p-polarized visible input, p-polarized IR input) and ppp. The $\chi^{(2)}_{eff,ssp}$ / $\chi^{(2)}_{eff,ppp}$ ratio can be calculated from the fitting results of SFG spectra. Then the $\chi^{(2)}_{eff,ssp}$ / $\chi^{(2)}_{eff,ppp}$ value can be converted to $\chi^{(2)}_{yyz}$ / $\chi^{(2)}_{zzz}$ by considering the Fresnel Coefficients:

$$\chi^{(2)}_{eff,yyz} = L_{yyz}\,\chi^{(2)}_{yyz} \tag{6}$$

$$\chi^{(2)}_{eff,zzz} = L_{zzz}\,\chi^{(2)}_{zzz} - L_{yzz}\,\chi^{(2)}_{yzy} + L_{zyy}\,\chi^{(2)}_{zyy} - L_{yyz}\,\chi^{(2)}_{yyz} \tag{7}$$

The relationship between the $\chi^{(2)}_{yyz}$ / $\chi^{(2)}_{zzz}$ ratio and the functional group (or molecule) orientation can be obtained, which will be discussed in detail below. Using the experimentally measured $\chi^{(2)}_{yyz}$ / $\chi^{(2)}_{zzz}$ value and the above relationship, the orientation of a function group or molecule, usually defined by the tilt and twist angles, can be deduced.

1.4 SFG Data Analysis Methodology on α-helix and β-sheet Structures

The experimentally measured effective second-order nonlinear optical susceptibility $\chi^{(2)}$ is related to the molecule's hyperpolarizability and orientation. The hyperpolarizability of the amide I mode of an α-helical structure can be calculated using the bond additivity model reported previously by our group.[53-54] In this model, an alpha-helical structure is treated as an ideal alpha-helix with a $C_{18/5}$ symmetry. According to the character table for a $C_{18/5}$ point group, two amide I vibrational modes, the A and E_1 modes, are both IR-active and Raman-active (thus SFG-active). The A and E_1 modes are parallel and perpendicular to the principal axis of an α-helix, respectively. The amide I mode IR transition dipole moment of a peptide unit inside the α-helix can be projected onto the parallel direction and the perpendicular direction vs. the principal axis, and then these projections can be summed up (after considering the phase of the amide I vibration of each peptide unit) to calculate the total IR transition dipole moment of an α-helix. Similarly, the amide I mode

Raman polarizability of an α-helix can be obtained from the Raman polarizability of a single peptide unit. Then the SFG hyperpolarizability of the amide I mode of an α-helix can be calculated. Quantitatively, the SFG hyperpolarizability can be expressed as:

$$\beta_{lmn,q} \propto \frac{\partial \alpha_{lm}^{*}}{\partial Q_q} \frac{\partial \mu_n}{\partial Q_q} \tag{8}$$

where l,m,n are the molecular coordinates, and $\frac{\partial \alpha_{lm}^{*}}{\partial Q_q}$ and $\frac{\partial \mu_n}{\partial Q_q}$ are Raman polarizability and IR transition dipole moment derivatives with respect to the normal coordinate of the qth vibrational mode, respectively.

With the calculated SFG hyperpolarizability components and their relations with experimentally measured SFG susceptibility components, the relationships between the ratios of SFG amide I susceptibility components and the α-helix orientation can be determined, which can be used to deduce α-helix orientation. This methodology has been successfully applied to study the straight α-helical magainin 2 peptides and bent α-helical LL-37 (by summing the Raman polarizability and IR transition dipole moment for two alpha-helical segments) associated with lipid membranes,[53] as well as chemically immobilized α-helical antimicrobial peptides on SAM before and after bacteria contact.[46]

The above method can also be extended to study protein orientation. Andrew et al. developed a python software package based on the bond additivity model that can automatically locate the alpha-helical segments inside a protein crystal structure and calculate the overall SFG responses (e.g., the $\chi_{xxz}^{(2)}$ / $\chi_{zzz}^{(2)}$ ratios) of all the α-helical structures inside the protein as a function of protein orientation (tilt and twist angles). Such calculated orientation dependent SFG responses can be compared with experimentally measured SFG responses to generate a heatmap, showing the matching qualities between the experimental data and the calculated data at different protein

orientations. This protein orientations with the highest matching scores are the most likely orientations. This method was successfully applied to determine the orientations of several membrane proteins including a protein complex formed by G protein-coupled receptor kinase 2 (GRK2) and heterotrimeric G proteins βγ subunits (G-βγ) at a lipid bilayer.[43]

For some proteins and peptides, this method could lead to multiple possible orientations that may hamper the structure analysis, indicating that the limited number of SFG measurements are not adequate to determine a unique protein orientation in these cases. ATR-FTIR is commonly used as a complementary tool for SFG to narrow down the range of possible orientations. ATR-FTIR does not have intrinsic monolayer surface sensitivity as SFG, but if there is only one monolayer of proteins, ATR-FTIR signals must be contributed by the monolayer protein molecules. ATR-FTIR measures different orientation parameters from SFG. For example, for a tilt angle θ, SFG measures $<\cos\theta>$ and $<\cos^3\theta>$, while ATR-FTIR measurement obtains $<\cos^2\theta>$ (here < > means average). By combining SFG and ATR-FTIR techniques, a complicated orientation distribution of alpha-helical melittin inside a DPPG lipid bilayer was successfully deduced.[55] This methodology was also applied to study other proteins, such as surface-immobilized nitro-reductase (NfsB),[45] the G proteins Gαiβ1γ2 and Gβ1γ2 on a lipid membrane,[56] and the two-point tethered NfsB on the maleimide-terminated SAM surface.[38]

The analysis of β-sheet, another widely existed secondary structure, is more complicated than that of α-helix. The anti-parallel β-sheet can be treated as having D_2 symmetry,[57-59] so there are three IR active modes (B_1, B_2, and B_3) and four Raman active modes (A, B_1, B_2, and B_3). Due to the D_2 symmetry, the orientation requires both the tilt angle (θ) and the twist angle (ψ) to define. Here the SFG signal collected in the ssp and ppp polarization combinations are dependent on each other. Therefore, the intensity ratio $\chi_{ssp}^{(2)} / \chi_{ppp}^{(2)}$ remains constant and is irrelevant to the orientation

of β-sheet structure, and one additional independent measurement is required to deduce the orientation of a β-sheet structure, Khoi et al. combined the SFG measurements with ATR-FTIR to successfully deduce the orientation of a β-sheet antimicrobial peptide, tachyplesin I, at interface.[60]

These systematic methodologies have been successfully used for deducing the orientations of a variety of proteins and peptides containing α-helix and β-sheet structures. However, these methods have their own limitations. For example, the method to use SFG signals contributed from α-helices assumes that the detected SFG amide I signal centered around 1650 cm^{-1} is only contributed from the α-helical structure, and it does not consider the responses from amino acids with other structures. Although the ~1650 cm^{-1} signal is dominated by α-helical segments, it is not reasonable to completely exclude the possibilities for other amino acids to contribute to this signal. In this method, the α-helical segments inside the proteins or peptides were all treated as ideal α-helices to apply the helical symmetry and simplify the orientation analysis. However, not all the α-helical structures are ideal for many proteins or peptides. The β-sheet method was successfully applied to study simple anti-parallel β-sheet peptide, tachyplesin I, but it is difficult to use this method to study β-sheet structures with more than two strands in protein. Therefore, further efforts need to be invested for SFG protein orientation analysis based on both α-helix and β-sheet structures, as well as other amino acids.

1.5 SFG-Hamiltonian Analysis Method

Hamiltonian analysis method can be used to calculate SFG spectra from a protein/peptide using the transition dipole coupling model and one-exciton Hamiltonian. This method will read the coordinates of all the atoms of the input protein/peptide structure (pdb) file and construct the amide I local mode for each peptide bond. The IR transition dipole μ and the Raman polarizability α can be assigned to all the amide I local modes. The amide I modes inside the protein/peptide

structure are strongly coupled with each other, and the coupling effects are quantified by using the transition dipole coupling model between each pair of the amide I local modes. This method was published previously and was applied to study the site-specific orientation of ovispirin-1 (an α-helical peptide) on PS surface and at model membrane interface by combining with the isotope-labeled SFG technique.[47-48] This SFG-Hamiltonian method was further developed in this thesis research into a generally applicable method so it can be used to study orientations and conformations of many proteins/peptides with complicated secondary structures.[61-62] The details of the Hamiltonian spectral calculation and the calculated – collected spectral matching process will be presented in Chapter 2.

1.6 SFG Instrumentation

In this thesis, two SFG systems were used for SFG signal acquisition: a picosecond (ps) SFG system and a femtosecond (fs) SFG system. Details of the SFG setup and data collection of ps-SFG[63-64] and fs-SFG[65-67] have been published and will not be repeated here. The following is a brief introduction:

(1) The ps-SFG system:

An EKSPLA PL 2250 (Vilnius, Lithuania) SFG spectrometer was used for SFG measurements. This SFG system produces picosecond (ps) laser pulses (30 ps pulse width) at a repetition rate of 50 Hz. Two laser pulses, one with a fixed wavelength at 532 nm in the visible frequency range and the other with a tunable wavelength from 2.3 to 10 μm in the IR frequency range, overlap spatially and temporally at the examined interface. Nearly total reflection geometry was used for SFG data collection.

(2) The fs-SFG system:

In this system, laser pulses were generated from a Ti:sapphire regenerative amplifier (Solstice Ace, Spectra Physics), which centered at ~795 nm with ~35 femtoseconds pulse width. Part of the laser power was used in the optical parametric amplifier (OPA, TOPAS Prime, Spectra Physics) and difference frequency generator (DFG, TOPAS Prime, Spectra Physics) to produce the broadband IR beam. Then the broadband IR beam and the 795 nm beam were overlapped spatially and temporally at the sample interface. The incident angles of the 795 nm and the broadband IR beams were 65° and 55 ° versus the surface normal, respectively. The generated SFG signal was collected by a spectrograph (Kymera 328i, Andor) using the ssp and ppp polarization combinations.

1.7 Research Objective and Contents in This Thesis

This thesis focuses on further developing the SFG-Hamiltonian analysis method for studying the interfacial structures (orientations and conformations) of proteins/peptides on surfaces and at interfaces. This research is aimed to develop a well-organized and widely applicable SFG data analysis method to study peptides and proteins, which can be used together with molecular dynamics simulations and isotope labeling, based on all the amino acids in the protein, not limited by the amino acids in the helical and/or sheet structures only.

The chapter 1 (this chapter) briefly introduces the research background, SFG experiments and data analysis, especially the previous data analysis, methods used to study proteins and peptides, as well as the research focuses in each of the later thesis chapters

Chapter 2 presents the details of the developed the Hamiltonian spectral calculation methodology. The Hamiltonian spectral calculation method was integrated with MD simulations and spectral comparison between calculated and experimentally collected SFG spectra to

determine the most likely conformation and orientation of proteins/peptides at interface, which is also discussed in this chapter.

Chapters 3 to 6 present the applications of the developed methodology detailed in chapter 2 to study a variety of interfacial proteins and peptides. Chapter 3 demonstrates the feasibility of using SFG study with the Hamiltonian analysis method to investigate protein aggregation at interface. Particularly, we showed that the developed SFG experimental/data analysis method can be used to differentiate the bovine serum albumin (BSA) dimer and monomer adsorption on the silicone oil surface. It was reported that dithiothreitol (DTT) can cut the disulfide bonds in BSA dimer to change BSA dimer to monomers. Here, we successfully observed such a change of BSA dimer at the silicone oil interface caused by DTT using SFG and the Hamiltonian data analysis. The BSA dimer and monomer ratio at the silicone oil interface can be quantified after the DTT reaction.

In Chapter 4, we monitored the adsorption dynamics of fibrinogen on the silicone oil surface. Time-dependent SFG spectra were collected using the fs-SFG system. These time-dependent SFG spectra collected during the protein adsorption process were analyzed by using the Hamiltonian method to deduce the orientation change of the fibrinogen molecules while being adsorbed to the interface. It was found that the adsorbed fibrinogen molecules tend to lie down during the initial adsorption and then tilts up toward the solution due to the crowded surface covered by adsorbed fibrinogen molecules. The coverage change of fibrinogen on the surface during the adsorption was also deduced.

Chapter 5 discusses the orientation and structure analysis of two commercial antibody drug products at the silicone oil interface. The effects of a widely used surfactant in pharmaceutical industry, PS80, on the adsorption behavior of these two antibody drugs on silicone oil surface were

elucidated. With a certain bulk concentration, this surfactant can prevent the antibody molecules from adsorption. Also, even below this concentration, the surfactant could retain the native structures of the adsorbed antibodies adsorbed on silicone oil.

In Chapter 6, along with MD simulations, we applied the development Hamiltonian analysis method and SFG experiments to investigate the conformation and orientation of barnacle cement peptides (BCP) on polystyrene surface, providing molecular level understanding on marine biofouling mechanisms.

This thesis developed a systematic approach to determine conformation and orientation of proteins and peptides at buried interfaces in situ in real time. This approach integrates SFG experiments, MD simulations, Hamiltonian spectral calculations, and experimental – calculated spectra comparisons together. For proteins and peptides with no crystal structure, input structures for Hamiltonian calculation can be deduced from structural prediction software with sequences. Therefore, this approach can be applied to study many different interfacial peptides and proteins with or without crystal structures known.

1.8 References

1. Bajpai, A., Fibrinogen adsorption onto macroporous polymeric surfaces: correlation with biocompatibility aspects. *Journal of Materials Science: Materials in Medicine* **2008,** *19* (1), 343-357.

2. Horbett, T. A., Biological activity of adsorbed proteins. *Surfactant science series* **2003,** *110*, 393-413.

3. Gerhardt, A.; Bonam, K.; Bee, J. S.; Carpenter, J. F.; Randolph, T. W., Ionic strength affects tertiary structure and aggregation propensity of a monoclonal antibody adsorbed to silicone oil–water interfaces. *Journal of pharmaceutical sciences* **2013,** *102* (2), 429-440.

4. Perera, H. G.; Lu, T.; Fu, L.; Zhang, J.; Chen, Z., Probing the Interfacial Interactions of Monoclonal and Bispecific Antibodies at the Silicone Oil–Aqueous Solution Interface by Using Sum Frequency Generation Vibrational Spectroscopy. *Langmuir* **2019,** *35* (44), 14339-14347.

5. Frokjaer, S.; Otzen, D. E., Protein drug stability: a formulation challenge. *Nature reviews drug discovery* **2005,** *4* (4), 298-306.

6. Peña-Bahamonde, J.; Nguyen, H. N.; Fanourakis, S. K.; Rodrigues, D. F., Recent advances in graphene-based biosensor technology with applications in life sciences. *Journal of nanobiotechnology* **2018,** *16* (1), 1-17.

7. Li, X.; Li, S.; Huang, X.; Chen, Y.; Cheng, J.; Zhan, A., Protein-mediated bioadhesion in marine organisms: A review. *Marine Environmental Research* **2021,** *170*, 105409.

8. Tang, L.; Thevenot, P.; Hu, W., Surface chemistry influences implant biocompatibility. *Current topics in medicinal chemistry* **2008,** *8* (4), 270-280.

9. Castner, D. G.; Ratner, B. D., Biomedical surface science: Foundations to frontiers. *Surface Science* **2002,** *500* (1-3), 28-60.

10. Jones, L. S.; Kaufmann, A.; Middaugh, C. R., Silicone oil induced aggregation of proteins. *Journal of pharmaceutical sciences* **2005,** *94* (4), 918-927.

11. Rosenberg, A. S., Effects of protein aggregates: an immunologic perspective. *The AAPS journal* **2006,** *8* (3), E501-E507.

12. Thirumangalathu, R.; Krishnan, S.; Ricci, M. S.; Brems, D. N.; Randolph, T. W.; Carpenter, J. F., Silicone oil-and agitation-induced aggregation of a monoclonal antibody in aqueous solution. *Journal of pharmaceutical sciences* **2009,** *98* (9), 3167-3181.

13. Vázquez‐Rey, M.; Lang, D. A., Aggregates in monoclonal antibody manufacturing processes. *Biotechnology and bioengineering* **2011,** *108* (7), 1494-1508.

14. Demirel, Y. K.; Uzun, D.; Zhang, Y.; Fang, H.-C.; Day, A. H.; Turan, O., Effect of barnacle fouling on ship resistance and powering. *Biofouling* **2017,** *33* (10), 819-834.

15. Kermani, A. A., A guide to membrane protein X‐ray crystallography. *The FEBS journal* **2020**.

16. Hu, Y.; Cheng, K.; He, L.; Zhang, X.; Jiang, B.; Jiang, L.; Li, C.; Wang, G.; Yang, Y.; Liu, M., NMR-based methods for protein analysis. *Analytical Chemistry* **2021**, *94* (4), 1866-1879.

17. Glassford, S. E.; Byrne, B.; Kazarian, S. G., Recent applications of ATR FTIR spectroscopy and imaging to proteins. *Biochimica et Biophysica Acta (BBA)-Proteins and Proteomics* **2013,** *1834* (12), 2849-2858.

18. Cheng, Y., Membrane protein structural biology in the era of single particle cryo-EM. *Current opinion in structural biology* **2018,** *52*, 58-63.

19. Dupont-Gillain, C., Orientation of adsorbed antibodies: in situ monitoring by QCM and random sequential adsorption modeling. In *Proteins at interfaces III state of the art*, ACS Publications: 2012; pp 453-469.

20. Zhao, X.; Pan, F.; Cowsill, B.; Lu, J. R.; Garcia-Gancedo, L.; Flewitt, A. J.; Ashley, G. M.; Luo, J., Interfacial immobilization of monoclonal antibody and detection of human prostate-specific antigen. *Langmuir* **2011,** *27* (12), 7654-7662.

21. Zhao, X.; Pan, F.; Garcia-Gancedo, L.; Flewitt, A. J.; Ashley, G. M.; Luo, J.; Lu, J. R., Interfacial recognition of human prostate-specific antigen by immobilized monoclonal antibody: effects of solution conditions and surface chemistry. *Journal of The Royal Society Interface* **2012,** *9* (75), 2457-2467.

22. Wang, X.; Wang, Y.; Xu, H.; Shan, H.; Lu, J. R., Dynamic adsorption of monoclonal antibody layers on hydrophilic silica surface: A combined study by spectroscopic ellipsometry and AFM. *Journal of colloid and interface science* **2008,** *323* (1), 18-25.

23. Lu, X.; Shephard, N.; Han, J.; Xue, G.; Chen, Z., Probing molecular structures of polymer/metal interfaces by sum frequency generation vibrational spectroscopy. *Macromolecules* **2008,** *41* (22), 8770-8777.

24. Lu, X.; Li, D.; Kristalyn, C. B.; Han, J.; Shephard, N.; Rhodes, S.; Xue, G.; Chen, Z., Directly probing molecular ordering at the buried polymer/metal interface. *Macromolecules* **2009,** *42* (22), 9052-9057.

25. Lu, X.; Clarke, M. L.; Li, D.; Wang, X.; Xue, G.; Chen, Z., A sum frequency generation vibrational study of the interference effect in poly (n-butyl methacrylate) thin films sandwiched between silica and water. *The Journal of Physical Chemistry C* **2011,** *115* (28), 13759-13767.

26. Lu, X.; Xue, G.; Wang, X.; Han, J.; Han, X.; Hankett, J.; Li, D.; Chen, Z., Directly probing molecular ordering at the buried polymer/metal interface 2: Using P-polarized input beams. *Macromolecules* **2012,** *45* (15), 6087-6094.

27. Myers, J. N.; Zhang, X.; Bielefeld, J.; Lin, Q.; Chen, Z., Nondestructive in situ characterization of molecular structures at the surface and buried interface of silicon-supported low-k dielectric films. *The Journal of Physical Chemistry B* **2015,** *119* (4), 1736-1746.

28. Lu, X.; Zhang, C.; Ulrich, N.; Xiao, M.; Ma, Y.-H.; Chen, Z., Studying polymer surfaces and interfaces with sum frequency generation vibrational spectroscopy. *Analytical chemistry* **2016,** *89* (1), 466-489.

29. Zhang, X.; Myers, J. N.; Huang, H.; Shobha, H.; Chen, Z.; Grill, A., SFG analysis of the molecular structures at the surfaces and buried interfaces of PECVD ultralow-dielectric constant pSiCOH. *Journal of Applied Physics* **2016,** *119* (8), 084101.

30. Wang, J.; Even, M. A.; Chen, X.; Schmaier, A. H.; Waite, J. H.; Chen, Z., Detection of amide I signals of interfacial proteins in situ using SFG. *Journal of the American Chemical Society* **2003,** *125* (33), 9914-9915.

31. Clarke, M. L.; Wang, J.; Chen, Z., Conformational changes of fibrinogen after adsorption. *The Journal of Physical Chemistry B* **2005,** *109* (46), 22027-22035.

32. Wang, J.; Chen, X.; Clarke, M. L.; Chen, Z., Detection of chiral sum frequency generation vibrational spectra of proteins and peptides at interfaces in situ. *Proceedings of the National Academy of Sciences* **2005,** *102* (14), 4978-4983.

33. Wang, J.; Clarke, M. L.; Chen, X.; Even, M. A.; Johnson, W. C.; Chen, Z., Molecular studies on protein conformations at polymer/liquid interfaces using sum frequency generation vibrational spectroscopy. *Surface Science* **2005,** *587* (1-2), 1-11.

34. Clarke, M. L.; Chen, Z., Polymer surface reorientation after protein adsorption. *Langmuir* **2006,** *22* (21), 8627-8630.

35. Wang, J.; Chen, X.; Clarke, M. L.; Chen, Z., Vibrational spectroscopic studies on fibrinogen adsorption at polystyrene/protein solution interfaces: hydrophobic side chain and secondary structure changes. *The Journal of Physical Chemistry B* **2006,** *110* (10), 5017-5024.

36. Wang, J.; Lee, S.-H.; Chen, Z., Quantifying the ordering of adsorbed proteins in situ. *The Journal of Physical Chemistry B* **2008,** *112* (7), 2281-2290.

37. Sarroukh, R.; Goormaghtigh, E.; Ruysschaert, J.-M.; Raussens, V., ATR-FTIR: a "rejuvenated" tool to investigate amyloid proteins. *Biochimica et Biophysica Acta (BBA)-Biomembranes* **2013,** *1828* (10), 2328-2338.

38. Zou, X.; Wei, S.; Badieyan, S.; Schroeder, M.; Jasensky, J.; Brooks III, C. L.; Marsh, E. N. G.; Chen, Z., Investigating the effect of two-point surface attachment on enzyme stability and activity. *Journal of the American Chemical Society* **2018,** *140* (48), 16560-16569.

39. Li, Y.; Pan, D.; Nashine, V.; Deshmukh, S.; Vig, B.; Chen, Z., Understanding Protein-Interface Interactions of a Fusion Protein at Silicone Oil-Water Interface Probed by Sum Frequency Generation Vibrational Spectroscopy. *Journal of pharmaceutical sciences* **2018,** *107* (2), 682-689.

40. Zou, X.; Wei, S.; Jasensky, J.; Xiao, M.; Wang, Q.; Brooks III, C. L.; Chen, Z., Molecular interactions between graphene and biological molecules. *Journal of the American Chemical Society* **2017,** *139* (5), 1928-1936.

41. Wei, S.; Zou, X.; Tian, J.; Huang, H.; Guo, W.; Chen, Z., Control of protein conformation and orientation on graphene. *Journal of the American Chemical Society* **2019,** *141* (51), 20335-20343.

42. Xiao, M.; Wei, S.; Chen, J.; Tian, J.; Brooks III, C. L.; Marsh, E. N. G.; Chen, Z., Molecular Mechanisms of Interactions between Monolayered Transition Metal Dichalcogenides and Biological Molecules. *Journal of the American Chemical Society* **2019,** *141* (25), 9980-9988.

43. Boughton, A. P.; Yang, P.; Tesmer, V. M.; Ding, B.; Tesmer, J. J.; Chen, Z., Heterotrimeric G protein β1γ2 subunits change orientation upon complex formation with G protein-coupled receptor kinase 2 (GRK2) on a model membrane. *Proceedings of the National Academy of Sciences* **2011,** *108* (37), E667-E673.

44. Liu, Y.; Jasensky, J.; Chen, Z., Molecular interactions of proteins and peptides at interfaces studied by sum frequency generation vibrational spectroscopy. *Langmuir* **2012,** *28* (4), 2113-2121.

45. Ding, B.; Jasensky, J.; Li, Y.; Chen, Z., Engineering and characterization of peptides and proteins at surfaces and interfaces: a case study in surface-sensitive vibrational spectroscopy. *Accounts of chemical research* **2016,** *49* (6), 1149-1157.

46. Xiao, M.; Jasensky, J.; Gerszberg, J.; Chen, J.; Tian, J.; Lin, T.; Lu, T.; Lahann, J.; Chen, Z., Chemically immobilized antimicrobial peptide on polymer and self-assembled monolayer substrates. *Langmuir* **2018,** *34* (43), 12889-12896.

47. Ding, B.; Laaser, J. E.; Liu, Y.; Wang, P.; Zanni, M. T.; Chen, Z., Site-specific orientation of an α-helical peptide ovispirin-1 from isotope-labeled SFG spectroscopy. *The Journal of Physical Chemistry B* **2013,** *117* (47), 14625-14634.

48. Ding, B.; Panahi, A.; Ho, J.-J.; Laaser, J. E.; Brooks III, C. L.; Zanni, M. T.; Chen, Z., Probing site-specific structural information of peptides at model membrane interface in situ. *Journal of the American Chemical Society* **2015,** *137* (32), 10190-10198.

49. Shen, Y., Surface properties probed by second-harmonic and sum-frequency generation. *Nature* **1989,** *337* (6207), 519.

50. Zhuang, X.; Miranda, P.; Kim, D.; Shen, Y., Mapping molecular orientation and conformation at interfaces by surface nonlinear optics. *Physical Review B* **1999,** *59* (19), 12632.

51. Moad, A. J.; Simpson, G. J., A unified treatment of selection rules and symmetry relations for sum-frequency and second harmonic spectroscopies. *The Journal of Physical Chemistry B* **2004,** *108* (11), 3548-3562.

52. Shen, Y., *Fundamentals of sum-frequency spectroscopy*. Cambridge University Press: 2016.

53. Ding, B.; Soblosky, L.; Nguyen, K.; Geng, J.; Yu, X.; Ramamoorthy, A.; Chen, Z., Physiologically-relevant modes of membrane interactions by the human antimicrobial peptide, LL-37, revealed by SFG experiments. *Scientific reports* **2013,** *3* (1), 1-8.

54. Nguyen, K. T.; Le Clair, S. V.; Ye, S.; Chen, Z., Orientation determination of protein helical secondary structures using linear and nonlinear vibrational spectroscopy. *The Journal of Physical Chemistry B* **2009,** *113* (36), 12169-12180.

55. Chen, X.; Wang, J.; Boughton, A. P.; Kristalyn, C. B.; Chen, Z., Multiple orientation of melittin inside a single lipid bilayer determined by combined vibrational spectroscopic studies. *Journal of the American Chemical Society* **2007,** *129* (5), 1420-1427.

56. Yang, P.; Boughton, A.; Homan, K. T.; Tesmer, J. J.; Chen, Z., Membrane orientation of Gαiβ1γ2 and Gβ1γ2 determined via combined vibrational spectroscopic studies. *Journal of the American Chemical Society* **2013,** *135* (13), 5044-5051.

57. Suzuki, E., A quantitative study of the amide vibrations in the infra-red spectrum of silk fibroin. *Spectrochimica Acta Part A: Molecular Spectroscopy* **1967,** *23* (8), 2303-2308.

58. Fraser, R.; Suzuki, E., A quantitative study of the Amide I vibrations in the infra-red spectrum of β-keratin. *Spectrochimica Acta Part A: Molecular Spectroscopy* **1970,** *26* (2), 423-426.

59. Marsh, D., Dichroic ratios in polarized Fourier transform infrared for nonaxial symmetry of beta-sheet structures. *Biophysical journal* **1997,** *72* (6), 2710-2718.

60. Nguyen, K. T.; King, J. T.; Chen, Z., Orientation determination of interfacial β-sheet structures in situ. *The Journal of Physical Chemistry B* **2010,** *114* (25), 8291-8300.

61. Guo, W.; Zou, X.; Jiang, H.; Koebke, K. J.; Hoarau, M.; Crisci, R.; Lu, T.; Wei, T.; Marsh, E. N. G.; Chen, Z., Molecular Structure of the Surface-Immobilized Super Uranyl Binding Protein. *The Journal of Physical Chemistry B* **2021,** *125* (28), 7706-7716.

62. Lu, T.; Guo, W.; Datar, P. M.; Xin, Y.; Marsh, E. N. G.; Chen, Z., Probing protein aggregation at buried interfaces: distinguishing between adsorbed protein monomers, dimers, and a monomer–dimer mixture in situ. *Chemical Science* **2022,** *13* (4), 975-984.

63. Chen, Z.; Shen, Y.; Somorjai, G. A., Studies of polymer surfaces by sum frequency generation vibrational spectroscopy. *Annual review of physical chemistry* **2002,** *53* (1), 437-465.

64. Richmond, G., Molecular bonding and interactions at aqueous surfaces as probed by vibrational sum frequency spectroscopy. *Chemical reviews* **2002,** *102* (8), 2693-2724.

65. Tan, J.; Zhang, B.; Luo, Y.; Ye, S., Ultrafast Vibrational Dynamics of Membrane‐Bound Peptides at the Lipid Bilayer/Water Interface. *Angewandte Chemie* **2017,** *129* (42), 13157-13161.

66. McGuire, J. A.; Shen, Y. R., Ultrafast vibrational dynamics at water interfaces. *Science* **2006,** *313* (5795), 1945-1948.

67. Zhang, Z.; Piatkowski, L.; Bakker, H. J.; Bonn, M., Ultrafast vibrational energy transfer at the water/air interface revealed by two-dimensional surface vibrational spectroscopy. *Nature chemistry* **2011,** *3* (11), 888.

Chapter 2 Development of Hamiltonian Analysis Method

2.1 Introduction

This chapter will discuss the development of the Hamiltonian analysis method that can calculate SFG spectra and determine molecular structure (orientation and conformation) of interfacial proteins/peptides. The calculation of this Hamiltonian method is based on the one-exciton Hamiltonian matrix of the vibrational exciton, which has been discussed in previous publications.[1-5] These excellent research results showed that the Hamiltonian method can study structures and orientations of large biomolecules, such as DNA oligomers and self-assembled peptides, by analyzing the 2D-SFG or 2D-IR spectra. It is well known that the amide I modes of amino acids in a protein or peptide are strongly coupled with each other. Such coupling effects need to be considered when applying the Hamiltonian method for SFG spectra calculation. The transition dipole model is commonly used to address the coupling terms inside the one-exciton Hamiltonian matrix. Many efforts have been made to improve the accuracy of this model, such as the nearest-neighbor coupling correction[2-3, 6] and the antiparallel β-sheet coupling correction.[7-9] However, improving the accuracy of this model by adding corrections is still an ongoing area of research, and this thesis research will only focus on the transition dipole model. Nevertheless, SFG spectroscopy with the Hamiltonian data analysis method is a unique and valuable tool for unveiling the molecular structures of interfacial proteins/peptides which are difficult to achieve by other techniques. Previous studies from our group showed that the Hamiltonian method could be used to interpret the SFG signals of isotope-labeled ovisipirin-1 in lipid layers, which successfully

elucidated the site-specific structural information by determining the coupling effects among amide I modes and the isotope-label effects.

The Hamiltonian method in this thesis refers to a MATLAB program that calculates 1D-SFG spectra based on protein/peptide structures by considering the amide I local mode vibration of each peptide unit and the coupling effects between the amide I modes of any two peptide bonds. This Hamiltonian method was adopted and developed based on a prototype MATLAB script that can only calculate SFG signal amplitude of each amide I normal mode at one protein/peptide orientation at a time. The method developed in this thesis can now be used to calculate SFG spectra of peptides and proteins as a function of peptide/protein orientation. Furthermore, in this thesis, MD simulated peptide/protein structures can be used as input structures for the Hamiltonian method for SFG spectral calculation to consider the conformational changes of the peptides/proteins from crystal structures due to interfacial interactions. In addition, the calculated orientation dependent SFG spectra can be compared to the experimentally collected SFG spectra to generate matching score heat maps to deduce the interfacial peptide/protein orientation. Therefore, based on the Hamiltonian analysis and SFG results, a systematic and generally applicable methodology was developed in this thesis to determine conformations and orientations of proteins or peptides at interfaces.

2.2 Theory of the Hamiltonian Local Mode Approximation

The main calculation part in this Hamiltonian analysis program is similar to the previously published version but with slight modifications. The details of the SFG spectra calculation will be discussed in this section.

Firstly, a protein data bank (pdb) structure (for a protein crystal structure) or a MD simulated protein structure is loaded into the MATLAB main program. The atomic positions of C,

N, and O atoms in the protein backbone chain are selected and used for calculating the amide I modes later. The molecular frame axes of each local mode (amide I mode for each peptide unit) are also defined according to the C, N, and O atom positions. For each local mode, the z-axis is defined by the vector of the C=O bond, the x-axis is perpendicular to the C-N-O plane, and the y-axis is perpendicular to both the x and z axes pointing from C to N.

The transition dipole moment μ for the amide I mode in this molecular frame is defined as:

$$\mu = \begin{bmatrix} 0 \\ \sin\frac{25\pi}{180} \\ -\cos\frac{25\pi}{180} \end{bmatrix}$$

The angle between the μ and the C=O bond in the peptide unit is 25 degrees.[10-11] The position and location of the amide I mode transition dipole moment of the peptide unit is shown in Figure 2.1. The Raman polarizability tensor α of each local amide I mode is given by:[12]

$$\alpha = \begin{bmatrix} 0.25 & 0 & 0 \\ 0 & 1 & 0 \\ 0 & 0 & 5 \end{bmatrix}$$

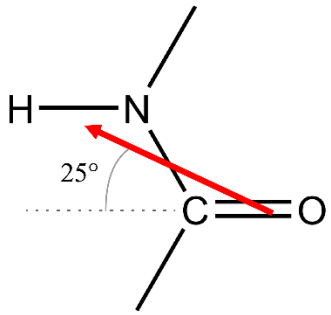


Figure 2.1 Diagram showing the direction and location of the IR amide I transition dipole of a peptide unit.

The angle between the z-axis of the Raman polarizability tensor and the C=O bond is 34 degrees, as shown in Figure 2.2. Therefore, the rotation matrix that maps from the molecular frame axes to the principal axes of the Raman polarizability tensor can be expressed as:

$$R_{Mol} = \begin{bmatrix} 1 & 0 & 0 \\ 0 & \cos\frac{34\pi}{180} & -\sin\frac{34\pi}{180} \\ 0 & \sin\frac{34\pi}{180} & \cos\frac{34\pi}{180} \end{bmatrix}$$

So, the Raman polarizability tensor of each amide I local mode α_{Local} can be calculated using the following equation:

$$\alpha_{Local} = R_{Mol} \cdot \alpha \cdot R'_{Mol}$$

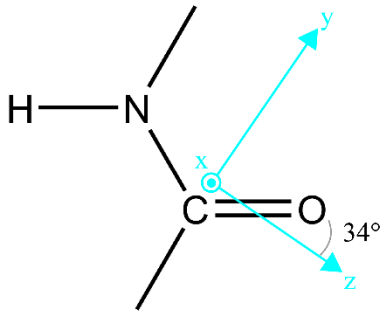


Figure 2.2 The principal axes of the Raman polarizability in the molecular frame of the amide I stretch mode.

The center of each local amide I mode is defined by:

$$\vec{r}_{amide-I} = \vec{r}_C + \vec{r}_{CO} * 0.665 + \vec{r}_{CN} * 0.256$$

where $\vec{r}_{CO}$ is normalized C=O vectors, and $\vec{r}_{CN}$ is normalized C-N vectors. The center of the amide I mode will be used for determining the distance between two local amide I modes for two peptide units, which is critical for calculating the coupling effects by the transition dipole model.

The coupling effects between two different local amide I modes can be calculated by the transition dipole coupling model:

$$\beta_{ij} = \frac{1}{4\pi\epsilon_0}\left[\frac{\vec{\mu}_i \cdot \vec{\mu}_j}{r_{ij}^3} - 3\frac{(\vec{r}_{ij} \cdot \vec{\mu}_i)(\vec{r}_{ij} \cdot \vec{\mu}_j)}{r_{ij}^5}\right]$$

where β_{ij} is the coupling term between modes i and j, $\vec{\mu}_i$ is the transition dipole of mode I, $\vec{r}_{ij}$ is the vector pointing from the center of mode i to mode j, and r_{ij} is the distance between the centers

of modes i and j. The Hamiltonian matrix was then constructed by using the coupling terms β as the off-diagonal elements and the local mode frequencies as the diagonal elements. The local mode frequency of 1644 cm^{-1} was used in this study unless otherwise specified. The constructed Hamiltonian matrix is shown below:

$$H = \begin{bmatrix} 1644 & \beta_{12} & \beta_{13} & \beta_{14} & \cdots \\ \beta_{21} & 1644 & \beta_{23} & \beta_{24} & \cdots \\ \beta_{31} & \beta_{32} & 1644 & \beta_{34} & \cdots \\ \beta_{41} & \beta_{42} & \beta_{43} & 1644 & \cdots \\ \vdots & \vdots & \vdots & \vdots & \ddots \end{bmatrix}$$

The Hamiltonian matrix is then diagonalized. The eigenvalues represent the frequencies of the normal modes of the protein, and the eigenvectors describe the contribution of each local mode to the normal mode. The transition dipole of N-th normal mode can be calculated by using:

$$\mu_N = \sum_m C_{Nm} \cdot \mu_m$$

where μ_m is the transition dipole of m-th local mode, and C_{Nm} is the corresponding element in the eigenvectors. The Raman polarizability tensor of the normal modes α_N can be calculated using a similar fashion:

$$\alpha_N = \sum_m C_{Nm} \cdot \alpha_m$$

The hyperpolarizability β of a normal mode of the protein can be calculated by the outer product of α and μ of this normal mode:

$$\beta = \alpha \otimes \mu$$

Then the calculated second-order nonlinear susceptibility χ_{Lab} in the lab frame is given by:[13-14]

$$\chi_{Lab} = N_s \cdot < R > \cdot \beta$$

where N_s is the surface number density, β represents the hyperpolarizability of a normal mode in the molecular frame, and R is the rotation matrix that transforms the response from the molecular frame to the lab frame. $< R >$ denotes the ensemble average over the orientation distribution, and the azimuthal angle ϕ is averaged out in this study. Only the tilt angle θ and the twist angle ψ are considered for the rotation in orientation. Since the calculation of the hyperpolarizability β is a very time-consuming process, β is only calculated once at the given starting orientation of the protein structure, then β is rotated by $< R >$ to calculate χ_{Lab} at different protein orientations.

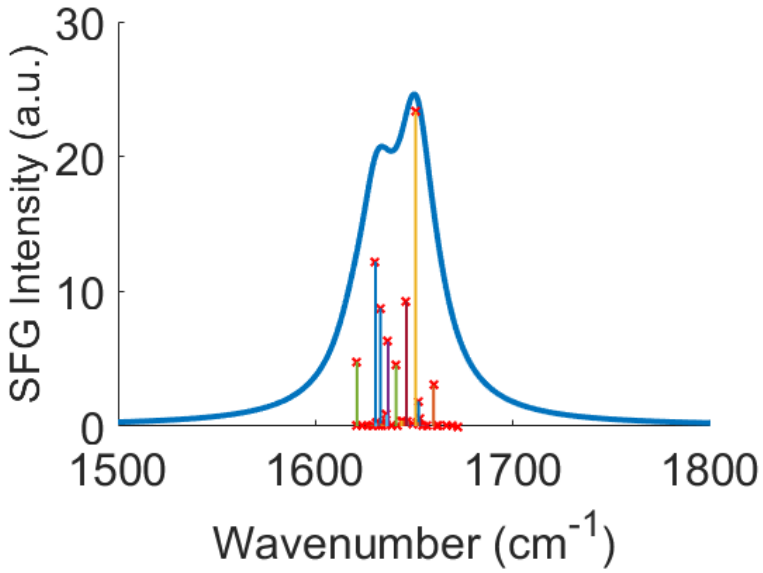


Figure 2.3 SFG amide I spectrum of a protein can be calculated based on the calculated frequencies and χ_{Lab} values of all the amide I normal modes.

The frequencies and χ_{Lab} values of all the amide I normal modes (plotted as lines in Figure 3.3) can be used to calculate the SFG spectra in the lab frame. Each normal mode is expanded by the Lorentzian function:

$$S_N(\omega) = \frac{\chi_{Lab,N}}{\omega - \omega_N + i\Gamma}$$

where $\chi_{Lab,N}$ is the calculated second order nonlinear susceptibility of N-th normal mode in the lab frame, ω is the frequency, ω_N is the calculated frequency of N-th normal mode, and Γ is the

width (or damping term) of the Lorentzian peak. By summing up the expanded Lorentzian peak across all the normal modes:

$$S_{Total}(\omega) = \sum_{N} S_N(\omega)$$

and calculating the product of $S_{Total}(\omega)$ with its complex conjugate, the SFG spectrum of the given input protein structure at a given orientation can be obtained, as shown in the Figure 2.3 (blue curve).

2.3 Matching Experimental Data with Calculated Spectra

In this thesis, the SFG spectra were calculated from a protein structure (either a crystal structure or a MD simulated structure) with the protein orientation of tilt angles ranging from 0 to 180 degrees and the twist angles ranging from 0 to 360 degrees. The calculated SFG spectra were then matched with the reconstructed SFG spectra obtained from the fitting results of the experimental data. It is necessary to use the reconstructed SFG experimental data instead of the original data because the SFG original data contains a non-resonant background. The SFG nonresonant background signal cannot be calculated with the Hamiltonian analysis method. The experimental SFG spectra were fitted with the Lorentzian function,[15] and the fitting parameters can be used to reconstruct the resonant signals by excluding the non-resonant term.

In this thesis study, the SFG spectra were collected using the ssp and ppp polarization combinations. The measured effective second-order nonlinear susceptibilities $\chi^{(2)}_{eff,ppp}$ and $\chi^{(2)}_{eff,ppp}$ can be converted to the χ components defined in the lab frame by Fresnel coefficients:

$$\chi^{(2)}_{eff,ssp} = F_{ssp,yyz}\,\chi_{yyz}$$

$$\chi^{(2)}_{eff,ppp} = F_{ppp,xxz}\,\chi_{xxz} + F_{ppp,xzz}\,\chi_{xzx} + F_{ppp,zxx}\,\chi_{zxx} + F_{ppp,zzz}\,\chi_{zzz}$$

In our SFG experiments, SFG spectra were collected using a prism geometry which will be described in more detail below in Chapter 3. The Fresnel coefficients for the this SFG sample geometry showed that the $F_{ppp,zzz}$ term is much larger than $F_{ppp,xxz}$, $F_{ppp,xzx}$, and $F_{ppp,zxx}$, therefore only the $F_{ppp,zzz}\,\chi_{zzz}$ term needs to be considered as shown below.[16]

$$\chi^{(2)}_{eff,ppp} \approx F_{ppp,zzz}\,\chi_{zzz}$$

Then the reconstructed SFG ssp and SFG ppp spectra can be converted to reconstructed experimentally collected SFG yyz and SFG zzz spectra, respectively. The experimental SFG yyz and SFG zzz spectra can then be compared with the calculated SFG yyz and SFG zzz spectra from the Hamiltonian method.

For spectral matching (or comparison), the reconstructed experimental and calculated spectra were normalized to [0,1]. We then calculated the sum of the square of the difference between the normalized calculated and reconstructed experimental spectra at each wavenumber. We can show this process using the following equation:

$$SE_1 = \sum_{\omega} \left(Y_{\omega,cal} - Y_{\omega,exp}\right)^2$$

where $Y_{\omega,cal}$ and $Y_{\omega,exp}$ are the SFG signal intensity at wavenumber ω of normalized calculated and reconstructed SFG spectra, respectively. This SE value describes the matching quality of the spectral feature between the calculated and experimental spectra. We repeated this matching process for the protein with all the orientations for both the yyz and zzz spectra and calculated the sum of the square differences (SE) for each protein orientation.

We can generate two matching score heat maps with the summed square differences plotted against the protein orientation angles – one for the yyz spectral matching result and the other for

the zzz spectral matching result. These two heat maps match the spectral features between the calculated spectra and the experimental data. Next, we calculated the square of the difference of the yyz and zzz intensity ratio at 1645 cm^{-1} between the calculated spectra and the reconstructed experimental data to generate the third matching score heat map, which considers the yyz/zzz spectral intensity ratio.

$$SE_2 = \left(\left| \frac{Y_{1645,cal,yyz}}{Y_{1645,cal,zzz}} \right| - \left| \frac{Y_{1645,exp,yyz}}{Y_{1645,exp,zzz}} \right| \right)^2$$

By combining the above three matching score heat maps, we created an overall heat map $F(\theta, \Psi)$ by summing the three maps and taking the reciprocal for each score in the map.

$$SE_{Total}(\theta, \Psi) = SE_{1,ssp}(\theta, \Psi) + SE_{1,ppp}(\theta, \Psi) + SE_2(\theta, \Psi)$$

$$F(\theta, \Psi) = \frac{1}{SE_{Total}(\theta, \Psi)}$$

In the above final heat map, the highest score indicates that at that orientation, the calculated spectra and the experimental data have the best overall matching quality. Therefore, we can locate the most probable orientations of the protein (with the best matching) by identifying the highest matching score in the final matching score heat map. A summary flow chart of this calculation and matching process is shown in Figure 2.4.

2.4 Applications of the Hamiltonian Analysis Method

This newly developed Hamiltonian method has been successfully used for deducing the interfacial proteins at the buried solid/liquid interface. Wen et al. applied this method to investigate the surface-immobilized super uranyl binding protein (SUP).[17] The orientations of SUP on SAM surface before and after the uranyl ion binding were deduced, and SUP tends to lie down on SAM surface in both cases due to the strong hydrophobic interaction.

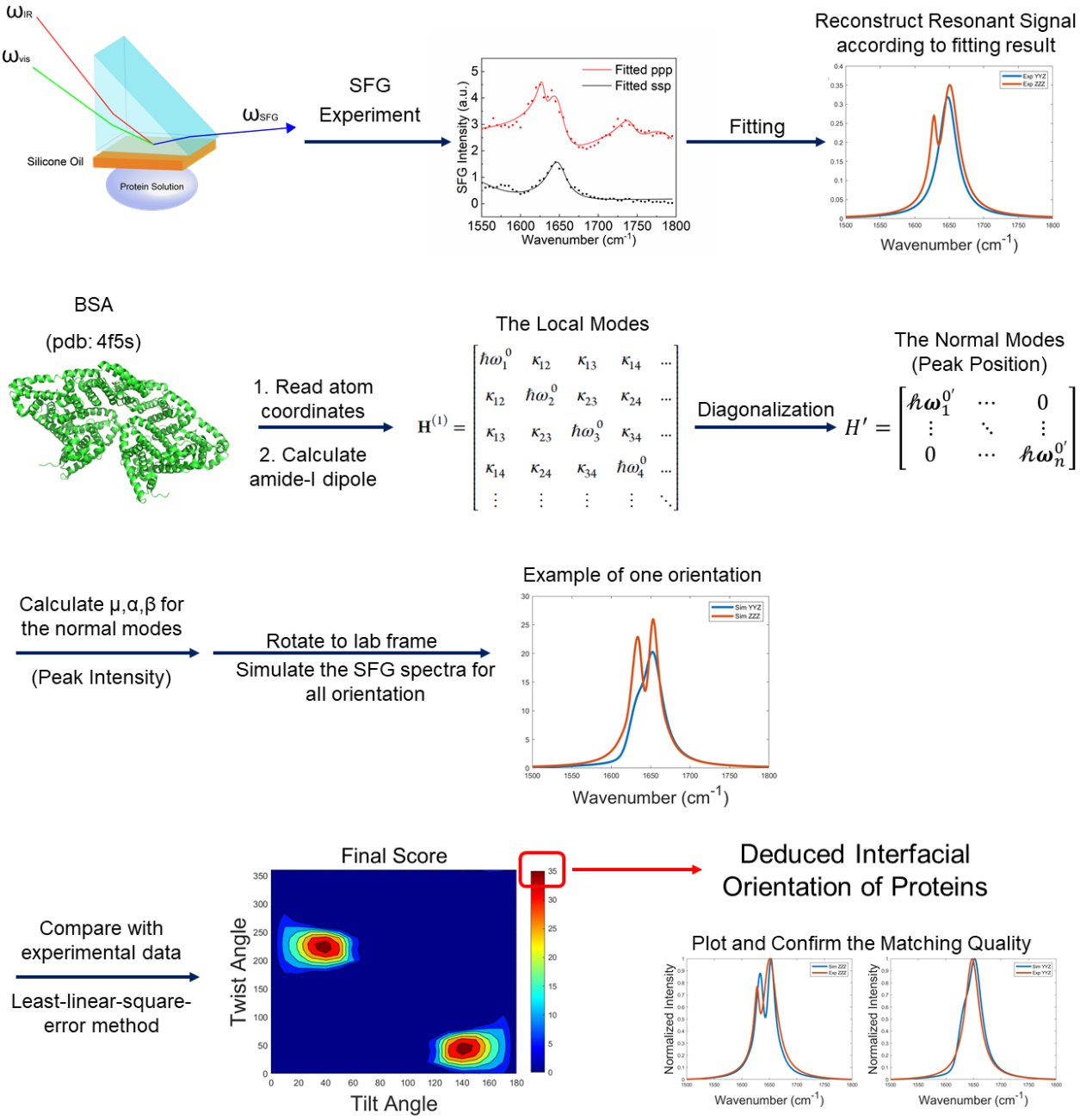


Figure 2.4 Flow chart showing the Hamiltonian data analysis method used to deduce protein orientation from experimentally collected SFG spectra. μ, α, and β are the IR transition dipole, Raman polarizability and SFG hyperpolarizability respectively.

Because the Hamiltonian method requires a protein structure file as the input, the quality of the input structure greatly impacts the final matching quality between the simulated and the experimental spectra. When different possible conformations of the protein are used as input

structures form Hamiltonian analysis, different highest matching scores in the final overall heat maps generated from different protein conformations can be observed. Thus, the Hamiltonian method can elucidate the orientation of proteins and provide insight into the most likely conformation(s) of the protein. By comparing the highest matching scores in the final overall heat maps calculated from different protein conformations, we can determine which protein structure can better represent the interfacial conformation of proteins.

In the next few chapters in this thesis, the application of the Hamiltonian analysis method will be presented to study interfacial structures of a variety of peptides/proteins including BSA, fibrinogen, antibody drugs, and barnacle peptides.

2.5 References

1. Laaser, J. E.; Skoff, D. R.; Ho, J.-J.; Joo, Y.; Serrano, A. L.; Steinkruger, J. D.; Gopalan, P.; Gellman, S. H.; Zanni, M. T., Two-dimensional sum-frequency generation reveals structure and dynamics of a surface-bound peptide. *Journal of the American Chemical Society* **2014,** *136* (3), 956-962.

2. Ho, J.-J.; Ghosh, A.; Zhang, T. O.; Zanni, M. T., Heterogeneous amyloid β-sheet polymorphs identified on hydrogen bond promoting surfaces using 2D SFG spectroscopy. *The Journal of Physical Chemistry A* **2018,** *122* (5), 1270-1282.

3. Ho, J.-J.; Skoff, D. R.; Ghosh, A.; Zanni, M. T., Structural characterization of single-stranded DNA monolayers using two-dimensional sum frequency generation spectroscopy. *The Journal of Physical Chemistry B* **2015,** *119* (33), 10586-10596.

4. Ghosh, A.; Ho, J.-J.; Serrano, A. L.; Skoff, D. R.; Zhang, T.; Zanni, M. T., Two-dimensional sum-frequency generation (2D SFG) spectroscopy: summary of principles and its application to amyloid fiber monolayers. *Faraday discussions* **2015,** *177*, 493-505.

5. Hamm, P.; Zanni, M., *Concepts and methods of 2D infrared spectroscopy*. Cambridge University Press: 2011.

6. la Cour Jansen, T.; Dijkstra, A. G.; Watson, T. M.; Hirst, J. D.; Knoester, J., Modeling the amide I bands of small peptides. *The Journal of chemical physics* **2006,** *125* (4), 044312.

7. Ham, S.; Kim, J.-H.; Lee, H.; Cho, M., Correlation between electronic and molecular structure distortions and vibrational properties. II. Amide I modes of NMA–n D 2 O complexes. *The Journal of chemical physics* **2003,** *118* (8), 3491-3498.

8. Lee, C.; Cho, M., Local amide I mode frequencies and coupling constants in multiple-stranded antiparallel β-sheet polypeptides. *The Journal of Physical Chemistry B* **2004,** *108* (52), 20397-20407.

9. Lu, H.; Schäfer, A.; Lutz, H.; Roeters, S. J.; Lieberwirth, I.; Muñoz-Espí, R.; Hood, M. A.; Bonn, M.; Weidner, T., Peptide-controlled assembly of macroscopic calcium oxalate nanosheets. *The journal of physical chemistry letters* **2019,** *10* (9), 2170-2174.

10. Torii, H.; Tasumi, M., Model calculations on the amide‐I infrared bands of globular proteins. *The Journal of chemical physics* **1992,** *96* (5), 3379-3387.

11. Krimm, S.; Bandekar, J., Vibrational spectroscopy and conformation of peptides, polypeptides, and proteins. *Advances in protein chemistry* **1986,** *38*, 181-364.

12. Nguyen, K. T.; Le Clair, S. V.; Ye, S.; Chen, Z., Orientation determination of protein helical secondary structures using linear and nonlinear vibrational spectroscopy. *The Journal of Physical Chemistry B* **2009,** *113* (36), 12169-12180.

13. Laaser, J. E.; Zanni, M. T., Extracting structural information from the polarization dependence of one-and two-dimensional sum frequency generation spectra. *The Journal of Physical Chemistry A* **2013,** *117* (29), 5875-5890.

14. Simpson, G. J., *Nonlinear optical polarization analysis in chemistry and biology*. Cambridge University Press: 2017.

15. Chen, Z.; Shen, Y.; Somorjai, G. A., Studies of polymer surfaces by sum frequency generation vibrational spectroscopy. *Annual review of physical chemistry* **2002,** *53* (1), 437-465.

16. Li, B.; Lu, X.; Han, X.; Wu, F.-G.; Myers, J. N.; Chen, Z., Interfacial Fresnel coefficients and molecular structures of model cell membranes: from a lipid monolayer to a lipid bilayer. *The Journal of Physical Chemistry C* **2014,** *118* (49), 28631-28639.

17. Guo, W.; Zou, X.; Jiang, H.; Koebke, K. J.; Hoarau, M.; Crisci, R.; Lu, T.; Wei, T.; Marsh, E. N. G.; Chen, Z., Molecular Structure of the Surface-Immobilized Super Uranyl Binding Protein. *The Journal of Physical Chemistry B* **2021,** *125* (28), 7706-7716.

Chapter 3 Probing Protein Aggregation at Buried Interfaces: Distinguishing Adsorbed Protein Monomer, Dimer, and Monomer-Dimer Mixture in Situ

Material covered in this chapter was published in *Chem. Sci.* 13, 975–984 (2022)

3.1 Introduction

As discussed in chapter 1, protein molecular behavior on surfaces or at interfaces determines protein property and function, which greatly impacts many applications and research fields, especially for those involving interfacial proteins such as biosensors, anti-fouling coatings, biomedical implants, membranes used for bio-separation, and protein antibody drugs.[1-11] In order to rationally design surfaces/interfaces to optimize interfacial protein properties and functions through controlling protein interfacial behavior, it is important to develop powerful tools to investigate molecular structure and molecular behavior of proteins at various interfaces. Many analytical techniques have been developed for characterizing protein structures and behavior, such as X-ray diffraction, nuclear magnetic resonance (NMR), attenuated total reflection – FTIR (ATR-FTIR), cryo-electron microscopy (cryo-EM), quartz crystal microbalance (QCM), etc., leading to important knowledge about protein molecules.[12-14] However, such techniques have some disadvantages in investigating protein molecules at buried solid/liquid or liquid/liquid interfaces in situ in real time. They either lack surface/interface sensitivity or require high vacuum to operate and are thus unable to be used for in situ study, or cannot provide detailed structural information at the molecular level.

As discussed in the previous two chapters, sum frequency generation vibrational spectroscopy (SFG) is a unique and powerful second-order nonlinear vibrational spectroscopic tool,[15-36] which can detect the amide I signals from interfacial protein molecules, providing molecular level information regarding protein structure.[18-19, 31, 37-38] According to the selection rule of a second-order nonlinear optical process, SFG is a highly surface/interface-sensitive method with a sub-monolayer specificity.[15-39] It allows to probe protein behavior at buried solid/liquid and liquid/liquid interfaces in situ directly.[18-19, 31, 39-40] SFG can monitor interfacial adsorption of proteins in real time and probe detailed structural information of interfacial proteins (such as protein orientation).[18-19, 31, 37-41] In the previous studies from our group, we have reported the successful detection and orientation analysis of many proteins at different interfaces, including cell membrane associated proteins,[42] surface chemically immobilized enzymes,[43] and physically adsorbed proteins.[37, 40]

In recent years, antibody drugs have been developed into important cures for many diseases, including cancers, autoimmune diseases, and chronic inflammatory diseases.[44] Since generally an antibody only binds to a corresponding antigen, antibody drugs are highly efficient and selective, which makes the antibody treatment a powerful method to treat tumors and other diseases that require targeted agents. More and more antibody drugs have become commercially available. During the antibody drug storage and administration, these protein drug molecules have opportunities to contact various surfaces. Silicone oil is commonly used as lubricant in pharmaceutical industry, such as the coating material for the wall of a syringe for protein antibody drug storage and injection. It has been shown that silicone oil can induce protein adsorption and possible aggregation, and thus potentially reduce the efficacy of protein drugs.[45-47] It is thus important to study protein behavior on silicone oil surface in situ at the molecular level, which has

been rarely reported due to the lack of appropriate methods which can be used to study interfacial proteins at the silicone oil/solution interface in situ at the molecular level.

In this study, we applied SFG to study interfacial protein behavior at the silicone oil/protein solution interface in situ in real time at the molecular level, using bovine serum albumin (BSA) as a model. BSA has been widely used as a model protein for studying protein adsorption and interfacial protein behavior in various systems.[48-51] It has also been widely used as passivation coating for different surfaces.[52] Despite the large number of publications reporting the BSA interfacial adsorption, in situ studies on the detailed BSA interfacial structure at the molecular level are still rare. Previous research has shown that adsorbed BSA can adopt dimer form – For example, it was reported that BSA molecules can form dimers in aged solutions through di-sulfide bonds, which causes protein aggregation and fouling on membranes.[53] In these studies, HPLC was frequently used to study the BSA dimer formation, but such an experimental approach cannot be used to probe adsorbed protein molecules on surface in situ to elucidate the protein interfacial behavior directly at the molecular level.[54-56]

Here SFG spectra were directly collected from the adsorbed BSA at the silicone oil/protein solution interface. These SFG spectra were analyzed with the Hamiltonian local mode approximation method which was presented in detail in the chapter 2 above.[57-60] As we mentioned in chapter 2, we have shown in our previous publication that such Hamiltonian data analysis approach can be used along with SFG results to deduce interfacial protein orientation and conformation.[60] Here in this research, using the Hamiltonian method, we can calculate SFG spectra of adsorbed BSA as a function of orientation. The calculated BSA orientation dependent SFG spectra from BSA monomer and dimer are markedly different. The comparison between the measured SFG spectra and calculated SFG spectra leads to the identification of BSA monomer or

dimer at interface and the determination of adsorbed BSA monomer or dimer orientation. We also showed that this method can be used to study BSA monomer-dimer mixture at the buried silicone oil/protein solution interface. Dimerization is a crucial initial step for protein aggregation.[61-63] Our research demonstrates that with the help of the Hamiltonian data analysis method, SFG can be used to study protein aggregation in situ. Previously we used SFG to study adsorption behavior of fusion protein and antibody onto silicone oil surface, but no detailed structural information was reported.[64-65] The methodology developed in this study is generally applicable, which can be used to study aggregation of many different proteins including fusion and antibody protein drugs at interfaces. It is worth mentioning that protein aggregation plays significant roles in many biological and biomedical process.[66-70]

3.2 Experimental Details

3.2.1 Sum Frequency Generation (SFG) Vibrational Spectroscopy

Details of SFG instrumentation and SFG theories have been extensively published[15-43, 71-77] and discussed in Chapter 1. SFG experiments were conducted using an EKSPLA PL 2250 SFG system (Vilnius, Lithuanian). To generate a sum frequency signal, a 532 nm visible beam and a frequency tunable IR beam (wavelength ranges from 2.3 to 10 μm) were overlapped spatially and temporally on the sample surface/interface. The sample geometry used in this study to collect SFG spectra from the silicone oil/solution interface is shown in Figure 3.1. Time-dependent SFG signal was first collected by tracking the signal intensity of the characteristic peak from α-helices in BSA after the silicone oil surface was placed in contact with the BSA solution (with a 1 s time step). After the adsorption reached an equilibrium (evidenced by a constant SFG signal intensity), static SFG spectra were collected in ssp (s-polarized SFG signal, s-polarized visible beam, and p-polarized input IR

beam) and ppp polarization combinations. All the SFG spectra presented here are averaged by three scans. The resolution of the SFG spectrometer is about 5 cm^{-1}.

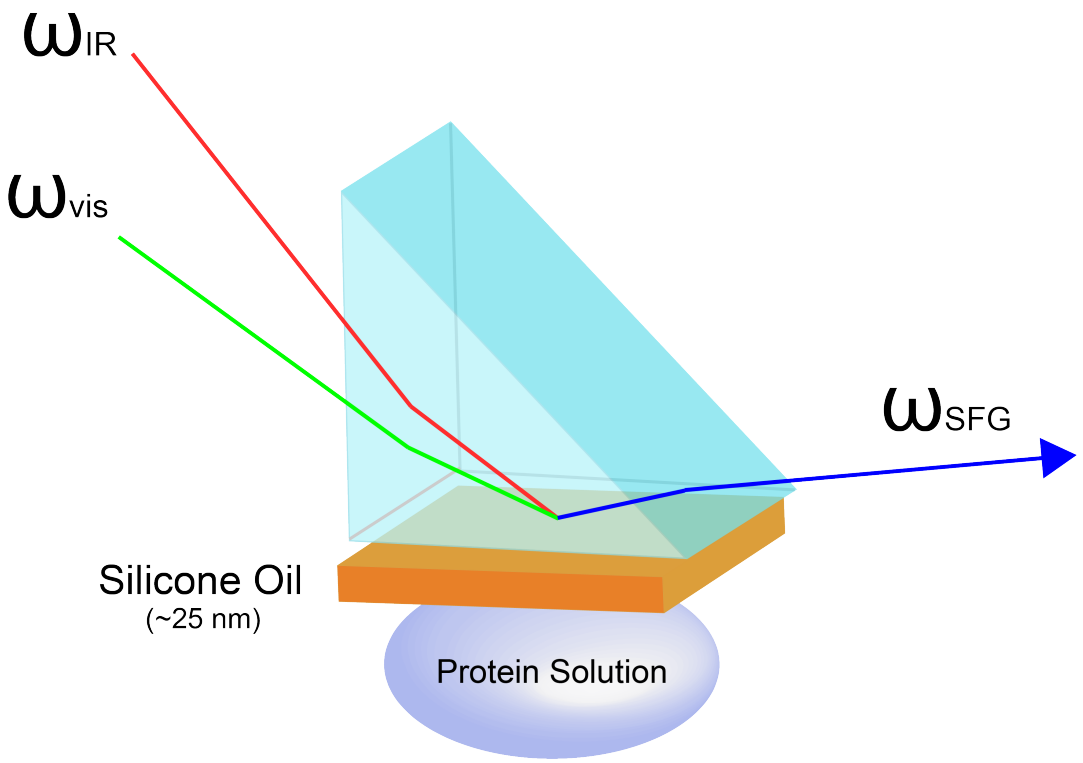


Figure 3.1 Schematic of the SFG sample geometry used in this experiment.

3.2.2 Samples and materials

BSA and dithiothreitol (DTT) samples were purchased from Sigma-Aldrich (St. Louis, MO). The BSA solution concentration used in this study is 0.1 mg/ml in deionized water. DTT solution with a concentration of 50 mM was prepared by dissolving DTT in deionized water. Medical-grade silicone oil (360 Medical Fluid 1000 Cst) was purchased from Dow Corning (Midland, MI). CaF_2 prisms used for SFG study were bought from Altos Photonics (Bozeman, MT).

3.2.3 Silica-coated CaF_2 prisms

Silica coated CaF_2 prisms were used as substrates to prepare silicone oil films. For cleaning, CaF_2 prisms were soaked in toluene for 24 h, immersed in acetone and methanol each for 10 mins, rinsed thoroughly by deionized water (18 MΩ·cm), and dried with nitrogen gas flow. Then the prisms were treated by oxygen and argon plasma (Glen 1000P Plasma Cleaner) to remove (if any) residue organic contaminants. Next, the cleaned prisms were transferred into the chamber of Angstrom Engineering Evovac Evaporator to deposit a 100 nm of SiO_2 film on each CaF_2 prism via physical vapor deposition.

3.2.4 Preparation of Silicone Oil Thin Film

Silicone oil thin film was prepared by spin-coating silicone oil onto silica-coated CaF_2 prism with the published method.[65] Silicone oil was dissolved in toluene to make a concentration of 0.5 wt% solution. The silicone oil solution was dropped on the prism surface and spin-coated at 2000 rpm for 30 s. The silicone oil coated prism was dried in air. The silicone oil thickness was measured by using ellipsometry (EP3 Nanofilm, Germany) to be about 25 nm.

3.2.5 Circular Dichroism

The secondary structure of adsorbed BSA on silicone oil was studied by using circular dichroism (CD) spectra collected with a J-1500 CD spectrometer (Jasco Inc., Japan). For CD studies, a silicone oil film was prepared on a quartz slide by the same spin-coating procedure used to prepare silicone oil film on prism for SFG studies presented above. To prepare adsorbed BSA on silicone oil samples for CD study, the BSA solution was dropped on the silicone oil surface on quartz slides and then washed by deionized water for 30 mins to remove loosely adsorbed BSA. Seven quartz slides with silicone oil film and with adsorbed BSA were stacked for taking CD spectra to improve signal/noise ratio. After the CD data collection was complete, the 50 mM DTT

solution was dropped on the silicone oil surface and CD spectra of adsorbed BSA after DTT treatment were collected. Each CD spectrum was collected from 190 to 240 nm with 1-nm step. The scan rate was set at 50 nm/min and each presented CD spectrum was obtained by averaging 10 scans.

3.2.6 Native-PAGE Experiments

The native PAGE experiment was performed using a 4-20% Mini-PROTEAN TGX polyacrylamide gel (Bio-Rad). 10 μL of samples were mixed with 20 μL Native sample buffer (Bio-Rad) and 10 μL of this was loaded onto gels. Electrophoresis was performed at 30 V and 4 ℃ for 14 hrs in Tris/Glycine buffer (Bio-Rad). The gel was stained using InstantBlue Commassie Protein Stain (Novus Biologicals) and visualized via ChemiDoc Touch Imager (Bio-Rad). Protein bands were quantified using Image Lab (Bio-Rad).

3.3 Results and Discussions

3.3.1 SFG Experiment Result

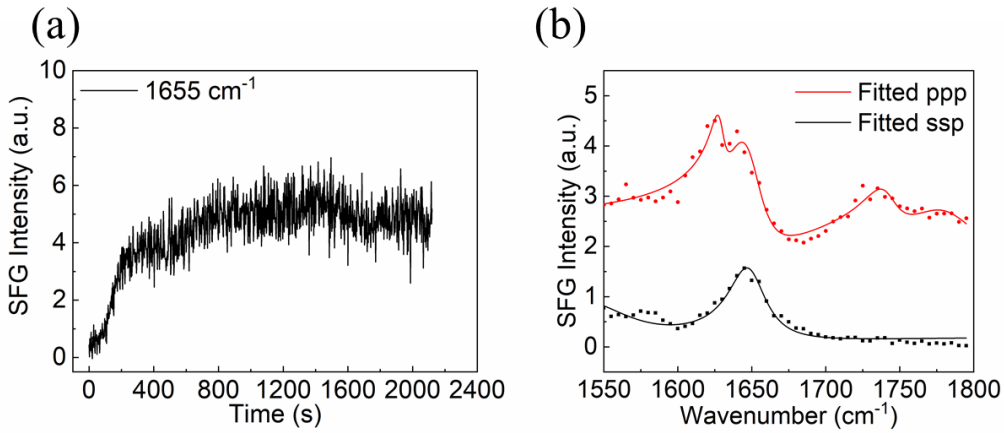


Figure 3.2 (a) Time-dependent SFG ssp signal intensity observed at ~1650 cm^{-1} during the BSA adsorption process onto silicone oil (b) SFG ssp and ppp spectra of adsorbed BSA collected from the silicone oil/BSA solution interface. The spectra are offset. Dots are experimental data and the lines are fitted spectra.

No SFG signal could be detected between 1500 and 1800 cm^{-1} from silicone oil in air and in water. After the BSA solution was placed in contact with silicone oil, SFG signal intensity at ~1650 cm^{-1} increased at the silicone oil/BSA solution interface (Figure 3.2a), showing that BSA molecules adsorbed onto the silicone oil surface. The SFG signal intensity increased very fast in the first several minutes, then slowly increased and more or less reached a plateau after 20 minutes (Figure 3.2a), indicating the BSA adsorption reached equilibrium. SFG ssp and ppp spectra were then collected from the silicone oil/BSA solution interface (Figure 3.2b). The amide I signals from adsorbed BSA on silicone oil can be clearly seen. The peak at around 1645 cm^{-1} in both ssp and ppp spectra is contributed from the alpha-helical structure in BSA. We also noticed that there is a second peak at 1627 cm^{-1} in the ppp spectrum. More details regarding this assignment will be discussed later.

Since the collected SFG spectra contain a non-resonant contribution, we cannot compare the experimental data to the calculated spectra using the Hamiltonian method directly. It is necessary to extract the resonant spectral contribution from the experimental data. We fitted the SFG spectra using the standard SFG spectral fitting method.[77] With the fitted parameters listed in Table 3.1, we reconstructed the resonant yyz and zzz SFG spectra using the fitted parameters (Figure 3.3a and 3.3b, red spectra), which were used to compare to the calculated spectra.

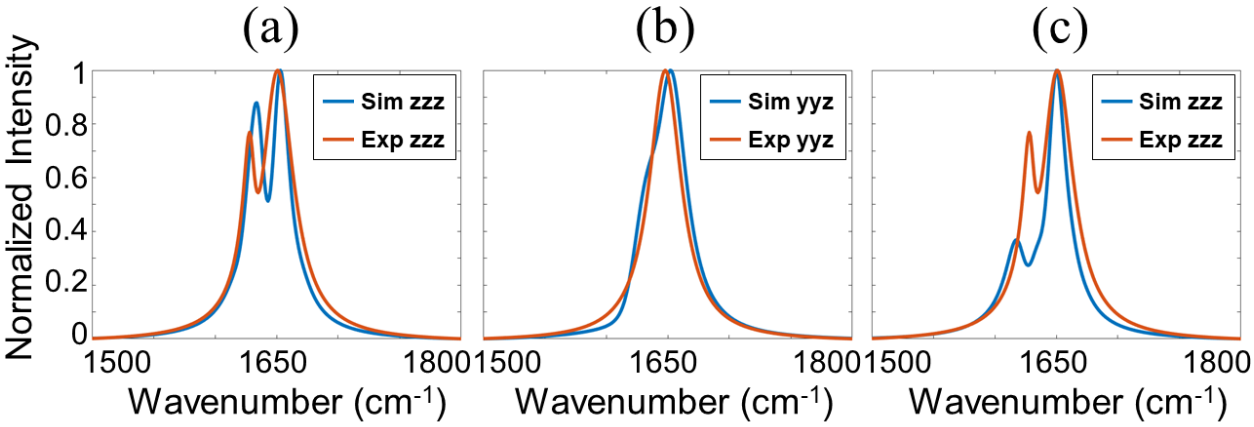


Figure 3.3 Comparison between simulated and experimental SFG spectra. (a) Red: reconstructed resonant SFG zzz spectrum from the experiment data. Blue: Calculated zzz SFG spectrum based on BSA dimer. (b) Red: reconstructed resonant SFG yyz spectrum from the experiment data. Blue: Calculated yyz SFG spectrum based on BSA dimer. (c) Red: reconstructed resonant SFG zzz spectrum from the experiment data. Blue: Calculated zzz SFG spectrum based on BSA monomer. The ssp and ppp spectra can be converted to yyz and zzz spectra after considering the Fresnel coefficients.

	ssp	ppp
Offset	0.16	-0.07
NR	-0.378	-0.643
A1	16.7	2.26
x01	1648	1629
w1	15.8	5.4
A2	0.454	16.5
x02	2195	1650
w2	50.0	15.7
A3	31.5	21.2
x03	1546	1786
w3	50.0	30.7
A4	0.520	6.43
x04	1501	1742
w4	0.323	14.0

Table 3.1 Fitting parameters of the SFG spectra of BSA on silicone oil shown in Figure 3.2(b).

3.3.2 Hamiltonian Data Analysis and Protein Orientation Determination Method

We applied the Hamiltonian data analysis method to calculate SFG polarized (e.g., yyz and zzz) spectra of BSA as a function of BSA orientation. A schematic to show the Hamiltonian method and the calculation details were included in the Chapter 2. For BSA with a certain

orientation, the Hamiltonian method started with a data matrix with diagonal elements as the peak centers of the uncoupled amide I signal of each amino acid (e.g., 1645 cm^{-1}) and off-diagonal elements with couplings between each pair of the amino acids. In this study, we applied the Hamiltonian method to calculate BSA orientation dependent SFG yyz and zzz spectra using the crystal structure of BSA dimer (PDB:4f5s) or monomer (chain A in PDB:4f5s) as the input structure file. SFG spectra of BSA were calculated with the tilt angle range from 0 to 180 degree, and the twist angle range from 0 to 360 degree. The calculation angle step size for tilt or twist angle is 10 degrees. The orientations (0, 0 - with both tilt and twist angles of zero) for BSA dimer and monomer are defined by using the BSA dimer and monomer orientations shown in the PDB (PDB:4f5s and chain A in 4f5s). Such reference orientations are shown in Figure 3.4.

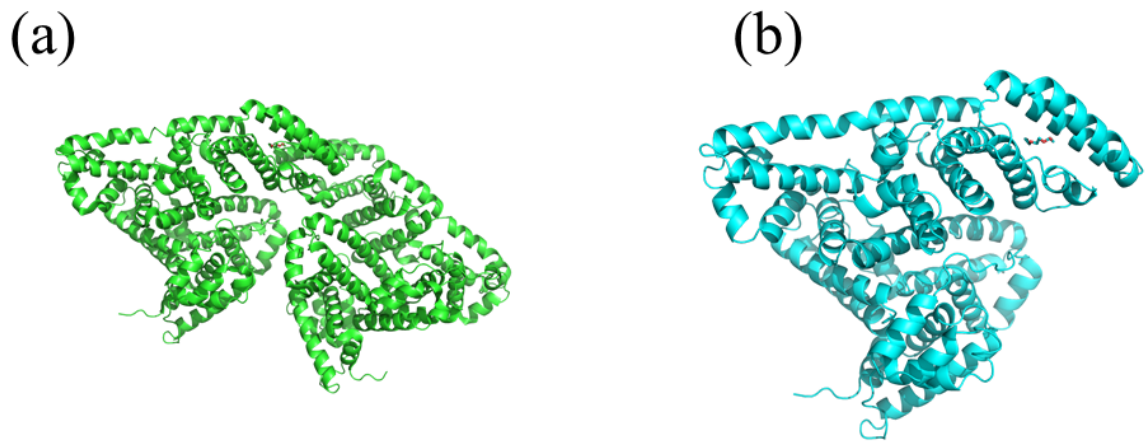


Figure 3.4 Reference orientations (Tilt=0, Twist=0) of (a) BSA dimer and (b) BSA monomer.

The calculated orientation dependent SFG spectra were then compared to the SFG resonant spectra extracted from the experimental data after deconvoluting the non-resonant contribution. The best matching between the calculated and fitted spectra provides the most likely protein orientation. The matching process has been presented in detail in Chapter 2 and will not be repeated here. After the matching process, the most likely protein orientation can be identified from the

final matching score heat map. The most likely BSA orientation can be determined by an overall heat map which combines the heat maps for yyz spectrum, zzz spectrum, and yyz/zzz signal strength ratio.

3.3.3 Orientation and Structure Analysis by Hamiltonian Method

Before we present the detailed SFG data analysis results of BSA on silicone oil, we want to mention that BSA – silicone oil interaction can be complicated, leading to the existence of BSA monomers as well as oligomers (e.g., dimers, trimers, tetramers, etc.) at the silicone oil interface. In the bulk environment, it has been shown that BSA dimer is the most probable oligomer form,[78] which is also shown by our PAGE experiments (see Section 3.3.6). Here we hypothesize that the dominating BSA forms on silicone oil are monomer and/or dimer forms. Our data analysis shown below demonstrates that the calculated SFG spectra based on the structures of BSA monomer and/or BSA dimer could well match the experimental data, showing that the above hypothesis is valid. Certainly we could not completely rule out the formation of other oligomers, which will not be considered in this research.

We calculated SFG yyz and zzz spectra of BSA as a function of BSA orientation using the Hamiltonian method based on BSA monomer crystal structure and BSA dimer crystal structure. The calculated SFG spectra were compared to the reconstructed resonant SFG spectra from the experimental data using the method presented in the method section above to create heat maps. Figure. 3.5a and 3.5b display the final score heat maps generated from BSA monomer and dimer respectively. Clearly the highest matching scores in the heat map generated based on the BSA dimer are much higher compared to those in the heat map generated based on the BSA monomer, indicating that adsorbed BSA does not have monomer as the dominating form, which is different from the bulk solution case (see native-PAGE results in Section 3.3.6). Based on our hypothesis

stated above, likely BSA mainly adopts the dimer form on the silicone oil surface. Figure 3.5b shows that the BSA dimer orientation with a tilt angle of 40° and a twist angle of 220° has the highest matching score, which is the most likely orientation of BSA dimer on silicone oil. This orientation is plotted in Figure 3.5c. The calculated SFG yyz and zzz spectra from the most likely BSA dimer orientation (tilt angle of 40° and twist angle of 220°) are plotted in Figure 3.3a and 3.3b, which are very similar to the reconstructed resonant SFG yyz and zzz spectra from the experimental data. For comparison, the SFG zzz spectrum calculated from the most likely orientation in the heat map deduced based on BSA monomer is plotted in Figure 3.3c, which is more different from the experimentally generated resonant zzz spectrum compared to that based on the BSA dimer (Figure 3.3a).

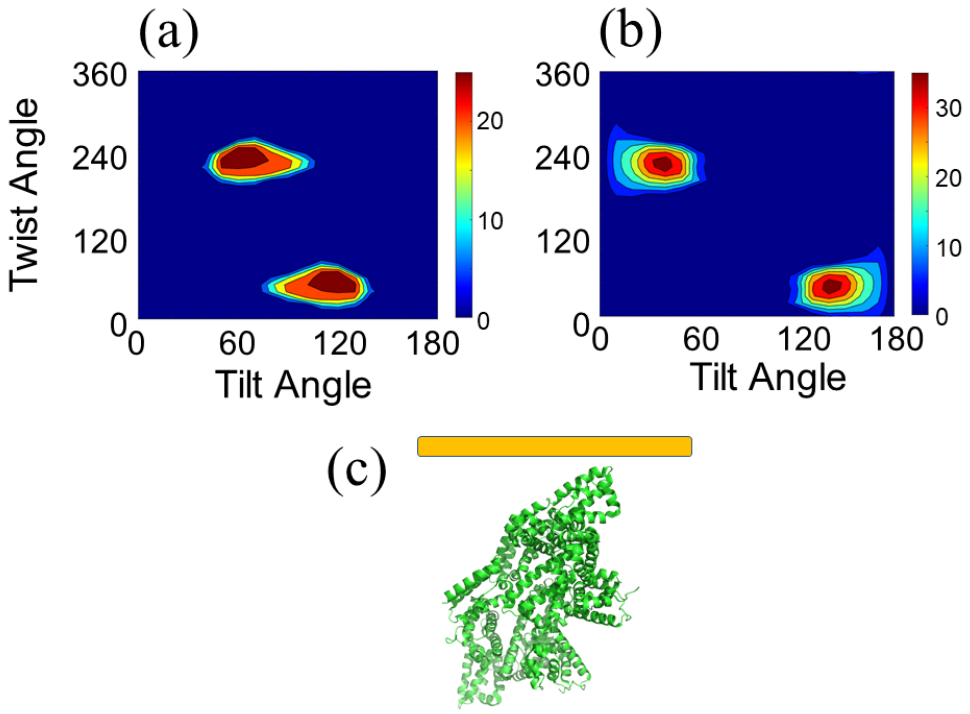


Figure 3.5 (a) Heat map showing the matching quality between the reconstructed resonant SFG spectra and calculated orientation dependent SFG spectra based on BSA monomer. (b) Heat map showing the matching quality between the reconstructed resonant SFG spectra and calculated orientation dependent SFG spectra based on BSA dimer. (c) Most likely orientation of BSA dimer on silicone oil. Each heat map shows two most likely orientations, with different absolute orientations (up and down). Since BSA dimer has two identical monomers, it is not necessary to differentiate the two orientations.

A BSA dimer can be formed by the di-sulfide bond between two monomers,[79] and DTT can be used to reduce the di-sulfide bond and turn a dimer into two monomers.[53, 80] It is worth mentioning again that various oligomers may form at silicone oil interface. According to the hypothesis we proposed, here we will only consider BSA monomers and dimers. To further test our SFG and Hamiltonian spectral analysis approach to study BSA dimer/monomer, we exposed adsorbed BSA molecules on silicone oil to DTT. Specifically, after the above SFG experiments on adsorbed BSA on silicone oil, we replaced BSA solution in contact with silicone oil with water and replaced the water with fresh water for additional two times to remove BSA solution left on the silicone oil surface. We then contacted the silicone oil (with adsorbed BSA) to a 50 mM DTT solution and SFG ppp and ssp spectra were collected from the silicone oil/DTT solution interface, as shown in Figure 3.6a and 3.6b (red spectra).

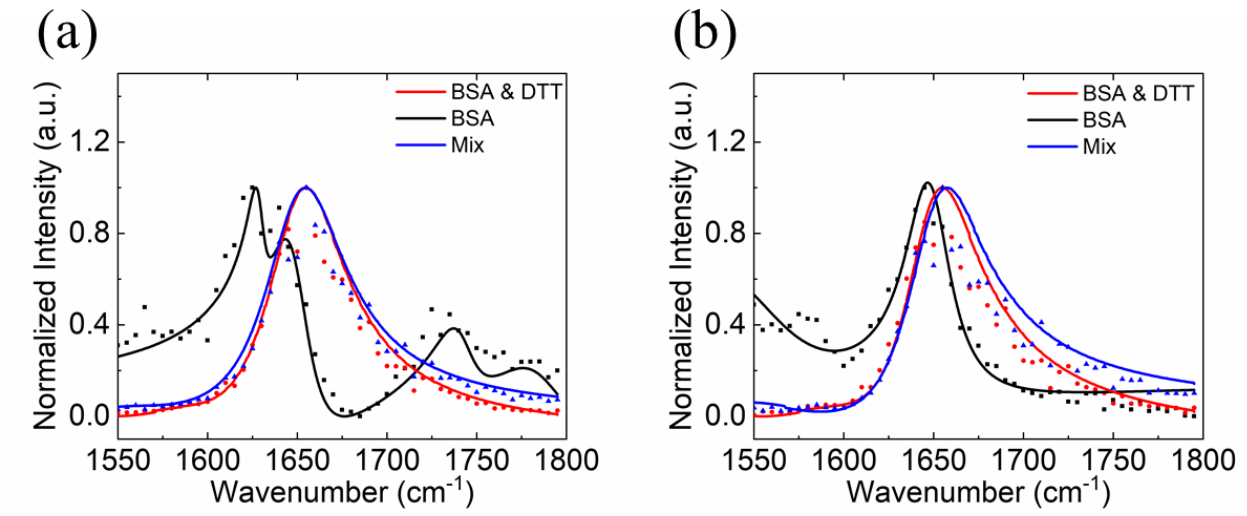


Figure 3.6 SFG ppp (a) and ssp (b) spectra of BSA with DTT treatment. The SFG spectra collected from BSA before the DTT treatment, BSA after the DTT treatment, and BSA pre-mixed with the DTT are displayed in black, red, and blue color, respectively.

We also conducted a separate SFG experiment using BSA-DTT mixture solution. BSA and DTT solutions were mixed to reach a concentration of 0.1 mg/ml of BSA and 50 mM of DTT. A prism with silicone oil film was then placed in contact with the BSA-DTT mixture and SFG ppp

and ssp spectra were collected from the silicone oil/BSA-DTT mixture solution interface, as shown in in Figure 3.6a and 3.6b (blue spectra). For comparison purpose, SFG spectra collected from the original silicone oil/BSA solution interface are replotted in in Figure 3.6a and 3.6b (black spectra).

Figure 3.6 shows clearly that the SFG spectra collected from the adsorbed BSA on silicone oil treated by DTT solution and those collected from the silicone oil/BSA-DTT mixture solution interface are quite similar, but are very different from the original SFG spectra collected from the silicone oil/BSA solution interface (without DTT treatment). This demonstrated that DTT can change the BSA behavior on silicone oil surface. As we reported above, adsorbed BSA on silicone oil mainly adopts the dimer form. Since DTT can dissociate BSA dimer, the different SFG spectra before and after DTT treatment indicate at least some of the BSA dimers changed to monomers. The similar SFG spectra obtained from the silicone oil/pre-mixed BSA-DTT solution interface and the adsorbed BSA after the DTT treatment likely indicate that DTT has a similar effect on BSA in solution and adsorbed BSA at the interface.

	BSA / DTT		BSA-DTT Mix	
	ssp	Ppp	ssp	ppp
Offset	-0.48	-0.43	-0.043	-0.099
NR	0.432	0.258	0.327	0.195
A1	41.4	57.2	31.7	40.2
x01	1643	1647	1646	1650
w1	25.5	27.1	26.9	27.9
A2	25.1	17.5	19.8	13.1
x02	1577	1577	1531	1552
w2	50.0	42.2	50.0	50.0
A3	34.5	26.8		
x03	1504	1511		
w3	50.0	50.0		

Table 3.2 Fitting parameters of the SFG spectra of BSA on silicone oil after the DTT treatment and the BSA-DTT mixture shown in Figure 3.6.

We fitted SFG spectra collected from adsorbed BSA treated by DTT to remove the non-resonant contribution. With the fitted parameters listed in Table 3.2, we reconstructed the resonant

SFG spectra. We then compared the spectra to the calculated SFG spectra using the Hamiltonian method based on the BSA monomer crystal structure to generate heat map (shown in Figure 3.7). However, we found that the heat map cannot provide a good matching for any of the BSA monomer orientations. Clearly not all the adsorbed BSA dimer molecules after the DTT treatment turned into the monomer form. Likely, some of the adsorbed BSA dimers dissociated into monomers because of DTT, while others stayed in the dimer form, leading to a mixture of BSA dimer and monomer on the silicone oil. This is reasonable since the DTT treatment was conducted at room temperature. The mild reaction condition cannot result in a 100% dissociation yield.

We then calculated SFG spectra using the Hamiltonian method based on a 60:40 mixture of the BSA dimer and monomer as a function of monomer orientation, assuming that the dimer remains the same orientation before and after the DTT treatment. The calculated SFG spectra were compared to the reconstructed SFG spectra from experimental data to generate a heat map (shown in Figure 3.8). It was found that the matching quality in the heat map for certain monomer orientation can be very high. Figure 3.8 shows the comparison between the calculated and reconstructed experimental spectra with the highest matching score, indicating that the spectra match with each other very well. This suggests that likely 25% of the BSA dimers adsorbed on silicone oil can be dissociated by DTT to turn to BSA monomers.

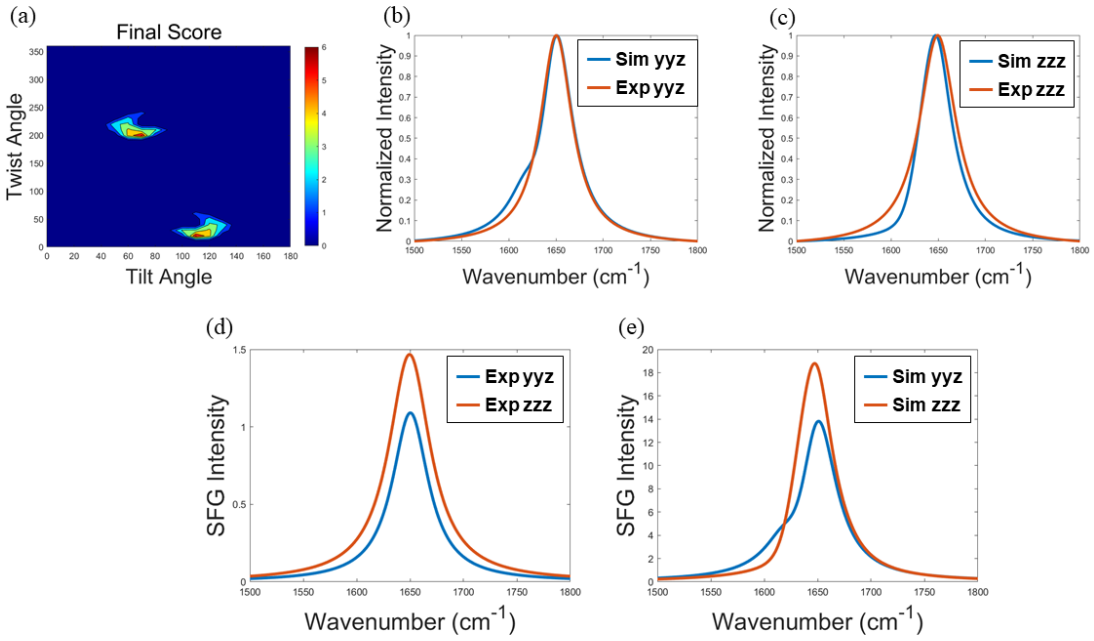


Figure 3.7 Matching qualities between the experimental data and calculated spectra based on BSA monomer structure for BSA after the DTT treatment: (a) Heat map showing the matching quality between the reconstructed resonant SFG spectra of BSA after the DTT treatment and calculated SFG spectra using the BSA monomer structure. The blue spectra in (b) and (c) show the calculated SFG yyz (b) and zzz (c) spectra of BSA after the DTT treatment with the best matching quality with the reconstructed resonant SFG spectra (shown in red). The matching qualities of the spectra are much worse than those shown in Figure 3.8 below based on BSA dimer-monomer mixture. The SFG spectra shown in (d) are replotted fitted experimentally collected SFG spectra. The spectra shown in (e) are calculated SFG yyz (blue) and zzz (red) spectra with the best matching quality. The matching qualities of the spectral features can be seen from (b) and (c), while the matching quality for the ssp and ppp intensity ratio can be seen from (d) and (e).

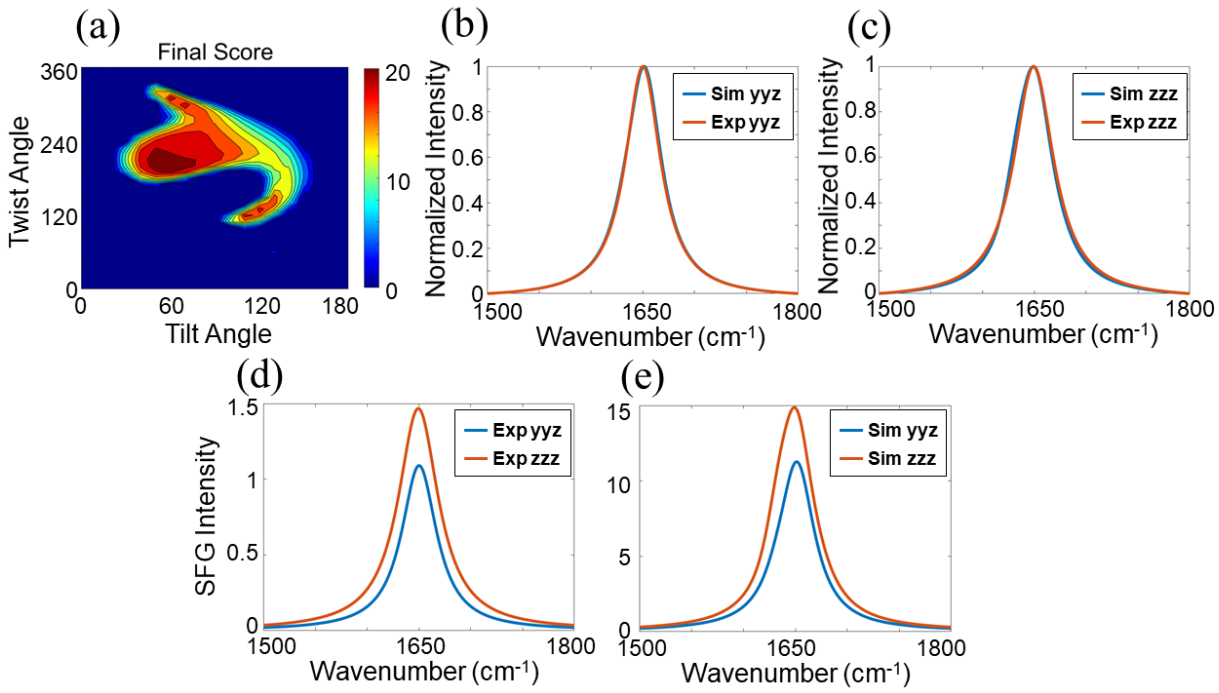


Figure 3.8 Matching qualities between the experimental data and calculated spectra based on BSA dimer-monomer mixture of a 60:40 ratio for BSA after the DTT treatment: (a) Heat map showing the matching quality between the reconstructed resonant SFG spectra of BSA after the DTT treatment and calculated SFG spectra using the BSA dimer-monomer mixture ratio of 60:40. The BSA dimer was assumed to have the same orientation as deduced previously while the orientation angles are the BSA monomer orientations. The blue spectra in (b) and (c) show the calculated SFG yyz (b) and zzz (c) spectra of BSA after the DTT treatment with the best matching quality with the reconstructed resonant SFG spectra (shown in red). The SFG spectra shown in (d) are replotted fitted experimentally collected SFG spectra. The spectra shown in (e) are calculated SFG yyz (blue) and zzz (red) spectra with the best matching quality. The matching qualities of the spectral features can be seen from (b) and (c), while the matching quality for the ssp and ppp intensity ratio can be seen from (d) and (e).

Figure 3.9 shows the schematic of some adsorbed BSA dimers on silicone oil dissociated into BSA monomers. The orientations of the BSA dimers and BSA monomers displayed in Figure 3.9 are the orientations with the best matching scores in the heat maps shown in Figure 2.5 b for BSA dimer and Figure 3.8a for BSA monomer. Both BSA dimer and monomer are tilting on the silicone oil surface, with similar orientations. The adsorption regions or contact areas for BSA dimer and monomer on the silicone oil surface are also similar. The DTT molecules can cleave an adsorbed BSA dimer into two monomers, but do not change the adsorbed BSA orientation on silicone oil. In addition to the 60:40 mixture, we also compared the calculated SFG spectra with the fitted experimental spectra for other BSA dimer-monomer mixture ratios. To quantify which

BSA dimer-monomer mixture ratio can generate calculated SFG spectra with the best matching quality with the experimental data, we varied the dimer-monomer mixture ratio from 1:9 to 9:1, calculated SFG spectra as a function of orientation, and matched the calculated spectra with the experimental data. Table 3.3 lists the difference square sum of the SFG spectra with best matching quality for each dimer-monomer ratio, showing that the calculated SFG spectra based on the BSA dimer-monomer ratio of 60:40 has the lowest value of the square difference (best matching quality) among all the ratios. This provides evidence that the silicone oil surface is likely covered by 60% BSA dimer and 40% monomer after the DTT treatment. The differences between the calculated and fitted experimental spectra of other mixtures are larger than that from the mixture with a 60:40 ratio.

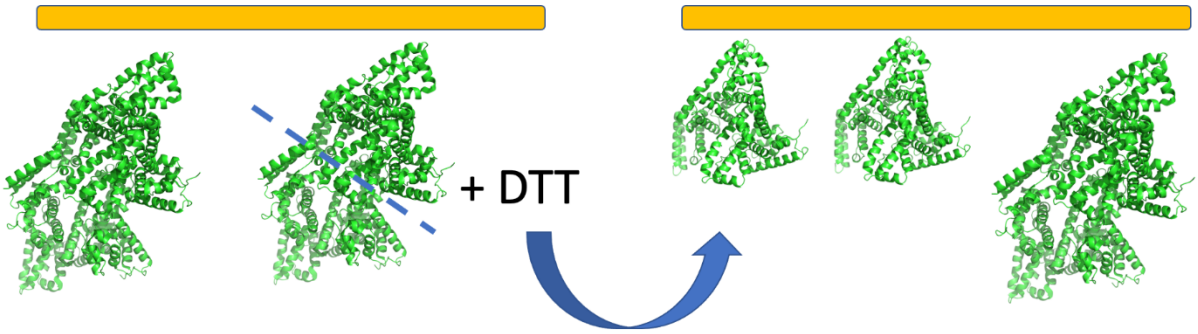


Figure 3.9 Schematic showing the interfacial reaction between DTT and BSA dimer on the silicone oil surface and the deduced orientations of BSA monomer and BSA dimer on the silicone oil surface after the DTT treatment.

Dimer:monomer ratio	1:9	2:8	3:7	4:6	5:5	6:4	7:3	8:2	9:1
Sum of the square of the difference	2.048	1.578	1.204	0.7161	0.3888	0.3142	0.4559	0.7809	1.263

Table 3.3 The sum of the difference square of the SFG spectra with best matching quality for each dimer-monomer ratio. The calculated SFG spectra based on the BSA dimer-monomer ratio of 60:40 has the lowest value of the square difference (or the best matching quality).

It is worth mentioning that since protein aggregation may occur through various ways,[78] DTT may reduce the disulfide bonds, and may also be considered an external modulator of the dynamic oligomerization pathway of BSA. Nevertheless, the use of DTT in this study is aimed to decrease the BSA dimer/monomer ratio, which is successful for interfacial BSA according to our SFG results presented above and also for bulk BSA according to the PAGE data shown in Section 3.3.6.

3.3.4 Circular Dichroism Spectroscopic Study Result

The above SFG data analysis indicates that DTT can cleave BSA dimers into monomers. We believe that the DTT treatment would not substantially change the BSA molecular structure, e.g., secondary structure. To confirm this, we studied the secondary structures of adsorbed BSA on silicone oil by CD experiments. Figure 3.10 shows that the CD spectra collected from adsorbed BSA on silicone oil before and after the DTT treatment are very similar, both of which exhibiting two negative peaks at 210 and 222 nm - the two characteristic peaks of the α-helical structure. The similar CD spectra from adsorbed BSA before and after the DTT treatment indicate that there is no significant change in the secondary structures of the adsorbed BSA, suggesting that DTT does not alter the BSA conformation substantially and the spectral changes observed in the SFG experiments should mainly be due to the change from BSA dimer to monomer as analyzed above.

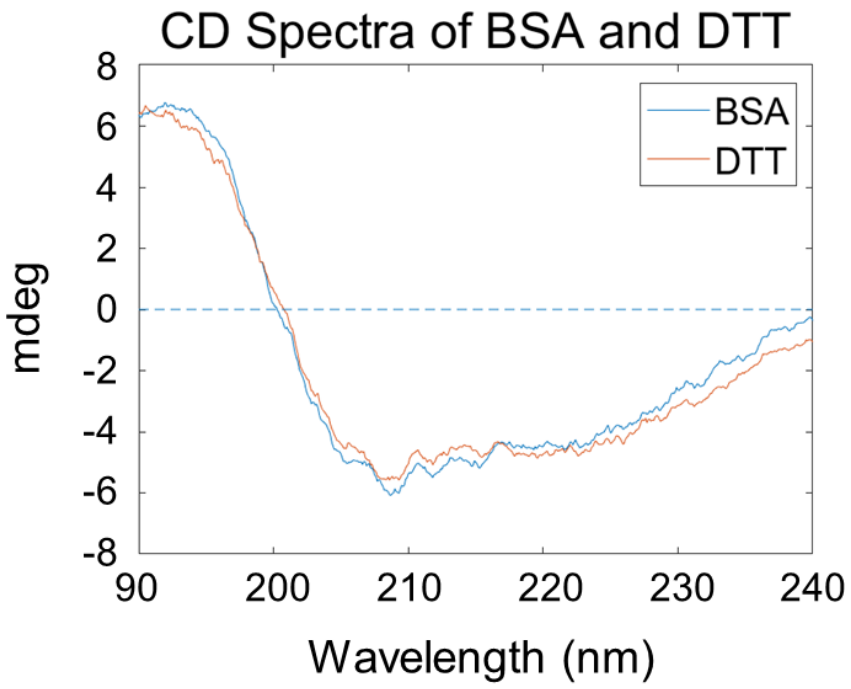


Figure 3.10 CD spectra of BSA on silicone oil before and after the DTT treatment.

3.3.5 Solvent Accessible Surface Area Analysis

BSA molecules have been extensively used as passivation coatings to prevent nonspecific adsorption of other molecules on the surface.[52] We have shown that the excellent passivation property of BSA is related to its strong surface hydration, contributed by its high surface coverage of amino acids glutamic acid (E) and lysine (K).[81] E and K behave as zwitterionic pairs and provide anti-fouling property.[82] Here we quantified the E/K ratio on the surface of BSA by calculating the solvent accessible surface area (SASA) to further understand the adsorption behavior of BSA on silicone oil. The number of E and K residues in the sequence considers both E/K on the protein surface and E/K in the interior of the protein, while E/K SASA considers the effect of protein surface E/K. We propose that the E/K SASA is more significant than the number of E and K

residues in the sequence since the BSA adsorption behavior is mainly affected by the outer surface of the protein.

E and K SASA considered the effect of surface E and K on BSA while the total number of E or K in the sequence may not be related to the BSA surface property. The SASA calculation was done in VMD[83] and the result is shown in Figure 3.11. The orientation of BSA shown in Figure 3.11 is the same as the deduced BSA orientation displayed in Figure 3.5 above. We selected the adsorption region on BSA dimer which is adjacent to the silicone oil surface (yellow region in Figure 3.11) and then calculated the ratio of SASA between E and K to be 1.339. Then all residues other than the adsorption site (red region in Figure 3.11) were selected and the calculated SASA E/K ratio is 0.919. Since the E and K can behave as zwitterionic pair, the protein (or a part of the protein) will exhibit more anti-fouling property if the E/K ratio is closer to 1. From Figure 3.11, we can see that the E/K SASA ratio of the adsorption site is higher than 1 and that of other parts of BSA is closer to 1, suggesting that the adsorption site has a less zwitterionic property and thus may have a stronger interaction with the silicone oil surface. This explains why a BSA dimer tends to tilt on the silicone oil surface with the region marked in yellow in contact with the silicone oil.

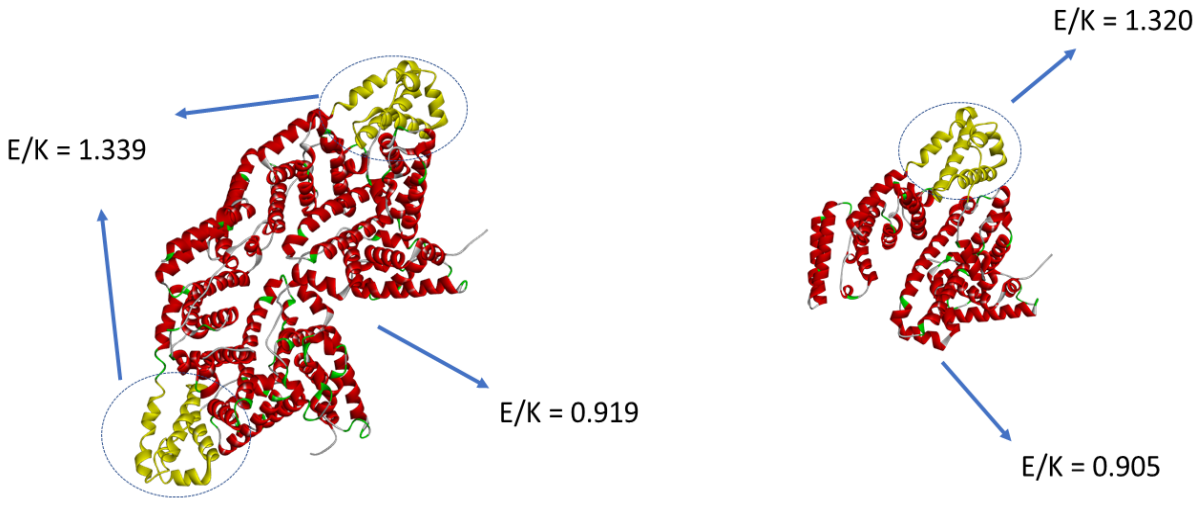


Figure 3.11 Solvent accessible surface area (SASA) analysis of E/K ratio of the adsorption site and other parts of a BSA dimer and a BSA monomer.

Besides the E/K ratio analysis, we also measured the SASA of positively charged, negatively charged, and hydrophobic amino acid residues. The result is summarized in Table 3.4. It has been shown that the silicone oil carries negative charges,[84-85] and BSA is slightly negatively charged in a pH=7 solution since the isoelectric point of BSA is 4.8. From the SASA values of positively and negatively charged amino acids as shown in Table 3.4, we can see that both the BSA adsorption part and the other part of the BSA surface are negative. If charge interaction plays the dominating role in the protein – silicone oil interaction, then BSA should not be adsorbed to the silicone oil surface. The observation of BSA adsorption on silicone oil indicates that the charge interaction does not play a major role in the BSA adsorption phenomenon. Since the BSA adsorption part has much less amino acids compared to the rest of the BSA protein, the SASA value of the other part of BSA is much larger than that of the adsorption part. For a better comparison, the SASA values are divided by the number of amino acids to get the average value for each amino acid. The average SASA result is shown in Table 3.5.

Table 3.5 shows that the adsorption parts of both the BSA dimer and monomer have higher average negative SASA values compared to the average positive SASA values in these parts, as well as the average negative SASA values of the other BSA parts, again suggesting that the negative charge repulsion between silicone oil surface and BSA is not the determining factor in BSA adsorption onto silicone oil. The average SASA values of the hydrophobic amino acids of the adsorption part are slightly higher than those of the other BSA parts for both the dimer and the monomer, which indicates that the hydrophobic interaction between BSA and the silicone oil is also important. To summarize, we believe that the E/K ratio or the zwitterionic effect and the hydrophobic interaction are the two main factors that affect the adsorption and the orientation of BSA on the silicone oil surface.

SASA Value ($Å^2$)	Dimer Adsorption Part	Dimer Rest Part	Monomer Adsorption Part	Monomer Rest Part
Positively charged amino acid (R,K,H)	2072.63	13407.80	1040.10	6883.96
Negatively charged amino acid (D,E)	3403.04	13864.99	1667.00	7030.07
Hydrophobic	2216.07	11022.60	1106.81	5503.20

Table 3.4 Solvent accessible surface area (SASA) calculation results of positively charged, negatively charged, and hydrophobic amino acids in the adsorption and the rest parts of BSA dimer and monomer.

SASA Value ($Å^2$)	Dimer Adsorption Part	Dimer Rest Part	Monomer Adsorption Part	Monomer Rest Part
Positively charged amino acid (R,K,H)	23.82	27.03	11.96	13.88
Negatively charged amino acid (D,E)	39.11	27.95	19.16	14.17
Hydrophobic	12.74	11.11	12.72	11.10

Table 3.5 Average solvent accessible surface area results of positively charged, negatively charged, and hydrophobic amino acids in the adsorption and other parts of BSA dimer and monomer.

3.3.6 Native-PAGE Experiment Results

We performed native PAGE experiments to determine BSA monomer and dimer amounts in the BSA solution before and after silicone oil surface contact, and before and after the DTT treatment. A BSA solution of concentration 1.0 mg/mL with a volume of 10 mL was prepared in a glass container. A silica window coated with silicone oil was placed in the above BSA solution for 30 minutes. The silicone oil surface was then removed from the BSA solution. 10 μL of the BSA solutions before and after the silicone oil contact was used in the native PAGE experiment.

A new BSA solution of concentration 1.0 mg/mL with a volume of 10 mL was prepared in a glass container. 77 mg of DTT was added to the BSA solution. A silica window coated with silicone oil was placed in the above DTT added BSA solution for 30 minutes. The silicone oil surface was then removed from the DTT added BSA solution. 10 µL of the DTT added BSA solutions before and after the silicone oil contact each was used in the native PAGE experiment.

We performed several PAGE experiments and qualitative reproducible results were obtained. Figure 3.12 shows the results from one example run. The four samples are BSA solutions before (1) and after (2) silicone oil exposure and BSA solutions with DTT added before (3) and after (4) silicone oil exposure. Table 3.6 presents the quantitative results obtained from the PAGE data shown in Figure 3.12. Figure 3.12 clearly shows that all the samples are dominated by the BSA monomers, with substantial amounts of BSA dimers. After the DTT treatment, the dimer amounts in the solution reduced noticeably. However, for the BSA solution before and after silicone oil surface contact, the dimer/monomer ratios are not very different. Table 3.6 shows representative band intensities obtained after quantitatively analyzing the images from stained gels.

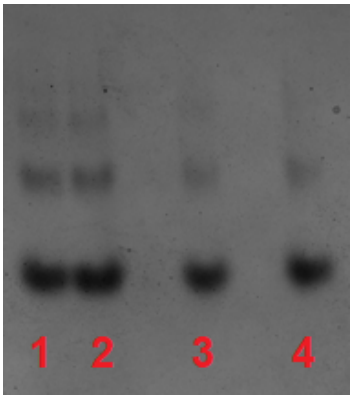


Figure 3.12 Native PAGE results of BSA solution before (1) and after (2) silicone oil surface contact, and DTT treated BSA solution before (3) and after (4) silicone oil surface contact.

	(1) BSA	(2) BSA Oil	(3) BSA DTT	(4) BSA Oil DTT
Dimer	4.6×10^6	5.0×10^6	2.5×10^6	2.5×10^6
Monomer	1.9×10^7	2.3×10^7	1.7×10^7	1.9×10^7
D/M	**1:4.1**	**1:4.6**	**1:6.8**	**1:7.6**

Table 3.6 Quantitative analysis results of the PAGE experiments. The first two rows are intensities of the BSA monomer and dimer bands in the gel. The third row is the ratios of the intensities from dimer vs. monomer.

Table 3.6 shows that the dimer/monomer ratios decreased after the DTT addition, indicating that DTT reduced some dimer molecules to monomers, as expected. We do not think that the native-PAGE experiments can provide quantitative correlations to SFG data. For quantitative correlations, after the silicone oil exposure, protein molecules (total intensity) should decrease, which was not observed. In the literature, similar methods were used to determine the possible monomer and dimer amounts adsorbed onto a surface. That is, a bulk method (e.g., PAGE) was used to measure the BSA dimer and monomer concentrations or amounts in a BSA solution. Then a surface was placed into contact with the solution. After that, the bulk solution (after the surface contact) was analyzed again using the bulk method to determine the BSA monomer and dimer amounts. According to the difference before and after the surface contact, possible amounts of BSA monomer and dimer on the surface were deduced. Unfortunately, the results obtained from this method may not be related to the amounts of BSA monomer and dimer on the (silicone oil) surface because BSA monomer and dimer can be re-equilibrated in the solution after the surface contact. Also, the interfacial interactions between adsorbed BSA and the surface may lead to dimer dissociation or monomer dimerization on the surface, which cannot be probed using the PAGE method. Here the only conclusions we can obtained from the native PAGE experiments are: (1) Both dimers and monomers exist in the BSA solution before and after silicone oil surface contact, and before and after DTT added. (2) After the DTT was added, the BSA monomer:dimer ratio

increases. (3) For both BSA solutions with and without added DTT, the BSA monomer:dimer ratios in the BSA solutions increase after the silicone oil surface contact.

3.4 Conclusions

It is important to understand protein behavior at interfaces. Protein aggregation at interfaces may greatly reduce protein function. To the best of our knowledge, the methodology to study protein aggregation at buried interfaces in situ, e.g., identify protein monomer or dimer at the buried solid/liquid or liquid/liquid interfaces, is lacking. Here, using widely studied and extensively applied BSA molecules, we demonstrated that SFG study along with Hamiltonian data analysis can be used to distinguish protein monomer, dimer, and monomer-dimer mixture at interfaces in situ in real time. It is worth reiterating that the protein – surface interaction can be complicated, leading to the formation of oligomers beyond dimers. Here we hypothesized that dimer is the most probable oligomer form, and tested this hypothesis using SFG data analysis based on the monomer and dimer structures. As shown above, our data analysis could well interpret the SFG data. Certainly we could not completely rule out the formation of other BSA oligomers on silicone oil, which is beyond the scope of this study.

Our studies reported here demonstrated that adsorbed BSA molecules on silicone oil are mainly in the dimer form. After the DTT treatment, about 25% of the BSA dimers turn into monomers because DTT can cleave the disulfide bond in the BSA dimer which connects the two monomers. The CD spectra collected from the adsorbed BSA on silicone oil show similar secondary structures of BSA on silicone oil before and after the DTT treatment, indicating that the DTT treatment does not alter the adsorbed BSA conformation, well correlated to our explanations on the SFG spectral change of adsorbed BSA on silicone oil after the DTT treatment.

It is worth mentioning that here we used BSA crystal structure in the Hamiltonian calculation for SFG data analysis. Since BSA is a globular protein with a rigid structure, we believe that the use of BSA crystal structure in the calculation is reasonable, which can be proved by the excellent matching results between the experimental data and the calculated results using the Hamiltonian approach based on the BSA crystal structure. For "soft proteins" which may undergo substantial conformational changes at interfaces, the use of protein crystal structure for Hamiltonian calculation may lead to large errors. As we will show in Chapter 4 below, the calculated SFG spectra from modified protein crystal structure of fibrinogen can match the SFG experimental data better, therefore under certain conditions it may need to modify the protein crystal structure to take account of the protein interfacial interactions. For proteins with no known crystal structures, we could predict the protein structure according to the protein sequenc\em, as we will show in chapter 6. For better include the protein-surface interaction into consideration, it is necessary to use the interfacial structure of the protein, e.g., obtained from molecular dynamics simulation, to calculate SFG spectra with the Hamiltonian method. The combined computer simulation and SFG studies can be used to identify the most likely protein conformation and orientation, as we demonstrated previously[60] and will also show in chapter 6. Such combined study can also cross-check the conclusions obtained from the simulation, and provide more detailed and more reliable structural information from SFG studies. Although this research only shows the capability of SFG to study BSA monomers and dimers, we believe that SFG is able to examine protein aggregates with more complicated structures such as trimer, tetramers etc. with the help of computer simulations.

Excellent research has been performed to apply various bulk analytical and biochemical methods to study complicated protein aggregates in bulk solutions.[86-87] It is possible to study such

protein aggregates at interfaces using SFG and Hamiltonian approach if reasonable models can be used for Hamiltonian calculation through MD simulations or other methods, which is beyond the current investigation.

The developed methodology in this research is generally applicable to study behavior of other proteins such as antibody protein drug molecules on silicone oil, which will lead to great impact on pharmaceutical research and applications. The developed method is also generally applicable to study protein molecules on other surfaces and interfaces beyond silicone oil surface, developing further understanding on interfacial protein behavior and its relationship to biocompatibility of biomaterials, performance of antifouling coatings, protein fouling on membranes used for bio-separation, sensitivity of biosensors, etc.

3.5 References

1. Coulet, P. R.; Blum, L. J., *Biosensor principles and applications*. CRC Press: 2019.

2. Del Grosso, C. A.; Leng, C.; Zhang, K.; Hung, H.-C.; Jiang, S.; Chen, Z.; Wilker, J. J., Surface hydration for antifouling and bio-adhesion. *Chemical Science* **2020,** *11* (38), 10367-10377.

3. Opdahl, A.; Koffas, T. S.; Amitay-Sadovsky, E.; Kim, J.; Somorjai, G. A., Characterization of polymer surface structure and surface mechanical behaviour by sum frequency generation surface vibrational spectroscopy and atomic force microscopy. *Journal of Physics: Condensed Matter* **2004,** *16* (21), R659.

4. Li, M.; Xiong, Y.; Qing, G., Smart bio-separation materials. *TrAC Trends in Analytical Chemistry* **2020,** *124*, 115585.

5. Zhao, C.; Li, L.; Wang, Q.; Yu, Q.; Zheng, J., Effect of film thickness on the antifouling performance of poly (hydroxy-functional methacrylates) grafted surfaces. *Langmuir* **2011,** *27* (8), 4906-4913.

6. Jiang, S.; Cao, Z., Ultralow‐fouling, functionalizable, and hydrolyzable zwitterionic materials and their derivatives for biological applications. *Advanced materials* **2010,** *22* (9), 920-932.

7. Sloan-Dennison, S.; Schultz, Z. D., Label-free plasmonic nanostar probes to illuminate in vitro membrane receptor recognition. *Chemical science* **2019,** *10* (6), 1807-1815.

8. Lu, J.; Xue, Y.; Shi, R.; Kang, J.; Zhao, C.-Y.; Zhang, N.-N.; Wang, C.-Y.; Lu, Z.-Y.; Liu, K., A non-sacrificial method for the quantification of poly (ethylene glycol) grafting density on gold nanoparticles for applications in nanomedicine. *Chemical science* **2019,** *10* (7), 2067-2074.

9. Wang, H.; Christiansen, D. E.; Mehraeen, S.; Cheng, G., Winning the fight against biofilms: the first six-month study showing no biofilm formation on zwitterionic polyurethanes. *Chemical science* **2020,** *11* (18), 4709-4721.

10. Shi, X.; Zhang, X.-N.; Chen, J.; Cheng, Q.; Pei, H.; Louie, S. G.; Zhang, Y., A poly-ADP-ribose polymer-based antibody-drug conjugate. *Chemical science* **2020,** *11* (34), 9303-9308.

11. Zhang, Y.; Shen, J.; Hu, R.; Shi, X.; Hu, X.; He, B.; Qin, A.; Tang, B. Z., Fast surface immobilization of native proteins through catalyst-free amino-yne click bioconjugation. *Chemical science* **2020,** *11* (15), 3931-3935.

12. Naidja, A.; Liu, C.; Huang, P., Formation of protein–birnessite complex: XRD, FTIR, and AFM analysis. *Journal of Colloid and Interface Science* **2002,** *251* (1), 46-56.

13. Bersch, B.; Dörr, J. M.; Hessel, A.; Killian, J. A.; Schanda, P., Proton‐detected solid‐state NMR spectroscopy of a zinc diffusion facilitator protein in native nanodiscs. *Angewandte Chemie International Edition* **2017,** *56* (9), 2508-2512.

14. Zhang, Y.; Sun, B.; Feng, D.; Hu, H.; Chu, M.; Qu, Q.; Tarrasch, J. T.; Li, S.; Kobilka, T. S.; Kobilka, B. K., Cryo-EM structure of the activated GLP-1 receptor in complex with a G protein. *Nature* **2017,** *546* (7657), 248-253.

15. Shen, Y., Surface properties probed by second-harmonic and sum-frequency generation. *Nature* **1989,** *337* (6207), 519.

16. Moad, A. J.; Simpson, G. J., A unified treatment of selection rules and symmetry relations for sum-frequency and second harmonic spectroscopies. *The Journal of Physical Chemistry B* **2004,** *108* (11), 3548-3562.

17. Zhuang, X.; Miranda, P.; Kim, D.; Shen, Y., Mapping molecular orientation and conformation at interfaces by surface nonlinear optics. *Physical Review B* **1999,** *59* (19), 12632.

18. Roy, S.; Covert, P. A.; FitzGerald, W. R.; Hore, D. K., Biomolecular structure at solid–liquid interfaces as revealed by nonlinear optical spectroscopy. *Chemical reviews* **2014,** *114* (17), 8388-8415.

19. Hosseinpour, S.; Roeters, S. J.; Bonn, M.; Peukert, W.; Woutersen, S.; Weidner, T., Structure and dynamics of interfacial peptides and proteins from vibrational sum-frequency generation spectroscopy. *Chemical reviews* **2020,** *120* (7), 3420-3465.

20. Ye, S.; Tong, Y.; Ge, A.; Qiao, L.; Davies, P. B., Interfacial structure of soft matter probed by sfg spectroscopy. *The Chemical Record* **2014,** *14* (5), 791-805.

21. Lu, X.; Zhang, C.; Ulrich, N.; Xiao, M.; Ma, Y.-H.; Chen, Z., Studying polymer surfaces and interfaces with sum frequency generation vibrational spectroscopy. *Analytical chemistry* **2017,** *89* (1), 466-489.

22. Fu, L.; Liu, J.; Yan, E. C., Chiral sum frequency generation spectroscopy for characterizing protein secondary structures at interfaces. *Journal of the American Chemical Society* **2011,** *133* (21), 8094-8097.

23. Bhattacharyya, D.; Montenegro, A.; Dhar, P.; Mammetkuliyev, M.; Pankow, R. M.; Jung, M. C.; Thompson, M. E.; Thompson, B. C.; Benderskii, A. V., Molecular orientation of poly-3-hexylthiophene at the buried interface with fullerene. *The journal of physical chemistry letters* **2019,** *10* (8), 1757-1762.

24. Geiger, F. M., Second harmonic generation, sum frequency generation, and χ (3): dissecting environmental interfaces with a nonlinear optical Swiss Army knife. *Annual review of physical chemistry* **2009,** *60*, 61-83.

25. Zuo, B.; Inutsuka, M.; Kawaguchi, D.; Wang, X.; Tanaka, K., Conformational relaxation of poly (styrene-co-butadiene) chains at substrate interface in spin-coated and solvent-cast films. *Macromolecules* **2018,** *51* (6), 2180-2186.

26. Ye, H.; Abu-Akeel, A.; Huang, J.; Katz, H. E.; Gracias, D. H., Probing organic field effect transistors in situ during operation using SFG. *Journal of the American Chemical Society* **2006,** *128* (20), 6528-6529.

27. Ye, H.; Huang, J.; Park, J.-R.; Katz, H. E.; Gracias, D. H., Correlations between SFG spectra and electrical properties of organic field effect transistors. *The Journal of Physical Chemistry C* **2007,** *111* (35), 13250-13255.

28. Peng, Q.; Chen, J.; Ji, H.; Morita, A.; Ye, S., Origin of the overpotential for the oxygen evolution reaction on a well-defined graphene electrode probed by in situ sum frequency generation vibrational spectroscopy. *Journal of the American Chemical Society* **2018,** *140* (46), 15568-15571.

29. Ge, A.; Peng, Q.; Qiao, L.; Yepuri, N. R.; Darwish, T. A.; Matsusaki, M.; Akashi, M.; Ye, S., Molecular orientation of organic thin films on dielectric solid substrates: a phase-sensitive vibrational SFG study. *Physical Chemistry Chemical Physics* **2015,** *17* (27), 18072-18078.

30. Xiao, M.; Wei, S.; Chen, J.; Tian, J.; Brooks Iii, C. L.; Marsh, E. N. G.; Chen, Z., Molecular Mechanisms of Interactions between Monolayered Transition Metal Dichalcogenides and Biological Molecules. *Journal of the American Chemical Society* **2019,** *141* (25), 9980-9988.

31. Ding, B.; Jasensky, J.; Li, Y.; Chen, Z., Engineering and characterization of peptides and proteins at surfaces and interfaces: a case study in surface-sensitive vibrational spectroscopy. *Accounts of chemical research* **2016,** *49* (6), 1149-1157.

32. Yang, Z.; Li, Q.; Chou, K. C., Structures of water molecules at the interfaces of aqueous salt solutions and silica: Cation effects. *The Journal of Physical Chemistry C* **2009,** *113* (19), 8201-8205.

33. Lovering, K. A.; Bertram, A. K.; Chou, K. C., Transient phase of ice observed by sum frequency generation at the water/mineral interface during freezing. *The journal of physical chemistry letters* **2017,** *8* (4), 871-875.

34. Tan, J.; Zhang, J.; Luo, Y.; Ye, S., Misfolding of a human islet amyloid polypeptide at the lipid membrane populates through β-sheet conformers without involving α-helical intermediates. *Journal of the American Chemical Society* **2019,** *141* (5), 1941-1948.

35. Yu, T.; Zhou, G.; Hu, X.; Ye, S., Transport and organization of cholesterol in a planar solid-supported lipid bilayer depend on the phospholipid flip-flop rate. *Langmuir* **2016,** *32* (44), 11681-11689.

36. Sun, V.; Jarisz, T. A.; Wunsch, L.; Hore, D. K., Monitoring early stages of bacterial adhesion at silica surfaces through image analysis. *Langmuir* **2020,** *36* (8), 2120-2128.

37. Wang, J.; Even, M. A.; Chen, X.; Schmaier, A. H.; Waite, J. H.; Chen, Z., Detection of amide I signals of interfacial proteins in situ using SFG. *Journal of the American Chemical Society* **2003,** *125* (33), 9914-9915.

38. Wang, J.; Chen, X.; Clarke, M. L.; Chen, Z., Detection of chiral sum frequency generation vibrational spectra of proteins and peptides at interfaces in situ. *Proceedings of the National Academy of Sciences* **2005,** *102* (14), 4978-4983.

39. Zhang, C.; Gao, J.; Hankett, J.; Varanasi, P.; Borst, J.; Shirazi, Y.; Zhao, S.; Chen, Z., Corn Oil–Water Separation: Interactions of Proteins and Surfactants at Corn Oil/Water Interfaces. *Langmuir* **2020,** *36* (15), 4044-4054.

40. Zou, X.; Wei, S.; Jasensky, J.; Xiao, M.; Wang, Q.; Brooks III, C. L.; Chen, Z., Molecular interactions between graphene and biological molecules. *Journal of the American Chemical Society* **2017,** *139* (5), 1928-1936.

41. Nguyen, K. T.; Le Clair, S. V.; Ye, S.; Chen, Z., Orientation determination of protein helical secondary structures using linear and nonlinear vibrational spectroscopy. *The Journal of Physical Chemistry B* **2009,** *113* (36), 12169-12180.

42. Boughton, A. P.; Yang, P.; Tesmer, V. M.; Ding, B.; Tesmer, J. J.; Chen, Z., Heterotrimeric G protein β1γ2 subunits change orientation upon complex formation with G

protein-coupled receptor kinase 2 (GRK2) on a model membrane. *Proceedings of the National Academy of Sciences* **2011,** *108* (37), E667-E673.

43. Zou, X.; Wei, S.; Badieyan, S.; Schroeder, M.; Jasensky, J.; Brooks III, C. L.; Marsh, E. N. G.; Chen, Z., Investigating the effect of two-point surface attachment on enzyme stability and activity. *Journal of the American Chemical Society* **2018,** *140* (48), 16560-16569.

44. Carter, P. J.; Lazar, G. A., Next generation antibody drugs: pursuit of the'high-hanging fruit'. *Nature Reviews Drug Discovery* **2018,** *17* (3), 197-223.

45. Frokjaer, S.; Otzen, D. E., Protein drug stability: a formulation challenge. *Nature reviews drug discovery* **2005,** *4* (4), 298-306.

46. Vázquez‐Rey, M.; Lang, D. A., Aggregates in monoclonal antibody manufacturing processes. *Biotechnology and bioengineering* **2011,** *108* (7), 1494-1508.

47. Wang, W.; Roberts, C. J., Protein aggregation–mechanisms, detection, and control. *International journal of pharmaceutics* **2018,** *550* (1-2), 251-268.

48. Baier, G.; Costa, C.; Zeller, A.; Baumann, D.; Sayer, C.; Araujo, P. H.; Mailänder, V.; Musyanovych, A.; Landfester, K., BSA adsorption on differently charged polystyrene nanoparticles using isothermal titration calorimetry and the influence on cellular uptake. *Macromolecular bioscience* **2011,** *11* (5), 628-638.

49. Frateur, I.; Lecoeur, J.; Zanna, S.; Olsson, C.-O.; Landolt, D.; Marcus, P., Adsorption of BSA on passivated chromium studied by a flow-cell EQCM and XPS. *Electrochimica Acta* **2007,** *52* (27), 7660-7669.

50. Swain, S. K.; Sarkar, D., Study of BSA protein adsorption/release on hydroxyapatite nanoparticles. *Applied Surface Science* **2013,** *286*, 99-103.

51. Zhao, Z.-P.; Wang, Z.; Wang, S.-C., Formation, charged characteristic and BSA adsorption behavior of carboxymethyl chitosan/PES composite MF membrane. *Journal of Membrane Science* **2003,** *217* (1-2), 151-158.

52. Park, J. H.; Jackman, J. A.; Ferhan, A. R.; Ma, G. J.; Yoon, B. K.; Cho, N.-J., Temperature-induced denaturation of BSA protein molecules for improved surface passivation coatings. *ACS applied materials & interfaces* **2018,** *10* (38), 32047-32057.

53. Kelly, S. T.; Zydney, A. L., Effects of intermolecular thiol–disulfide interchange reactions on bsa fouling during microfiltration. *Biotechnology and bioengineering* **1994,** *44* (8), 972-982.

54. Zsom, R. L., Dependence of preferential bovine serum albumin oligomer adsorption on the surface properties of monodisperse polystyrene latices. *Journal of colloid and interface science* **1986,** *111* (2), 434-445.

55. Okubo, M.; Azume, I.; Yamamoto, Y., Preferential adsorption of bovine serum albumin dimer onto polymer microspheres having a heterogeneous surface consisting of hydrophobic and hydrophilic parts. *Colloid and Polymer Science* **1990,** *268* (7), 598-603.

56. Chang, C.-S.; Suen, S.-Y., Modification of porous alumina membranes with n-alkanoic acids and their application in protein adsorption. *Journal of membrane science* **2006,** *275* (1-2), 70-81.

57. Hamm, P.; Zanni, M., *Concepts and methods of 2D infrared spectroscopy*. Cambridge University Press: 2011.

58. Ding, B.; Panahi, A.; Ho, J.-J.; Laaser, J. E.; Brooks III, C. L.; Zanni, M. T.; Chen, Z., Probing site-specific structural information of peptides at model membrane interface in situ. *Journal of the American Chemical Society* **2015,** *137* (32), 10190-10198.

59. Ding, B.; Laaser, J. E.; Liu, Y.; Wang, P.; Zanni, M. T.; Chen, Z., Site-specific orientation of an α-helical peptide ovispirin-1 from isotope-labeled SFG spectroscopy. *The Journal of Physical Chemistry B* **2013,** *117* (47), 14625-14634.

60. Guo, W.; Zou, X.; Jiang, H.; Koebke, K. J.; Hoarau, M.; Crisci, R.; Lu, T.; Wei, T.; Marsh, E. N. G.; Chen, Z., Molecular Structure of the Surface-Immobilized Super Uranyl Binding Protein. *The Journal of Physical Chemistry B* **2021,** *125* (28), 7706-7716.

61. Patel, D.; Kuyucak, S., Computational study of aggregation mechanism in human lysozyme [D67H]. *PloS one* **2017,** *12* (5), e0176886.

62. Frieden, C., Protein aggregation processes: in search of the mechanism. *Protein Science* **2007,** *16* (11), 2334-2344.

63. Woods, C. E. Understanding therapeutic monoclonal antibody aggregation mechanisms through biophysical, biochemical and biological characterization of two types of immunoglobulin G dimers. University of Kansas, 2015.

64. Li, Y.; Pan, D.; Nashine, V.; Deshmukh, S.; Vig, B.; Chen, Z., Understanding Protein-Interface Interactions of a Fusion Protein at Silicone Oil-Water Interface Probed by Sum Frequency Generation Vibrational Spectroscopy. *Journal of pharmaceutical sciences* **2018,** *107* (2), 682-689.

65. Perera, H. G.; Lu, T.; Fu, L.; Zhang, J.; Chen, Z., Probing the Interfacial Interactions of Monoclonal and Bispecific Antibodies at the Silicone Oil–Aqueous Solution Interface by Using Sum Frequency Generation Vibrational Spectroscopy. *Langmuir* **2019,** *35* (44), 14339-14347.

66. Rajan, R.; Ahmed, S.; Sharma, N.; Kumar, N.; Debas, A.; Matsumura, K., Review of the current state of protein aggregation inhibition from a materials chemistry perspective: special focus on polymeric materials. *Materials Advances* **2021,** *2* (4), 1139-1176.

67. Gandhi, J.; Antonelli, A. C.; Afridi, A.; Vatsia, S.; Joshi, G.; Romanov, V.; Murray, I. V.; Khan, S. A., Protein misfolding and aggregation in neurodegenerative diseases: a review of pathogeneses, novel detection strategies, and potential therapeutics. *Reviews in the Neurosciences* **2019,** *30* (4), 339-358.

68. Minakawa, E. N.; Nagai, Y., Protein aggregation inhibitors as disease-modifying therapies for polyglutamine diseases. *Frontiers in Neuroscience* **2021,** *15*, 75.

69. Alberti, S.; Hyman, A. A., Biomolecular condensates at the nexus of cellular stress, protein aggregation disease and ageing. *Nature Reviews Molecular Cell Biology* **2021,** *22* (3), 196-213.

70. Zhang, Y.; Liu, Y.; Tang, Y.; Zhang, D.; He, H.; Wu, J.; Zheng, J., Antimicrobial α-defensins as Multi-target Inhibitors Against Amyloid Formation and Microbial Infection. *Chemical Science* **2021**.

71. Ye, S.; Nguyen, K. T.; Le Clair, S. V.; Chen, Z., In situ molecular level studies on membrane related peptides and proteins in real time using sum frequency generation vibrational spectroscopy. *Journal of structural biology* **2009,** *168* (1), 61-77.

72. Lu, X.; Shephard, N.; Han, J.; Xue, G.; Chen, Z., Probing molecular structures of polymer/metal interfaces by sum frequency generation vibrational spectroscopy. *Macromolecules* **2008,** *41* (22), 8770-8777.

73. Lu, X.; Xue, G.; Wang, X.; Han, J.; Han, X.; Hankett, J.; Li, D.; Chen, Z., Directly probing molecular ordering at the buried polymer/metal interface 2: Using P-polarized input beams. *Macromolecules* **2012,** *45* (15), 6087-6094.

74. Lu, X.; Zhang, C.; Ulrich, N.; Xiao, M.; Ma, Y.-H.; Chen, Z., Studying polymer surfaces and interfaces with sum frequency generation vibrational spectroscopy. *Analytical chemistry* **2016,** *89* (1), 466-489.

75. Zhang, X.; Myers, J. N.; Huang, H.; Shobha, H.; Chen, Z.; Grill, A., SFG analysis of the molecular structures at the surfaces and buried interfaces of PECVD ultralow-dielectric constant pSiCOH. *Journal of Applied Physics* **2016,** *119* (8), 084101.

76. Wang, J.; Clarke, M. L.; Chen, X.; Even, M. A.; Johnson, W. C.; Chen, Z., Molecular studies on protein conformations at polymer/liquid interfaces using sum frequency generation vibrational spectroscopy. *Surface Science* **2005,** *587* (1-2), 1-11.

77. Wang, J.; Clarke, M. L.; Chen, Z., Polarization mapping: a method to improve sum frequency generation spectral analysis. *Analytical chemistry* **2004,** *76* (8), 2159-2167.

78. Levi, V.; Flecha, F. L. G., Reversible fast-dimerization of bovine serum albumin detected by fluorescence resonance energy transfer. *Biochimica et Biophysica Acta (BBA)-Proteins and Proteomics* **2002,** *1599* (1-2), 141-148.

79. Andersson, L.-O., Hydrolysis of disulfide bonds in weakly alkaline media II. Bovine serum albumin dimer. *Biochimica et Biophysica Acta (BBA)-Protein Structure* **1970,** *200* (2), 363-369.

80. Ueki, T.; Hiragi, Y.; Kataoka, M.; Inoko, Y.; Amemiya, Y.; Izumi, Y.; Tagawa, H.; Muroga, Y., Aggregation of bovine serum albumin upon cleavage of its disulfide bonds, studied by the time-resolved small-angle X-ray scattering technique with synchrotron radiation. *Biophysical chemistry* **1985,** *23* (1-2), 115-124.

81. Zhang, K.; Huang, H.; Hung, H.-C.; Leng, C.; Wei, S.; Crisci, R.; Jiang, S.; Chen, Z., Strong Hydration at the Poly (ethylene glycol) Brush/Albumin Solution Interface. *Langmuir* **2020,** *36* (8), 2030-2036.

82. White, A. D.; Nowinski, A. K.; Huang, W.; Keefe, A. J.; Sun, F.; Jiang, S., Decoding nonspecific interactions from nature. *Chemical Science* **2012,** *3* (12), 3488-3494.

83. Humphrey, W.; Dalke, A.; Schulten, K., VMD: visual molecular dynamics. *Journal of molecular graphics* **1996,** *14* (1), 33-38.

84. Kirby, B. J.; Hasselbrink Jr, E. F., Zeta potential of microfluidic substrates: 2. Data for polymers. *Electrophoresis* **2004,** *25* (2), 203-213.

85. Ludwig, D. B.; Carpenter, J. F.; Hamel, J. B.; Randolph, T. W., Protein adsorption and excipient effects on kinetic stability of silicone oil emulsions. *Journal of pharmaceutical sciences* **2010,** *99* (4), 1721-1733.

86. Borzova, V. A.; Markossian, K. A.; Kleymenov, S. Y.; Kurganov, B. I., A change in the aggregation pathway of bovine serum albumin in the presence of arginine and its derivatives. *Scientific reports* **2017,** *7* (1), 1-12.

87. Finn, T. E.; Nunez, A. C.; Sunde, M.; Easterbrook-Smith, S. B., Serum albumin prevents protein aggregation and amyloid formation and retains chaperone-like activity in the presence of physiological ligands. *Journal of Biological Chemistry* **2012,** *287* (25), 21530-21540.

Chapter 4 Monitoring Orientation and Conformation Changes of Fibrinogen during the Adsorption Process at the Buried Interface in Situ in Real Time

4.1 Introduction

As discussed in Chapter 1, protein adsorption can happen under various circumstances due to the surface-active property of proteins, which may lead to undesired fouling on surfaces or the unwanted conformational changes of the proteins. For example, protein adsorption is the first event that occurs when a biomedical implant is placed into contact with tissue or blood, which is influenced by the protein properties, the implant material, and environmental condition.[1-2] Unfavorable protein - implant interactions may lead to negative biological responses such as blood coagulation, unnecessary immune response etc.[3-4] Also the first step for marine biofouling to happen on a ship is the adsorption of adhesive proteins generated by marine organisms onto the ship hull - Their interactions determine whether the marine organisms could adhere to the ship or not.[5-7] Therefore, it is important to investigate the protein adsorption onto various surfaces to understand protein-surface interaction mechanisms for (1) rational design of surfaces to prevent protein from adsorption and/or (2) ensuring adsorbed protein adopts reasonable structure which would not cause a negative effect.

Protein adsorption has been a long active research focus for several decades. Extensive research has been performed to characterize the adsorption behavior of different proteins using many different analytical techniques. Examples of such analytical tools include ellipsometry, neutron reflection, AFM, quartz crystal microbalance (QCM), surface plasmon resonance (SPR), attenuated total reflection FTIR (ATR-FTIR), surface enhanced Raman spectroscopy (SERS), etc.[8]

Excellent research results have been obtained in the studies by using these techniques.[9-16] However, all of these techniques have some limitations; thus it is still challenging to directly monitor the adsorption process of the proteins at a buried solid/liquid or liquid/liquid interface in situ in real time with the detailed molecular level protein structural information. As discussed in the previous Chapters, sum frequency generation (SFG) vibrational spectroscopy has been developed into a powerful tool to study interfacial protein structure in situ.

In this study, we applied SFG to follow the adsorption behavior of fibrinogen adsorbed onto silicone oil at buried silicone oil/protein solution interface in situ in real time and followed fibrinogen structural changes during the adsorption process. Fibrinogen is an important blood protein. Fibrinogen adsorption has been a focus for many protein-adsorption studies due to its critical role in blood clot formation. Undesired adsorption and aggregation of fibrinogen may cause blood clot formation in a deep vein, called deep vein thrombosis.[17] The thromboembolism can cause severe outcomes if left unattended,[18-19] and it has been so common that it is considered an epidemic.[20-22] Understanding the adsorption of fibrinogen onto surfaces with related structural changes in the adsorption process is an important step to unveil fibrinogen's interfacial interaction and aggregation mechanism, providing a basis for developing better thrombolytic therapies in the future. In the past, our group has reported using of SFG technique to characterize the adsorption and conformation changes of fibrinogen on various polymer surfaces,[12, 23-27] but the detailed molecular structure (including both the conformation and orientation) of adsorbed fibrinogen has not been determined. In this study, SFG was applied to elucidate the fibrinogen structural changes during the adsorption process onto silicone oil.

The silicone oil was chosen in this study as a surface for protein adsorption due to its strong hydrophobicity and wide application as the lubricant in the pharmaceutical industry. For protein

drug (e.g., antibody drug) storage and administration, silicone oil was extensively used as a coating material for drug containers or injectors (e.g., a syringe).[28] It has been shown that the silicone oil coating can induce protein adsorption and possible aggregation, reducing the antibody drug effectiveness.[29-33] In this study, with a femtosecond broad-band SFG spectrometer, we examined the adsorption dynamic of fibrinogen onto silicone oil in situ and in real time at the molecular level. SFG spectra were collected from the silicone oil/fibrinogen solution interface during the fibrinogen adsorption process with different polarizations of the input and outgoing beams. With the help of the Hamiltonian analysis method, we successfully deduced the time-dependent fibrinogen confirmation and orientation changes during adsorption. This technique is generally applicable, which can be applied to study molecular adsorption mechanisms of many different types of proteins at buried interfaces.

4.2 Experimental Details

4.2.1 Material and Sample Preparation

IR-grade CaF_2 right angle prisms were purchased from Altos Photonics Inc. (Bozeman, MT). Fibrinogen from bovine plasma, toluene, acetone, and methanol were purchased from Sigma-Aldrich (St. Louis, MO) and used as received. Medical-grade silicone oil (360 Medical Fluid 1000 Cst) was purchased from the Dow Chemical Company (Midland, MI). The procedures of CaF_2 prism cleaning, SiO_2 film coating, and silicone oil film deposition were the same as those presented in the Chapter 3 and will not be repeated here.

4.2.2 Instrumentation

Details of the SFG theory and instrumentation have been discussed in Chapter 1 previously[34-42] and will not be repeated here. SFG spectra were collected using a broadband

femtosecond SFG setup as mentioned in Chapter 1. In this system, laser pulses were generated from a Ti:sapphire regenerative amplifier (Solstice Ace, Spectra Physics) which centered at ~795 nm with ~35 femtoseconds pulse width. Part of the laser power was used in the optical parametric amplifier (OPA, TOPAS Prime, Spectra Physics) and difference frequency generator (DFG, TOPAS Prime, Spectra Physics) to produce the broadband IR beam. Then the broadband IR beam and the 795 nm beam were overlapped spatially and temporally at the silicone oil/protein solution interface. The incident angles of the 795 nm and the broadband IR beams were 65° and 55° versus the surface normal, respectively. The generated SFG signal was collected by a spectrograph (Kymera 328i, Andor) using the ssp (s-polarized SFG output, s-polarized 795nm input, p-polarized IR input) and ppp polarization combinations. The schematic of the fs-SFG sample geometry used in this experiment is the same as that shown in Figure 3.1.

4.2.3 Hamiltonian Method for SFG Spectral Analysis

The Hamiltonian local mode approximation method was used in this study to calculate polarized SFG spectra (ssp and ppp) of fibrinogen as a function of protein orientation. The details of this method have been described in Chapter 2 [43-46] and will only be discussed briefly here. The SFG spectra of fibrinogen with a given orientation can be calculated based on the local frequency of amide I stretch of each amino acid, and the coupling terms between each pair of the amino acids by applying the transition dipole approximation. The SFG spectra of fibrinogen were calculated with the fibrinogen orientation of tilt angles ranging from 0 to 180 degrees, and the twist angles ranging from 0 to 360 degrees. The step size for the tilt or the twist angle is 10 degrees. To calculate the SFG spectra, a protein structure is required as the input for the Hamiltonian method. In this study, the fibrinogen crystal structure (pdb:3ghg) was used as the input file. The bent angles between the two long coiled-coils were varied. More details will be discussed later.

4.3 Result and Discussion

4.3.1 SFG Experiment Result

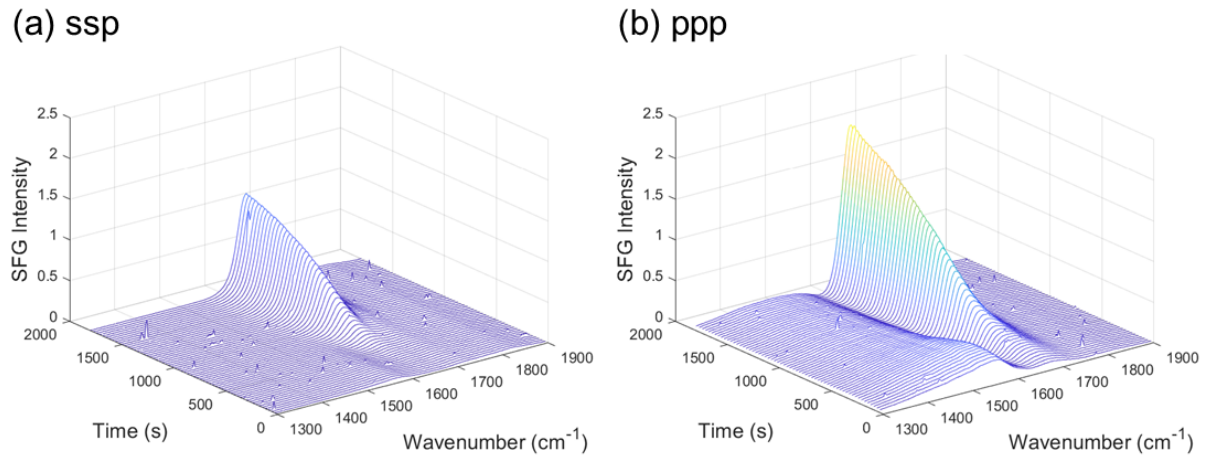


Figure 4.1 SFG (a) ssp and (b) ppp spectra collected from the silicone oil/fibrinogen solution interface to follow the fibrinogen adsorption process onto the silicone oil surface. The exposure time for each spectrum is 30 s. The fibrinogen solution was placed into contact with silicone oil at t = 0 s.

The time-dependent SFG ssp and ppp spectra collected from the silicone oil/fibrinogen solution interface are shown in Figure 4.1. Silicone oil should not generate any SFG signals in the amide I frequency region. Indeed, no discernable SFG protein amide I signal could be detected from the silicone oil surface before the fibrinogen solution contact. After the fibrinogen solution was placed into contact with silicone oil, for the first 300 s, the SFG signal did not change substantially, indicating that the adsorption rate was slow during the initial adsorption process. After the silicone oil surface was contacted with the fibrinogen solution for more than 300 s, the amide I signals gradually became stronger and could be seen clearly in the SFG spectra. The peak at around 1645 cm^{-1} in both ssp and ppp can be attributed to the helical structure in fibrinogen. The SFG signal increased as a function of time, likely indicating that more fibrinogen molecules were adsorbed to silicone oil as the adsorption time increased. Since SFG signal intensity also depends on the molecular orientation, the time-dependent SFG signal increase may also be caused

by adsorbed fibrinogen orientation change. Therefore the time-dependent fibrinogen adsorption amount change and possible structure change need to be analyzed further, which will be discussed in detail below.

4.3.2 Conformation and Orientation Analysis by Hamiltonian

To determine the structure (conformation and orientation) of adsorbed fibrinogen on silicone oil, it is necessary to compare the calculated SFG spectra and the experimental data. As we discussed in the previous chapters, the experimental SFG data contain both the resonant contribution from the interfacial protein (which is fibrinogen here) and the non-resonant background, while the calculated SFG spectra from the Hamiltonian method do not have non-resonant contribution. Therefore, for comparison, it is necessary to remove the non-resonant contribution from the experimental data and reconstruct the SFG experimental spectra only with the resonant parts. Here the experimentally collected SFG spectra were fitted by the standard SFG spectral fitting method first, and then the resonant spectra were reconstructed using the fitting parameters. The ssp and ppp spectra can be converted to yyz and zzz spectra by Fresnel coefficients , respectively.

The yyz and zzz SFG spectra of fibrinogen can be calculated as a function of fibrinogen molecular orientation using the Hamiltonian method. To do so, the Hamiltonian method needs a structural input to build the Hamiltonian matrix for calculation. In this study, the fibrinogen crystal structure (pdb: 3ghg, shown in Figure 4.2a) was used as a possible input structure for the Hamiltonian method. For the fibrinogen crystal structure, the two long coiled coils connect the two D domains with the center E domain, like a long linear molecule. Our previous SFG results on fibrinogen adsorption to polystyrene[25-26], polyurethanes, and fluorinated polymers[12] demonstrated that adsorbed fibrinogen molecules likely adopt bent structures, instead of the linear structure as

shown in the crystal. Our previous studies also showed that the fibrinogen bent structures may change as a function of time upon adsorption.[12] For example, fibrinogen adopts a bent structure at the beginning of the adsorption on polyurethane, and then the bent angle between the two coiled-coils increases and becomes "more" linear as a function of time. Differently, on the silicone-poly(carbonate urethane) or on the perfluorinated polymer surfaces, the fibrinogen bent angle decreases, becoming a more bent structure as the adsorption process goes on.

Here, to identify which conformation (linear or bent) does fibrinogen adopt on the silicone oil surface, the original crystal structure (pdb: 3ghg) was modified with different bent angles and these bent fibrinogen crystal structures were used as input structures for SFG spectral calculations with the Hamiltonian method. Specifically, we rotated the chain A, chain B, and chain C of the fibrinogen structure by 30°, 45°, 60°, and 90° to approximate the four bent conformations of fibrinogen. It is worth mentioning that this angle is not the bent angle between the two coiled-coils in the molecule. All the fibrinogen structures that were used for calculation in this study are shown in Figure 4.2. Note that these structures solely served as the input structures for the SFG orientation

analysis and the evaluation for possible fibrinogen conformational changes. They were not fully stabilized by simulation.

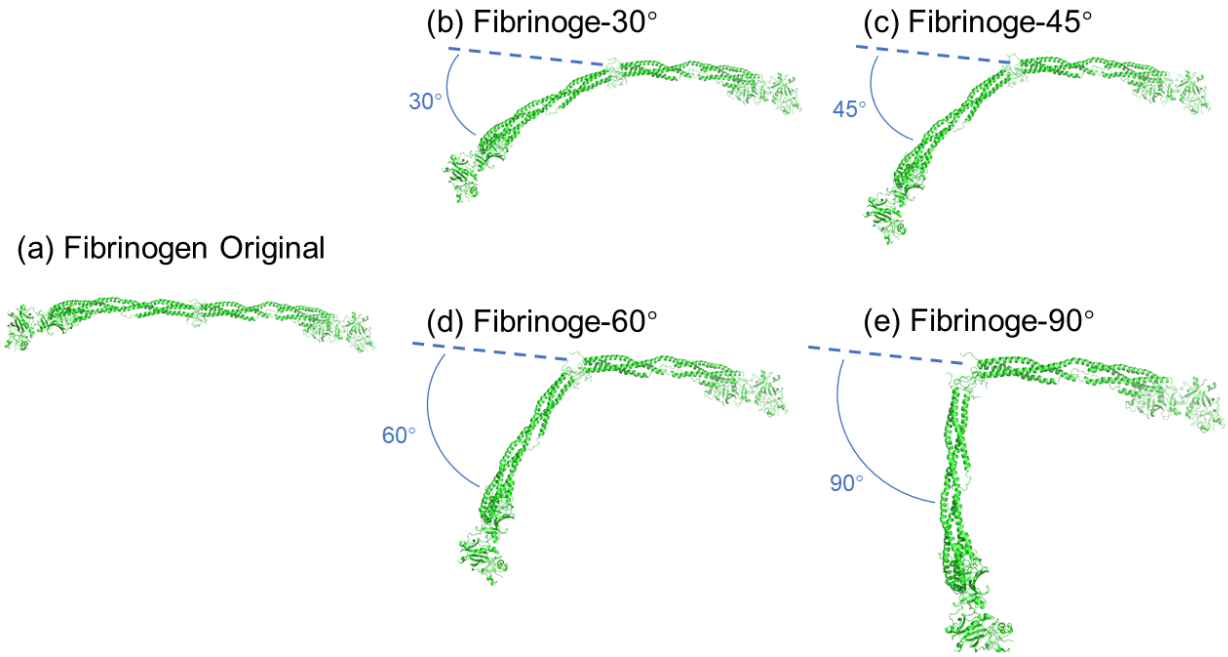


Figure 4.2 The structures of fibrinogen that were used for the Hamiltonian method in this study. (a) Fibrinogen original structure (pdb: 3ghg). Half of the protein structure (chain A, chain B, and chain C) was rotated by (a) 30 degrees, (b) 45 degrees, (c) 60 degrees, (d) 90 degrees to approximate the possible bent conformations of fibrinogen.

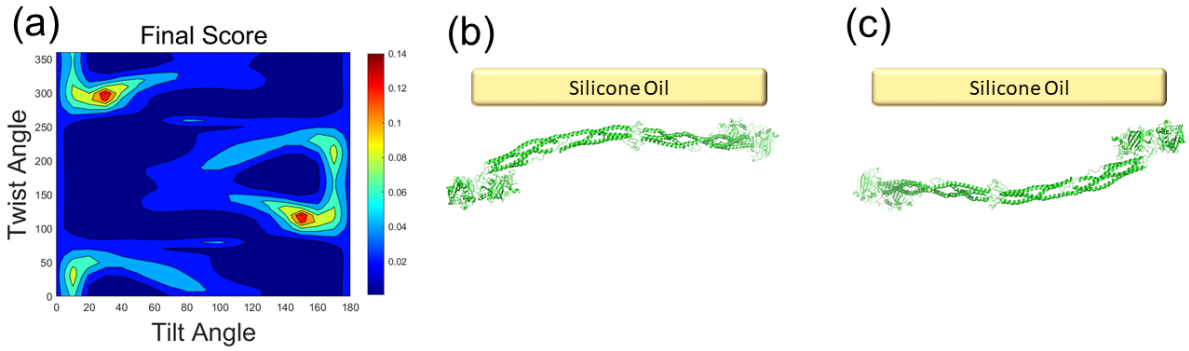


Figure 4.3 (a) The final matching score heat map showing the matching quality between the reconstructed resonant SFG experimental spectra (at t = 900 s) and the calculated orientation dependent SFG spectra based on the Fibrinogen-30° structure (shown in Figure 4.2b). (b) and (c) are the two most probable orientations of the adsorbed fibrinogen molecules on silicone oil.

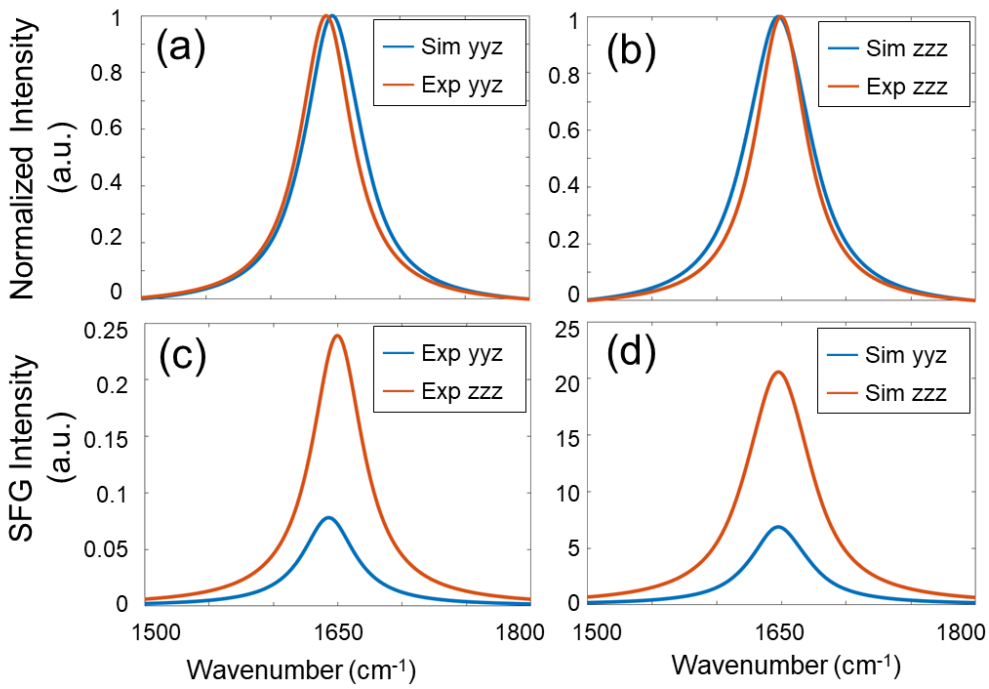


Figure 4.4 Comparison between reconstructed experimental data and calculated spectra based on the Fibrinogen-30° structure with the highest matching score. The blue spectra in (a) and (b) show the calculated SFG yyz (a) and zzz (b) spectra of adsorbed fibrinogen after 900 s adsorption with the highest matching score with the reconstructed experimental resonant SFG spectra (shown in orange). The unnormalized SFG spectra of (c) experimental data and (d) calculated spectra are plotted for evaluating the matching quality of the ssp and ppp spectral intensity ratio.

To probe the conformation and orientation change of fibrinogen adsorbed onto silicone oil as a function of time, the ssp and ppp spectra collected at t = 900 s, 1200 s, 1500 s, and 1800 s were compared with the calculated SFG spectra based on the five fibrinogen structures shown in Figure 4.2. No reliable fitting result can be obtained for the spectra collected before t = 900 s due to the low signal intensity. For the SFG spectra collected at t = 900 s, using the matching method we presented above, the final match score heat map after considering the ssp and ppp spectra features and the sss/ppp spectra intensity ratio can be obtained for each of the five confirmations with varied bent angles. It was found that the highest score in the matching score heat map calculated using the Fibrinogen-30° structure (shown in Figure 4.2b), is higher than those of the other four heat maps. Therefore, we believe that the Fibrinogen-30° structure is the most likely conformation adsorbed on the silicone oil at t = 900 s. According to the heat map shown in Figure

4.3a, the two most likely orientations are (tilt=150, twist=120) and (tilt=30, twist=300), shown in Figure 4.3b and 4.3c. These two orientations have the opposite absolution orientation. We believe that between these two orientations, Figure 4.3b is more reasonable because it has more contact area with silicone oil to support the large molecule on the surface, while Figure 4.3c is less likely because only one of the D domains is attached to the surface, which makes the adsorbed structure mechanically unstable on the surface. Thus, we believe that at t= 900 s, the fibrinogen adsorbed on silicone oil adopts a bent structure as that shown in Figure 4.3b with a (tilt=150, twist=120) orientation.

T	900 s		1200 s		1500 s		1800 s	
	ssp	ppp	ssp	ppp	ssp	ppp	ssp	ppp
Offset	-9.876E-5	0.05810	-0.01540	0.01270	-0.02840	-0.01580	-0.03930	-0.03760
NR	0.1088	0.06050	0.09930	0.1011	0.1032	0.1193	0.09930	0.1304
A1	14.22	23.23	21.57	30.09	25.08	34.04	27.77	36.81
x01	1643	1649	1644	1645	1644	1643	1644	1642
w1	24.54	24.13	24.58	25.07	24.49	25.33	25.07	25.56

Table 4.1 Fitting parameters of the SFG spectra of fibrinogen on silicone oil at t = 900 s, 1200 s, 1500 s, and 1800 s shown in Figure 4.1.

To appreciate the similarity of the calculated spectra and the reconstructed experimental data with the highest matching score at t = 900 s, both the calculated spectra and the reconstructed experimental spectra are shown in Figure 4.4. Figure 4.4a and 4.4b show the matching qualities of the spectral features for the ssp and ppp spectra respectively. Figure 4.4c and 4.4d show the matching quality of the ssp/ppp spectral intensity. Both spectral features and intensity ratio are well matched.

Similar method used for analyzing the t = 900 s data can be used to analyze the SFG spectra collected at t = 1200 s, 1500 s, and 1800 s. The final matching score heat maps with the highest matching scores for each time are shown in the Figure 4.5-4.7, with the spectral comparisons between the calculated spectra and reconstructed experimental data with the highest matching

scores. The highest matching scores of each fibrinogen conformation at each time step are listed in Table 4.2.

From Table 4.2, it shows that fibrinogen tends to adopt a bent structure rather than a linear structure after 900 s of the adsorption on silicone oil. The adsorbed fibrinogen molecules adopt a bent structure with a smaller bent angle (30 deg) or more linear when t = 900 s and 1200 s, and becomes slightly more bent (45 deg) after t = 1500 s. Here Fibrinogen-30° and Fibrinogen-45° structures were the most likely conformations at t=900 - 1200 s and t = 1500 - 1800s, respectively, because they have the largest matching scores. This result shows that the strong hydrophobic interaction between fibrinogen and silicone oil can induce the fibrinogen molecules to adopt a more bent structure as time increases, similar to what we observed for fibrinogen adsorption on hydrophobic fluorinated and silicone polymer surfaces previously.[12, 27]

Fibrinogen Structure	Highest Matching Score at Time (t) after the Adsorption			
	t=900s	t=1200s	t=1500s	t=1800s
Original	0.1116	0.09002	0.1025	0.1072
Fibrinogen-30°	**0.1423**	**0.2128**	0.1459	0.1330
Fibrinogen-45°	0.1185	0.1968	**0.1604**	**0.1384**
Fibrinogen-60°	0.08219	0.05906	0.05276	0.05143
Fibrinogen-90°	0.1083	0.1468	0.1155	0.1043

Table 4.2 Highest matching scores of calculated spectra based on different fibrinogen structures with the reconstructed resonant SFG spectra collected at different times during the fibrinogen adsorption process.

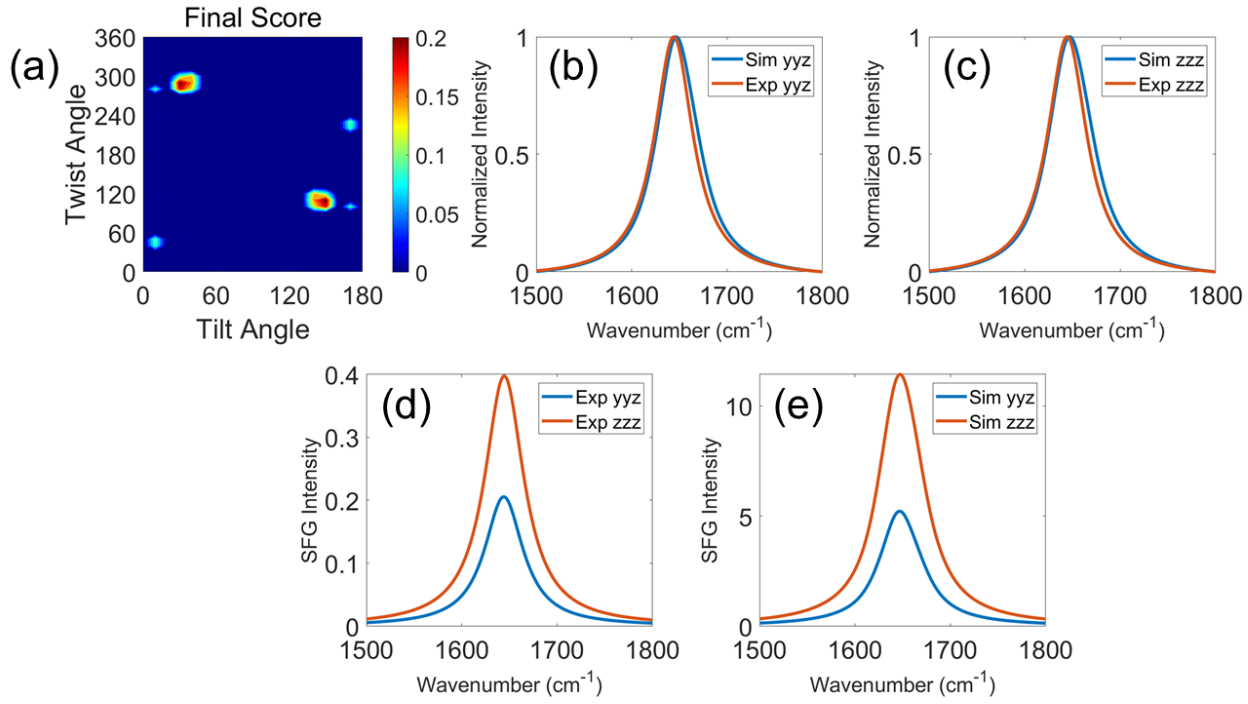


Figure 4.5 (a) The final matching score heat map showing the matching quality between the reconstructed resonant SFG experimental spectra (at **t = 1200 s**) and the calculated orientation dependent SFG spectra based on the **Fibrinogen-30°** structure. The blue spectra in (b) and (c) show the calculated SFG yyz (b) and zzz (c) spectra of adsorbed fibrinogen after 1200 s adsorption with the highest matching score with the reconstructed experimental resonant SFG spectra (shown in orange). The unnormalized SFG spectra of (d) experimental data and (e) calculated spectra are plotted for evaluating the matching quality of the ssp and ppp spectral intensity ratio.

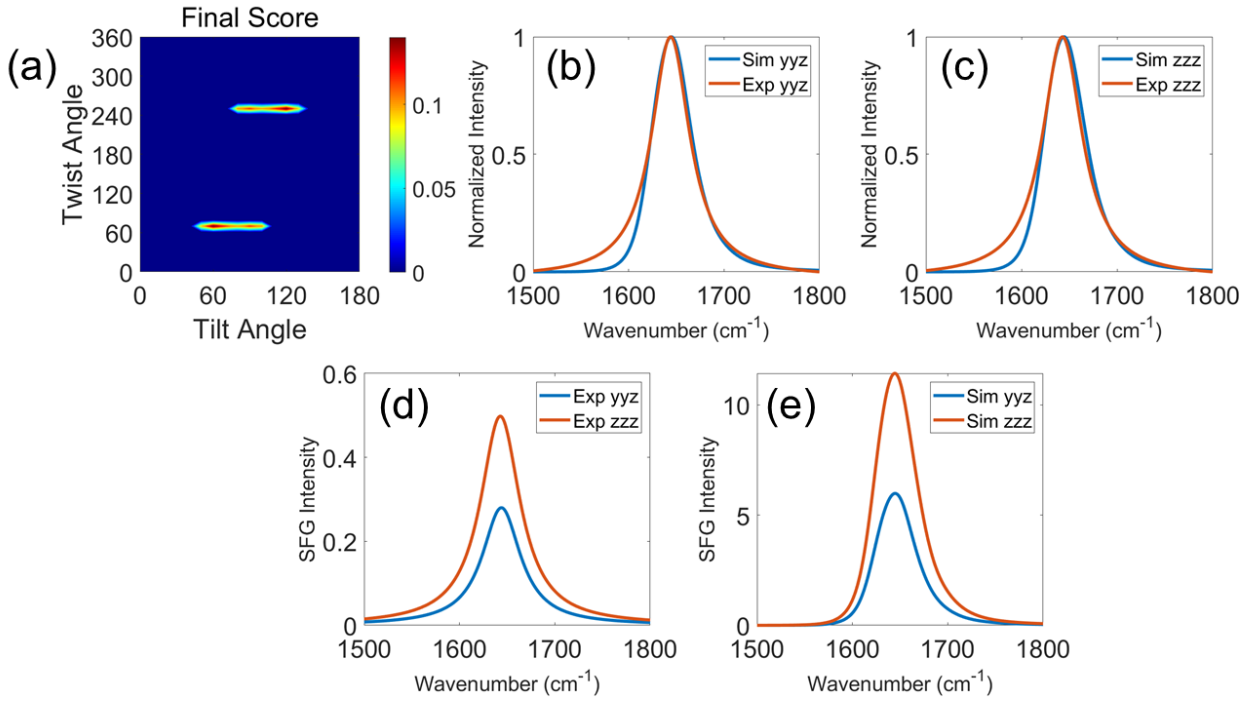


Figure 4.6 (a) The final matching score heat map showing the matching quality between the reconstructed resonant SFG experimental spectra (at **t = 1500 s**) and the calculated orientation dependent SFG spectra based on the **Fibrinogen-45°** structure. The blue spectra in (b) and (c) show the calculated SFG yyz (b) and zzz (c) spectra of adsorbed fibrinogen after 1500 s adsorption with the highest matching score with the reconstructed experimental resonant SFG spectra (shown in orange). The unnormalized SFG spectra of (d) experimental data and (e) calculated spectra are plotted for evaluating the matching quality of the ssp and ppp spectral intensity ratio.

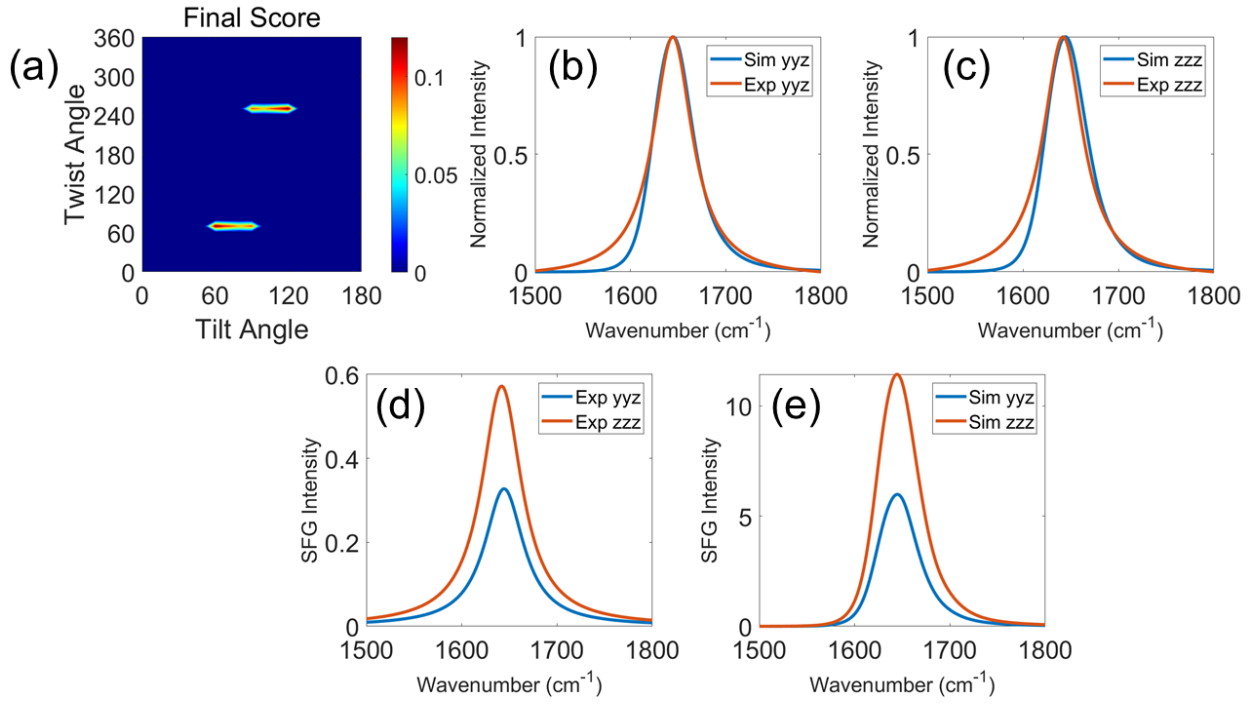


Figure 4.7 (a) The final matching score heat map showing the matching quality between the reconstructed resonant SFG experimental spectra (at **t = 1800 s**) and the calculated orientation dependent SFG spectra based on the **Fibrinogen-45°** structure. The blue spectra in (b) and (c) show the calculated SFG yyz (b) and zzz (c) spectra of adsorbed fibrinogen after 1800 s adsorption with the highest matching score with the reconstructed experimental resonant SFG spectra (shown in orange). The unnormalized SFG spectra of (d) experimental data and (e) calculated spectra are plotted for evaluating the matching quality of the ssp and ppp spectral intensity ratio.

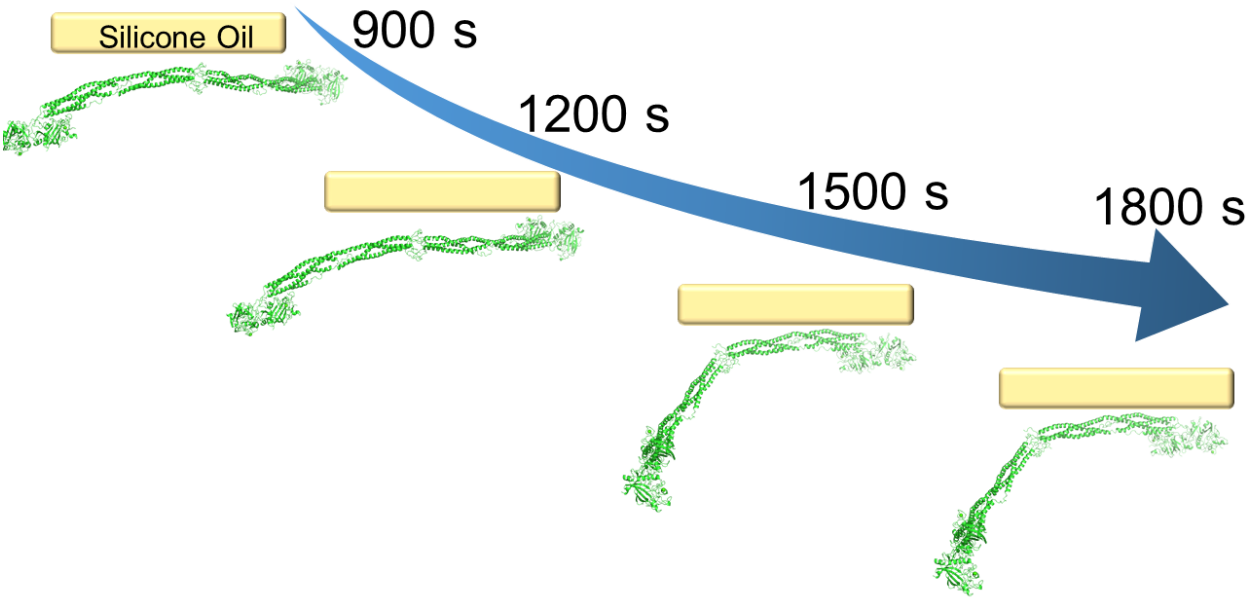


Figure 4.8 The most probable orientations of fibrinogen on silicone oil at different times during the adsorption process.

The deduced most probable orientations of the adsorbed fibrinogen molecules during the adsorption process on silicone oil are plotted in Figure 4.8. It can be clearly seen that the adsorbed fibrinogen molecules tend to lie down on the silicone oil surface at the initial stage of adsorption, and they can stand up more on the surface later. Possibly at first there are less adsorbed fibrinogen molecules, thus each molecule has more space. Later when more fibrinogen molecules were adsorbed, it is too crowded for the molecules to lie down.

4.3.3 Surface Coverage Analysis Result

The SFG signal intensity is affected by the number density and the orientation of the molecules, which can be shown as the following equation:

$$I \propto \left(\chi_{eff}^{(2)}\right)^2 = \left(Ns \cdot \beta_H^{(2)}\right)^2 \quad (1)$$

Here, $\chi_{eff}^{(2)}$ is the effective second order nonlinear optical susceptibility, which is obtained from the fitting results of the experimental spectra. Ns is the number density of the interfacial molecules, and $\beta_H^{(2)}$ is the SFG hyperpolarizability obtained from the fitting results of the calculated spectra using the Hamiltonian method. Here this SFG hyperpolarizability contains the orientation information along with the hyperpolarizability defined in the molecular frame. Therefore the orientation change of molecules will greatly affect the $\beta^{(2)}$ value.

The molecular number density Ns and the orientation can both contribute to the SFG signal intensity. When the orientation effect is known, it is then possible to get some information regarding the interfacial molecular number density. In this study, we have not calibrated the absolute SFG signal intensity, therefore we cannot deduce the absolute adsorption amounts of fibrinogen on silicone oil at different adsorption times. Here we want to determine the relative

adsorption amounts of fibrinogen at different times. Equation (1) can be used for evaluating the relative coverages of fibrinogen at different times during the adsorption process:

$$\frac{\chi^{(2)}_{eff,1}}{\chi^{(2)}_{eff,2}} = \frac{Ns_1 \cdot \beta^{(2)}_{H,1}}{Ns_2 \cdot \beta^{(2)}_{H,2}} \quad (2)$$

By comparing the $\chi^{(2)}_{eff}$ and $\beta^{(2)}_{H}$ values at different adsorption times, we can calculate the number density ratios of the adsorbed fibrinogen molecules. The $\chi^{(2)}_{eff}$ and $\beta^{(2)}_{H}$ values of the deduced orientation at each time step are shown in the Table 4.3. We assume the coverage of fibrinogen on silicone oil at t = 1800 s is 100%, and then we are able to calculate the coverage percentages of fibrinogen at t = 900 s, 1200 s, and 1500 s. The results of the fibrinogen coverages deduced by using the ssp and ppp measurements are shown in Table 4.3. The results from the ssp and ppp spectra are not identical, because the spectral fittings for the calculated SFG spectra may contain some minor errors, also the ppp/ssp intensity ratios for the reconstructed experimental spectra and the best-matched calculated spectra can be slightly different. Nevertheless, the fibrinogen coverage results determined from the ssp and ppp spectra are quite similar. We used the average number of the data deduced from ssp and ppp spectra as the relative coverage for each time point. Table 4.3 clearly shows that the fibrinogen coverage on silicone oil increases as a function of adsorption time.

	t=900s	t=1200s	t=1500s	t=1800s
$\chi^{(2)}_{eff,ssp}$	0.5749	0.8730	1.019	1.103
$\beta^{(2)}_{H,ssp}$	2.633	2.298	2.553	2.553
$Ns\ /\ Ns_{final}, ssp$	50.8%	87.8%	92.2%	100%*

$\chi^{(2)}_{eff,ppp}$	0.9626	1.202	1.345	1.442
$\beta^{(2)}_{H,ppp}$	4.575	3.413	3.533	3.533
$Ns\ /\ Ns_{final}, ppp$	51.5%	86.3%	93.3%	100%*

Table 4.3 Effective second order nonlinear optical susceptibility $\chi^{(2)}_{eff}$ and calculated $\beta^{(2)}_{H}$ values at different times during the adsorption. The coverage percentages of fibrinogen on silicone oil calculated by assuming 100% coverage at t=1800s and deconvoluting the orientation effect.

We were not able to fit the SFG spectra collected from fibrinogen for t < 900 s because of the low signal intensity. Instead of using fitted $\chi^{(2)}_{eff}$, we used the square root of the peak intensity integral from 1600 to 1750 cm^{-1} as $\chi^{(2)}_{eff}$ to measure the relative adsorption amounts or relative surface coverages at t = 300 s, t = 600 s, and t = 900 s. Since we know the relative surface coverages at t = 900 s deduced above, we could determine the relative surface coverages of t=300 s and t = 600 s. Here, we assumed the adsorbed fibrinogen molecules during the initial adsorption process have a constant orientation from t = 300 s to 900 s and the change of SFG signal intensity is only affected by the adsorption amount. For example, the relative coverage at t = 600 s can be calculated by dividing the square root of the peak intensity at t = 600 s by that at t = 900 s then multiplying by the coverage percentage deduced at t = 900 s above. The calculated relative coverage results for ssp and ppp measurements at t = 300 s and 600 s are shown in Table 4.4.

	t=300s	t=600s	t=900s
Sqrt of Peak Integral (ssp)	1.100	1.517	3.065
Relative Coverage (%)	18.6%	25.2%	50.8%*

Sqrt of Peak Integral (ppp)	2.545	3.757	5.141
Relative Coverage (%)	23.6%	34.1%	51.5%*

Table 4.4 Relative surface coverage percentages of the adsorbed fibrinogen on silicone oil at t = 300 s and 600 s of the adsorption.

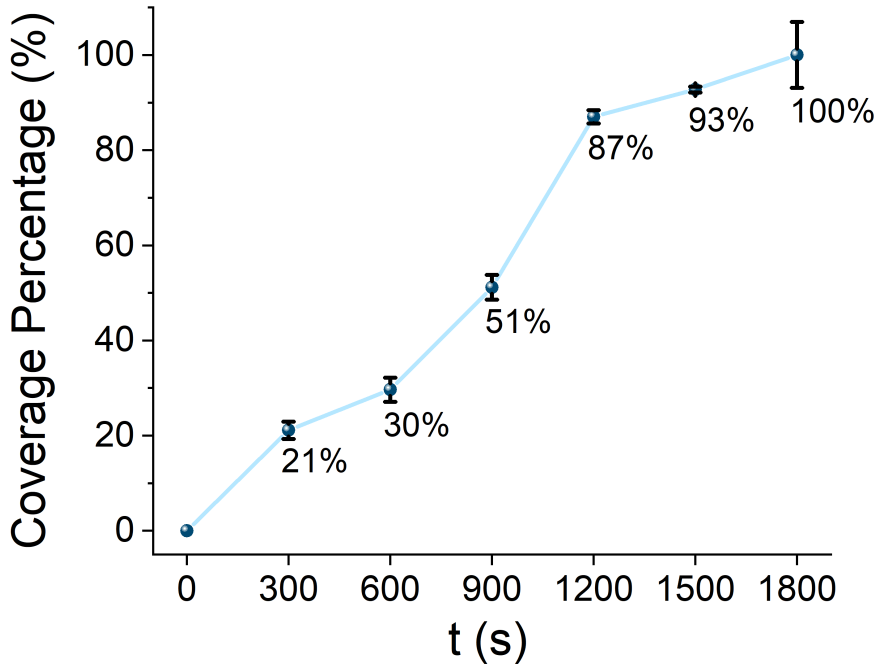


Figure 4.9 Surface coverage percentages of adsorbed fibrinogen on the silicone oil surface during the adsorption process.

The deduced surface coverage results from the ssp and ppp spectra for t = 300 s (also t = 600 s) are larger than those shown above for later times (t >= 900 s), likely showing that the adsorbed fibrinogen orientations changed in the early adsorption stage. They are not very different, thus we believe that they could provide semi-quantitative results on the fibrinogen surface coverages at t = 300 s and t = 600 s. The relative surface coverage results for all the time points were averaged and plotted in Figure 4.9. The trend in the coverage percentage plot clearly indicates

that the amount of the adsorbed fibrinogen molecules on silicone oil increases as a function of time and slowly approaches the equilibrium. Figure 4.9 shows that at t = 1800 s, surface coverage still continuously increases. The kinetics of fibrinogen adsorption may be influenced by both the adsorption/desorption balance at the interfaces as well as the diffusion of fibrinogen from bulk to interface. Our adsorption experiment was conducted using a static solution, which takes some time for protein to diffuse to the interface.

4.4 Conclusion

Fibrinogen adsorption at interface has been investigated extensively using many different analytical tools. For the first time, the orientation and conformation changes of fibrinogen during the interfacial adsorption process have been deduced in situ in real time by SFG, with the help of Hamiltonian SFG data analysis method. At the silicone oil/fibrinogen solution interface, the adsorption amount of fibrinogen increases as a function of time, and the adsorption kinetics can be monitored in real time with SFG. More importantly, it was found that fibrinogen molecules change conformations during the adsorption process. They do not adopt the crystal structure, instead they adopt bent structures on silicone oil. In addition to the conformational changes, orientation changes of adsorbed fibrinogen were also observed. For t = 900 s and t = 1200 s, fibrinogen adopts similar conformation and orientation, The detailed SFG data analysis shows that during this time period, one coiled coil slightly bends (by 30 degrees) towards the other coiled coil, with a more or less lying down orientation. The adsorption amounts are relatively small during this period of time; thus one fibrinogen molecule can have more space to have a more or less lying down orientation and stretched conformation. As time goes by, at t = 1500 s and t = 1800 s, the adsorbed fibrinogen molecule bends even more, with 45-degree bending of one coiled coil towards the other coil. This coiled-coil “stands up” more on the silicone oil surface. For these cases, more

fibrinogen was adsorbed, therefore each molecule has less space with a more compact structure. For all the cases, one coiled-coil contacts the silicone oil surface, enabling a stable structure of the adsorbed fibrinogen.

This study successfully elucidates the molecular structure including conformation and orientation of fibrinogen using in situ SFG study. Fibrinogen molecular structural changes were monitored in real time and the adsorption amount was deduced at the same time. The method developed in this research is general, which can be applied to study the adsorption process of many proteins in situ in real time at the molecular level.

4.5 References

1. Bajpai, A., Fibrinogen adsorption onto macroporous polymeric surfaces: correlation with biocompatibility aspects. *Journal of Materials Science: Materials in Medicine* **2008,** *19* (1), 343-357.

2. Horbett, T. A., Biological activity of adsorbed proteins. *Surfactant science series* **2003,** *110*, 393-413.

3. Castner, D. G.; Ratner, B. D., Biomedical surface science: Foundations to frontiers. *Surface Science* **2002,** *500* (1-3), 28-60.

4. Tang, L.; Thevenot, P.; Hu, W., Surface chemistry influences implant biocompatibility. *Current topics in medicinal chemistry* **2008,** *8* (4), 270-280.

5. Amara, I.; Miled, W.; Slama, R. B.; Ladhari, N., Antifouling processes and toxicity effects of antifouling paints on marine environment. A review. *Environmental toxicology and pharmacology* **2018,** *57*, 115-130.

6. Chen, S.; Li, L.; Zhao, C.; Zheng, J., Surface hydration: Principles and applications toward low-fouling/nonfouling biomaterials. *Polymer* **2010,** *51* (23), 5283-5293.

7. Wang, H.; Christiansen, D. E.; Mehraeen, S.; Cheng, G., Winning the fight against biofilms: the first six-month study showing no biofilm formation on zwitterionic polyurethanes. *Chemical science* **2020,** *11* (18), 4709-4721.

8. Society, A. C., *Proteins at Interfaces III State of the Art*. ACS Publications: 2012.

9. Zhao, X.; Pan, F.; Cowsill, B.; Lu, J. R.; Garcia-Gancedo, L.; Flewitt, A. J.; Ashley, G. M.; Luo, J., Interfacial immobilization of monoclonal antibody and detection of human prostate-specific antigen. *Langmuir* **2011,** *27* (12), 7654-7662.

10. Lu, J., Neutron reflection study of globular protein adsorption at planar interfaces. *Annual Reports Section" C"(Physical Chemistry)* **1999,** *95*, 3-46.

11. Wang, X.; Wang, Y.; Xu, H.; Shan, H.; Lu, J. R., Dynamic adsorption of monoclonal antibody layers on hydrophilic silica surface: A combined study by spectroscopic ellipsometry and AFM. *Journal of colloid and interface science* **2008,** *323* (1), 18-25.

12. Clarke, M. L.; Wang, J.; Chen, Z., Conformational changes of fibrinogen after adsorption. *The Journal of Physical Chemistry B* **2005,** *109* (46), 22027-22035.

13. Green, R.; Davies, J.; Davies, M.; Roberts, C.; Tendler, S., Surface plasmon resonance for real time in situ analysis of protein adsorption to polymer surfaces. *Biomaterials* **1997,** *18* (5), 405-413.

14. Glassford, S. E.; Byrne, B.; Kazarian, S. G., Recent applications of ATR FTIR spectroscopy and imaging to proteins. *Biochimica et Biophysica Acta (BBA)-Proteins and Proteomics* **2013,** *1834* (12), 2849-2858.

15. Lv, Y.; Qin, Y.; Svec, F.; Tan, T., Molecularly imprinted plasmonic nanosensor for selective SERS detection of protein biomarkers. *Biosensors and Bioelectronics* **2016,** *80*, 433-441.

16. Szekeres, G. P.; Kneipp, J., SERS probing of proteins in gold nanoparticle agglomerates. *Frontiers in Chemistry* **2019**, 30.

17. Kyrle, P. A.; Eichinger, S., Deep vein thrombosis. *The Lancet* **2005,** *365* (9465), 1163-1174.

18. Kakkar, V. V.; de Lorenzo, F., 4 Prevention of venous thromboembolism in general surgery. *Bailliere's clinical haematology* **1998,** *11* (3), 605-619.

19. Collins, R.; Scrimgeour, A.; Yusuf, S.; Peto, R., Reduction in fatal pulmonary embolism and venous thrombosis by perioperative administration of subcutaneous heparin. *New England Journal of Medicine* **1988,** *318* (18), 1162-1173.

20. Kearon, C., Epidemiology of postoperative venous thromboembolism: lessons from an administrative data base. *Thrombosis and haemostasis* **2003,** *90* (09), 367-368.

21. Lee, A. Y.; Levine, M. N.; Baker, R. I.; Bowden, C.; Kakkar, A. K.; Prins, M.; Rickles, F. R.; Julian, J. A.; Haley, S.; Kovacs, M. J., Low-molecular-weight heparin versus a coumarin for the prevention of recurrent venous thromboembolism in patients with cancer. *New England journal of medicine* **2003,** *349* (2), 146-153.

22. Dowling, N.; Austin, H.; Dilley, A.; Whitsett, C.; Evatt, B.; Hooper, W., The epidemiology of venous thromboembolism in Caucasians and African‐Americans: the GATE Study 1. *Journal of Thrombosis and Haemostasis* **2003,** *1* (1), 80-87.

23. Wang, J.; Clarke, M. L.; Chen, X.; Even, M. A.; Johnson, W. C.; Chen, Z., Molecular studies on protein conformations at polymer/liquid interfaces using sum frequency generation vibrational spectroscopy. *Surface Science* **2005,** *587* (1-2), 1-11.

24. Clarke, M. L.; Chen, Z., Polymer surface reorientation after protein adsorption. *Langmuir* **2006,** *22* (21), 8627-8630.

25. Wang, J.; Chen, X.; Clarke, M. L.; Chen, Z., Vibrational spectroscopic studies on fibrinogen adsorption at polystyrene/protein solution interfaces: hydrophobic side chain and secondary structure changes. *The Journal of Physical Chemistry B* **2006,** *110* (10), 5017-5024.

26. Wang, J.; Lee, S.-H.; Chen, Z., Quantifying the ordering of adsorbed proteins in situ. *The Journal of Physical Chemistry B* **2008,** *112* (7), 2281-2290.

27. Liu, Y.; Jasensky, J.; Chen, Z., Molecular interactions of proteins and peptides at interfaces studied by sum frequency generation vibrational spectroscopy. *Langmuir* **2012,** *28* (4), 2113-2121.

28. Kearns, V. R.; Williams, R. L., Drug delivery systems for the eye. *Expert review of medical devices* **2009,** *6* (3), 277-290.

29. Jones, L. S.; Kaufmann, A.; Middaugh, C. R., Silicone oil induced aggregation of proteins. *Journal of pharmaceutical sciences* **2005,** *94* (4), 918-927.

30. Thirumangalathu, R.; Krishnan, S.; Ricci, M. S.; Brems, D. N.; Randolph, T. W.; Carpenter, J. F., Silicone oil-and agitation-induced aggregation of a monoclonal antibody in aqueous solution. *Journal of pharmaceutical sciences* **2009,** *98* (9), 3167-3181.

31. Vázquez‐Rey, M.; Lang, D. A., Aggregates in monoclonal antibody manufacturing processes. *Biotechnology and bioengineering* **2011,** *108* (7), 1494-1508.

32. Gerhardt, A.; Bonam, K.; Bee, J. S.; Carpenter, J. F.; Randolph, T. W., Ionic strength affects tertiary structure and aggregation propensity of a monoclonal antibody adsorbed to silicone oil–water interfaces. *Journal of pharmaceutical sciences* **2013,** *102* (2), 429-440.

33. Woods, C. E. Understanding therapeutic monoclonal antibody aggregation mechanisms through biophysical, biochemical and biological characterization of two types of immunoglobulin G dimers. University of Kansas, 2015.

34. McGuire, J. A.; Shen, Y. R., Ultrafast vibrational dynamics at water interfaces. *Science* **2006,** *313* (5795), 1945-1948.

35. Ghosh, A.; Smits, M.; Bredenbeck, J.; Bonn, M., Membrane-bound water is energetically decoupled from nearby bulk water: An ultrafast surface-specific investigation. *Journal of the American Chemical Society* **2007,** *129* (31), 9608-9609.

36. Bonn, M.; Bakker, H. J.; Ghosh, A.; Yamamoto, S.; Sovago, M.; Campen, R. K., Structural inhomogeneity of interfacial water at lipid monolayers revealed by surface-specific vibrational pump− probe spectroscopy. *Journal of the American Chemical Society* **2010,** *132* (42), 14971-14978.

37. Eftekhari-Bafrooei, A.; Borguet, E., Effect of hydrogen-bond strength on the vibrational relaxation of interfacial water. *Journal of the American Chemical Society* **2010,** *132* (11), 3756-3761.

38. Zhang, Z.; Piatkowski, L.; Bakker, H. J.; Bonn, M., Ultrafast vibrational energy transfer at the water/air interface revealed by two-dimensional surface vibrational spectroscopy. *Nature chemistry* **2011,** *3* (11), 888.

39. Hsieh, C.-S.; Campen, R. K.; Okuno, M.; Backus, E. H.; Nagata, Y.; Bonn, M., Mechanism of vibrational energy dissipation of free OH groups at the air–water interface. *Proceedings of the National Academy of Sciences* **2013,** *110* (47), 18780-18785.

40. Singh, P. C.; Nihonyanagi, S.; Yamaguchi, S.; Tahara, T., Interfacial water in the vicinity of a positively charged interface studied by steady-state and time-resolved heterodyne-detected vibrational sum frequency generation. *The Journal of chemical physics* **2014,** *141* (18), 18C527.

41. Pandey, R.; Usui, K.; Livingstone, R. A.; Fischer, S. A.; Pfaendtner, J.; Backus, E. H.; Nagata, Y.; Fröhlich-Nowoisky, J.; Schmüser, L.; Mauri, S., Ice-nucleating bacteria control the order and dynamics of interfacial water. *Science advances* **2016,** *2* (4), e1501630.

42. Tan, J.; Zhang, B.; Luo, Y.; Ye, S., Ultrafast Vibrational Dynamics of Membrane‐Bound Peptides at the Lipid Bilayer/Water Interface. *Angewandte Chemie* **2017,** *129* (42), 13157-13161.

43. Guo, W.; Zou, X.; Jiang, H.; Koebke, K. J.; Hoarau, M.; Crisci, R.; Lu, T.; Wei, T.; Marsh, E. N. G.; Chen, Z., Molecular Structure of the Surface-Immobilized Super Uranyl Binding Protein. *The Journal of Physical Chemistry B* **2021,** *125* (28), 7706-7716.

44. Lu, T.; Guo, W.; Datar, P. M.; Xin, Y.; Marsh, E. N. G.; Chen, Z., Probing protein aggregation at buried interfaces: distinguishing between adsorbed protein monomers, dimers, and a monomer–dimer mixture in situ. *Chemical Science* **2022,** *13* (4), 975-984.

45. Ding, B.; Laaser, J. E.; Liu, Y.; Wang, P.; Zanni, M. T.; Chen, Z., Site-specific orientation of an α-helical peptide ovispirin-1 from isotope-labeled SFG spectroscopy. *The Journal of Physical Chemistry B* **2013,** *117* (47), 14625-14634.

46. Ding, B.; Panahi, A.; Ho, J.-J.; Laaser, J. E.; Brooks III, C. L.; Zanni, M. T.; Chen, Z., Probing site-specific structural information of peptides at model membrane interface in situ. *Journal of the American Chemical Society* **2015,** *137* (32), 10190-10198.

Chapter 5 Investigation of Antibody Adsorption Behavior onto Silicone Oil Surface

5.1 Introduction

Antibody plays an essential role in the immune system of human body, which can bind to specific antigens with high efficiency and selectivity. In the recent years, antibody molecules including the lab-produced antibodies have been widely used as drugs to treat a variety of diseases including cancer.[1] Especially recently therapeutic antibodies have been developed to treat COVID-19 patients.[2-4] The function of an antibody is heavily dependent on its structure, including the dominant secondary structures. It is therefore critical to study antibody structure in different conditions to understand the structure-function relations, providing knowledge on how the drug efficiency can be improved based on the structure optimization.

In pharmaceutical industry, silicone oil is commonly used as lubricant on various surfaces, e.g. the inner surface of a pre-filled syringe. Antibody drugs in solution are commonly stored and administrated with such syringes, thus antibody drug molecules have opportunities to contact with silicone oil lubricant coating directly. Some studies have shown that interactions between silicone oil and antibody molecules can change protein structures and induce antibody aggregation, leading to the loss of antibody function, potentially causing unforeseen problems in practical use of antibody drugs, such as causing the immunogenicity risk.[5-9] Therefore, it is important to examine the adsorption behavior of antibody onto silicone oil surface and the following structural changes induced by the silicone oil interaction. Previously, the adsorption behavior of a monoclonal antibody (mAb) and a bispecific antibody (BsAb) on silicone oil surface and the effect of PS80 surfactant on such behavior has been successfully investigated by using sum frequency generation

vibrational spectroscopy (SFG) in situ and in real time, but no detailed molecular structural information of adsorbed proteins was deduced in such studies.[10] It is worth mentioning that mAb binds to only one antigen, and BsAb can bind to two different types of antigens. The molecular structures of mAb and BsAb used in this study are shown in Figure 5.2.

As presented in the previous chapters, the Hamiltonian local mode approximation method was developed to calculate SFG spectra to study molecular structure of an interfacial protein molecule such as a protein adsorbed on a surface from a contacting solution. The details of the Hamiltonian method have been reported elsewhere[11-14] and discussed in Chapter 2. The molecular structural information deduced by the Hamiltonian method includes the information of protein conformation (in combination with computer simulations) and orientation. For example, here by combining the Hamiltonian method and the collected SFG data of mAb and BsAb on silicone oil, the structural information of adsorbed mAb and BsAb at the molecular level can be deduced. This structural information of adsorbed antibodies will provide deep insight towards the basic understanding of the adsorption mechanism of proteins onto hydrophobic surfaces as well as the interfacial interactions.

To prevent adsorption of antibodies to silicone oil, surfactant molecules were added to the antibody solution to interact with protein molecules. This chapter will demonstrate that SFG study allows us to find the lowest possible effective concentration of surfactant PS80 in the antibody solution to prevent the adsorption of antibodies onto silicone oil surface, and the successful application of Hamiltonian method for deducing the molecular structure information of adsorbed antibody. The adsorption kinetics of BsAb onto silicone oil surface were monitored with different concentrations of PS80 in solution in situ and in real time. The antibody solutions without and with

different concentrations of PS80 were tested by SFG to reveal the effects of addition of surfactant and its concentration on the antibody adsorption behavior and kinetics.

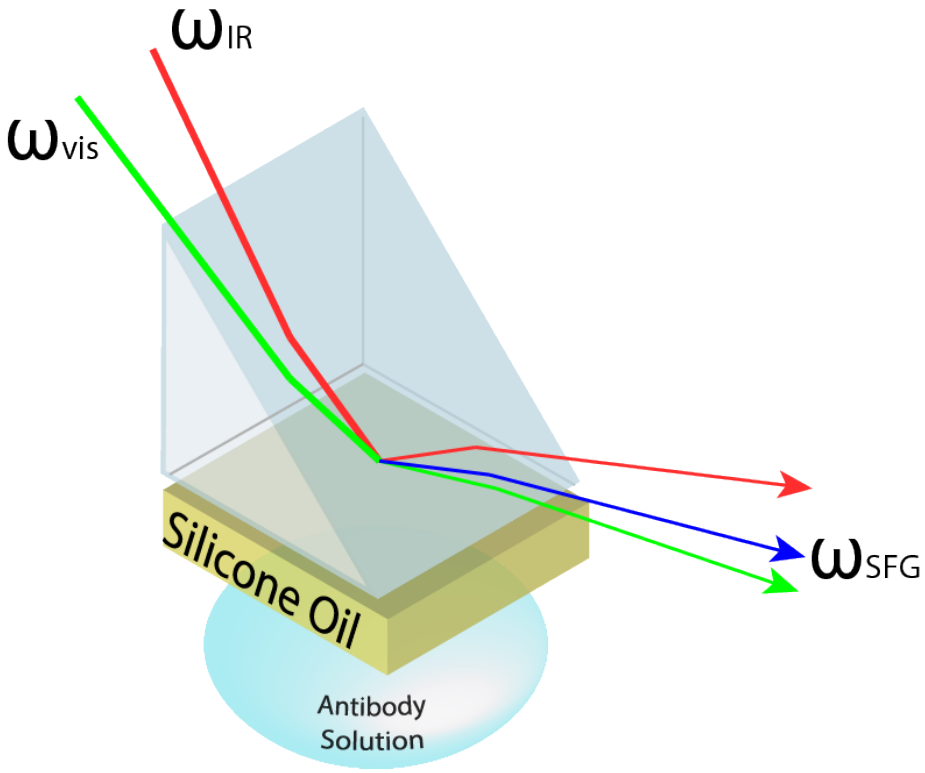
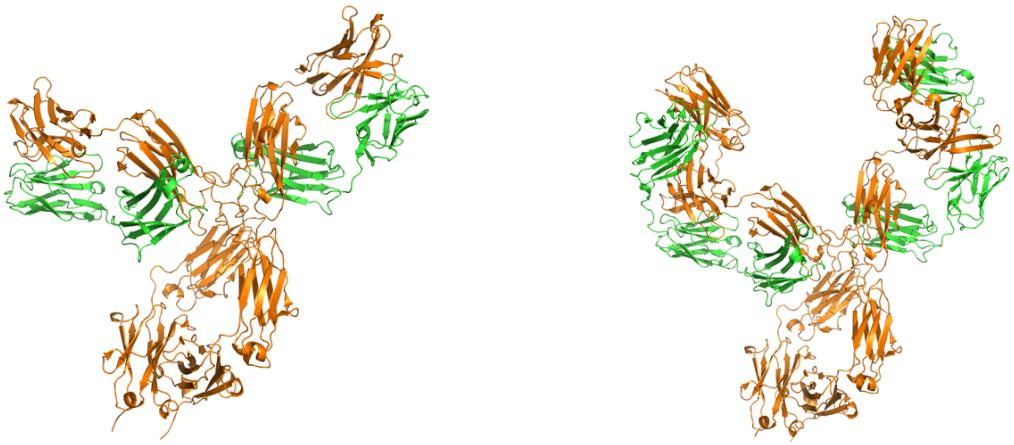


Figure 5.1 SFG sample geometry for monitoring the adsorption of antibodies on silicone oil. This sample geometry is the same as that used to study BSA adsorption, as shown in Figure 3.1.

It was found that the lowest possible effective concentrations for preventing two kinds of antibodies from adsorption to silicone oil surface are different. This indicates clearly that the adsorption affinity between different antibody products and silicone oil could be different. To effectively prevent the antibody adsorption on silicone oil, different surfactant concentrations may be required during the antibody drug formulation process. In this chapter, the structures of the adsorbed antibodies on silicone oil with and without surfactant in antibody solutions were also deduced. It was found that with surfactant, both antibodies (BsAb and mAb) could adopt solution conformations and their orientations on silicone oil can be deduced, which can be explained by hydrophobic interactions between the antibodies and the silicone oil surface. In contrast, without

surfactant, the calculated SFG spectra with the solution conformations of both antibodies could not well match the SFG data collected from antibodies on silicone oil, indicating that conformational changes occurred for the antibodies on silicone oil without surfactant caused by protein-surface interactions.



(a) Monoclonal Antibody (mAb)

(b) Bispecific Antibody (BsAb)

Figure 5.2 Structures of the monoclonal antibody (mAb) and the bispecific antibody (BsAb) used for Hamiltonian analysis.

5.2 Methods and Materials

5.2.1 Materials

Bispecific (BsAb) and monoclonal (mAb) antibodies, and PS80 surfactant were provided by Sanofi (Framingham, MA). The concentration of each antibody stock solution is 1.0 mg/mL. Acetate buffer (10 mM, pH=4.8) was prepared by using glacial acetic acid from J.T. Bakker (Radnor, PA), and NaOH from Sigma-Aldrich (St. Louis, MO). Medical-grade silicone oil (360 Medical Fluid 1000 Cst) was purchased from Dow Chemical Company (Midland, MI). Organic solvents including toluene, acetone, and methanol were purchased from Sigma-Aldrich (St. Louis,

MO) and used as received. Right-angle CaF_2 prisms were ordered from Altos Photonics Inc. (Bozeman, MT).

5.2.2 Silica-coated CaF_2 prisms

The same method used to prepare silica coated CaF_2 prisms as that presented in chapter 3 was used: The CaF_2 prisms were soaked in toluene for 24 h, immersed in acetone and methanol each for 10 mins, rinsed thoroughly by deionized water (18 MΩ·cm), and dried with nitrogen gas flow. Then the prisms were treated by oxygen and argon plasma (Glen 1000P Plasma Cleaner) to remove the organic contaminants. Next, the clean prisms were transferred into the chamber of Angstrom Engineering Evovac Evaporator to deposit a 100 nm of SiO_2 film on each CaF_2 prism via physical vapor deposition.

5.2.3 Preparation of silicone oil thin film

Silicone oil was dissolved in toluene and the concentration was 0.5 wt%. Then the solution was spin coated on silica-coated CaF_2 prisms at 2000 rpm for 30 s. The good silicone oil thin film quality was confirmed by measuring the SFG spectrum.[10, 15]

5.2.4 Preparation of antibody and surfactant mixture solutions

The antibody stock solution (1.0 mg/mL) was diluted to 0.6 mg/mL and 0.2 mg/mL for BsAb and mAb, respectively. A 4 wt% PS80 solution was made by sonicating the PS80 in deionized water, then was diluted to a series of different concentrations: 0.4 wt%, 0.04 wt%, and 0.004 wt%. After that a diluted antibody solution and a diluted PS80 solution were mixed with each other by equal volume to make an antibody-PS80 mixture solution.

5.2.5 SFG experiment setup

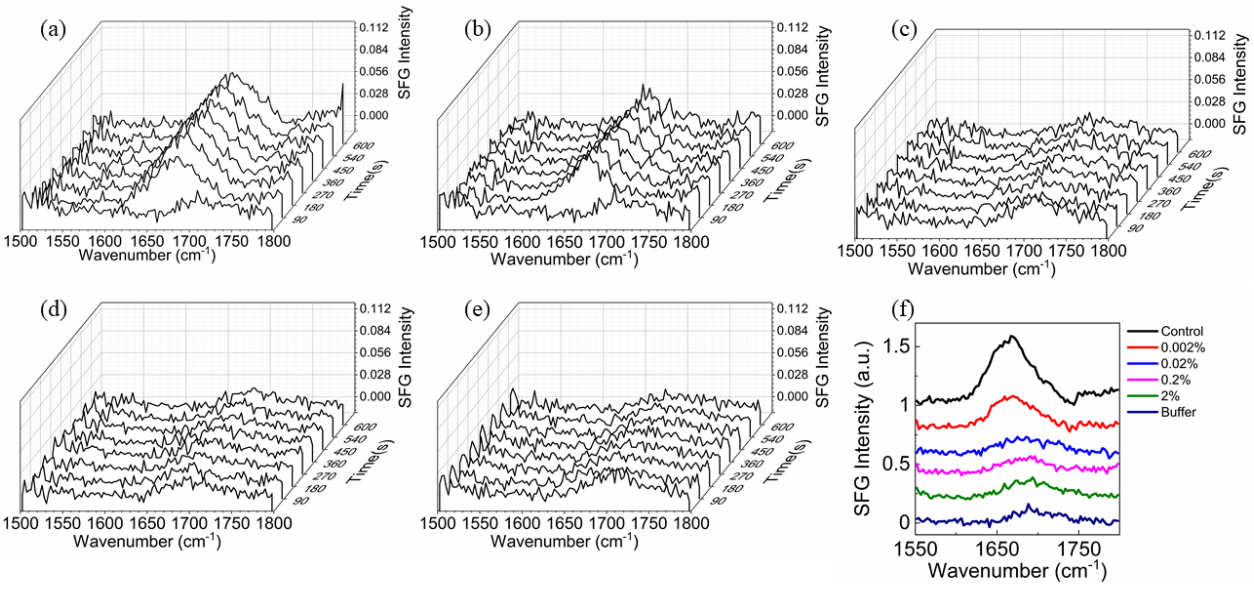
As presented in Chapter 1, SFG is a surface-sensitive characterization method that allows us to probe the structural information of molecules on surfaces or at interfaces,[16-21] which can be used to study the protein structure[15, 22-32] including antibody structure on silicone oil surface.[10] The details of SFG theory and instrumentation were presented in Chapter 1 and will not be repeated here. In this study, SFG spectra were collected from the silicone oil/solution interface (Figure 5.1) with the fs-SFG system.

5.3 Results and Discussion

5.3.1 Lowest possible effective concentration of PS80 to prevent antibody adsorption

To find the lowest possible effective concentration of PS80 that can completely prevent the antibody adsorption on silicone oil (refer to "adsorption prevention concentration"), different concentrations of PS80 were mixed with BsAb solution and tested. The signature SFG amide I signal (~1660 cm^{-1}) from the BsAb adsorbed at the silicone oil/protein solution interface and the optimized concentrations which can generate the highest SFG signal for both antibodies were previously reported by our group.[10] Therefore, in this study, the amide I signal (~1660 cm^{-1}) was selected as the indicator of the presence of antibody on silicone oil surface, and 0.3 mg/mL was chosen as the solution concentration of BsAb for SFG study. The SFG spectra collected from the interfaces between silicone oil and antibody solutions without and with different concentrations of PS80 are shown in Figure 5.3. Figure 5.3(a) shows the SFG spectra collected after the silicone oil surface was placed in contact with the BsAb solution without PS80 as a function of time. The amide I signals (~1660 cm^{-1}) from interfacial BsAb were clearly detected within 90 seconds, which indicates that BsAb could be adsorbed onto silicone oil surface very quickly. Figure 5.3(b) displays the time-dependent SFG spectra collected after the silicone oil surface was placed in contact with the BsAb solution with 0.002 wt% PS80. Similar to the case of the BsAb solution without PS80, the amide I signals (~1660 cm^{-1}) of BsAb were detected within 90 seconds, showing that BsAb could adsorb to the silicone oil surface quickly, therefore 0.002 wt% PS80 in the protein solution could not prevent

BsAb from adsorption to the silicone oil surface. Figure 5.3(c) shows the time-dependent SFG spectra collected after the silicone oil surface was placed in contact with the BsAb solution with 0.02 wt% PS80. Different from those shown in Figures 5.3(a) and 5.3(b), here no apparent amide I signals were detected, indicating that 0.02 wt% PS80 in the antibody solution could prevent the adsorption of BsAb to silicone oil. When the PS80 concentration further increased in the antibody solution, as shown in Figures 5.3(d) and 5.3(e), similar to the 0.02 wt% PS80 case, no BsAb amide I signals could be detected, showing the prevention of BsAb from adsorption to silicone oil. Figure 5.3(f) replots the SFG spectra collected from the silicone oil/BsAb solution (without and with PS80 of different concentrations) interfaces after the silicone oil was placed into contact with each solution for 10 mins. Figure 5.3(f) shows that the SFG amide I signal intensities from adsorbed antibody dropped when more PS80 was added to the antibody solutions for BsAb. Here, the lowest PS80 concentration when no SFG amide I signal could be detected from the silicone oil/antibody solution interface is defined as "the possible lowest effective PS80 concentration" that can possibly completely prevent the adsorption of antibody onto the silicone oil, or the "adsorption prevention concentration" of PS80. From Figure 5.3(f) and the above discussion, we can see that the possible lowest effective PS80 concentration to prevent BsAb adsorption is 0.02 wt%.



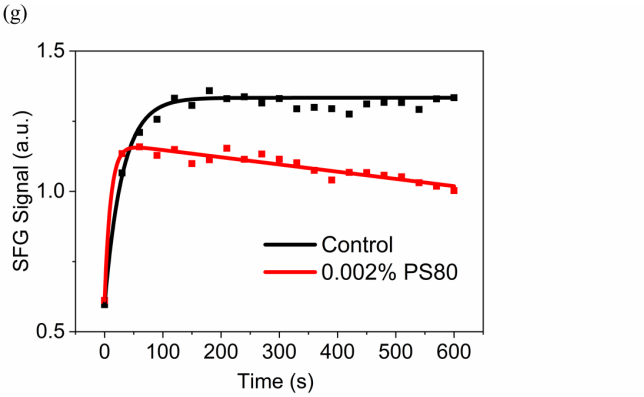


Figure 5.3 Time-dependent SFG ssp spectra collected from interfaces between silicone oil and BsAb without or with PS80 of different concentrations after the silicone oil surface was placed into contact with the solution: (a) no PS80, (b) 0.002 wt% PS80, (c) 0.02 wt% PS80, (d) 0.2 wt% PS80, (e) 2 wt% PS80 during the adsorption process. (f) SFG ssp spectra collected from the interfaces between silicone oil and BsAb solutions after the silicone oil was placed in contact with each solution for 10 mins. (g) Time-dependent SFG signal (calculated by peak integral) of amide I mode for BsAb without (black dots) or with 0.002 wt% PS80 (red dots). The lines are the fitted results. Each first spectrum shown at time zero in Figures (a) to (e) was collected from silicone oil/buffer solution (without BsAb) for comparison. Other spectra shown in these figures at 90 seconds or later were collected after the silicone oil was placed in contact with BsAb solutions without or with PS80. Each of these spectra is an averaged spectrum of three consecutively collected spectra (each collected with 30 seconds). The SFG signal shown in (g) is the signal from each 30-second spectrum.

5.3.2 Adsorption kinetics of BsAb onto Silicone Oil

The time dependent SFG signal intensities of the SFG amide I peak are shown in Figure 5.3(g) to compare the adsorption kinetics of BsAb onto silicone oil without PS80 and with 0.002 wt% PS80 in the solution. The half-life time of SFG signal increase of each sample is listed in Table 5.1, which shows the quantitative adsorption kinetics of the antibodies onto silicone oil. By comparing the half-life time listed in Table 5.1 and the time dependent SFG signal plot displayed in Figure 5.3(g), we can see that 0.002 wt% PS80 in the antibody solution substantially accelerated the adsorption kinetics of BsAb molecules.

It is interesting to observe that in Figure 5.3(g), when 0.002 wt% PS80 was present in the BsAb solution, the SFG antibody signal increased very fast initially with a gradual intensity

decrease later, indicating slow desorption or re-orientation of BsAb on silicone oil occurred with the presence of surfactant. Without PS80, no such a signal decrease was observed. The possible desorption/reorientation of BsAb on silicone oil shows that the interaction or binding between BsAb and silicone oil is not extremely strong with the presence of PS80.

It is worth mentioning that the absence of SFG signal detection from antibody at the interface for higher PS solution concentrations may be caused by the absence of protein adsorption, or the denaturation of the protein or the random orientation of the interfacial protein. We will show later that most likely in this study, the absence of the protein SFG signal is due to the lack of protein adsorption.

Antibody solution Composition	Signal Increase Half-life Time $t_{1/2}$ (s)
BsAb Control	24.64
BsAb + 0.002% PS80	7.67

Table 5.1 Half-life time of SFG signal increase of BsAb with and without PS80 in the solution.

5.3.3 Orientation analysis of BsAb by Hamiltonian method

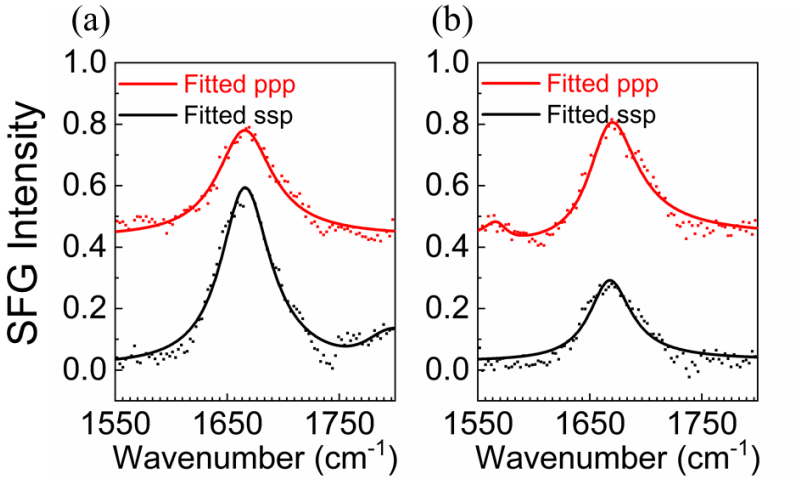


Figure 5.4 SFG spectra and the fitting results of (a) BsAb, and (b) BsAb with 0.002% PS80 mixture solution in contact with silicone oil for 10 mins. Dots are experimental data, and lines are fitting results.

Figures 5.4(a) and 5.4(b) show the ssp and ppp SFG spectra collected from the silicone oil/BsAb solution (without and with 0.002 wt% PS80) interfaces after 10 mins contact, along with the spectral fitting results. The fitting parameters for the spectra shown in Figure 5.4 are presented in Table 5.2. By comparing Figures 5.4(a) and 5.4(b), we can see that the ssp/ppp spectra intensity ratios are different, showing that the structure of adsorbed BsAb was greatly affected by PS80. The antibody structure plays an essential role for determining the interaction with silicone oil during the adsorption process and likely affects the "adsorption prevention concentration" of PS80.

	mAb without PS80		mAb+0.002 wt% PS80		BsAb without PS80		BsAb+0.002 wt% PS80	
	ssp	ppp	ssp	ppp	ssp	ppp	ssp	ppp
Offset	2.184E-4	-7.81E-3	-1.26E-3	-0.0121	0.0185	0.0319	0.0299	0.0245
NR	4.36E-3	0.0262	-5.45E-3	-0.0132	0.0727	0.0137	0.0232	0.0659
A1	6.106	3.349	7.003	2.562	20.17	17.65	11.68	15.90
x01	1659	1658	1666	1662	1665	1665	1667	1667
w1	17.22	17.82	24.67	14.04	27.10	29.92	22.86	26.38

Table 5.2 Fitting parameters of the SFG spectra (shown in Figure 5.4 and Figure 5.8) of BsAb and mAb on silicone oil without and with 0.002% PS80 in the protein solution.

To further understand the structure of the antibodies adsorbed on the silicone oil surface, the Hamiltonian data analysis method was applied to deduce the orientation of interfacial antibodies. As discussed in detail in the Chapter 2 above, this method computes the nonlinear response of each amino acid and coupling effect between each other by using the transition dipole model.[11-14] In the previous studies in our group, Bei et al. successfully used this method to study the structural disorder of a peptide, ovispirin-1, with the help of isotope-labeling.[13] Here, this Hamiltonian method was used to deduce the interfacial orientations of proteins, the results of which can be used to correlate the protein adsorption phenomenon to the adsorbed antibody structure.

As we presented in Chapter 2, the computer program with the Hamiltonian method can read a PDB file and then simulate the SFG amide I spectrum of a protein with a particular interfacial orientation collected with a certain polarization combination. This computer software has been developed to calculate the SFG spectra collected with different polarization combinations such as ppp and ssp as a function of interfacial protein orientation by rotating the protein. In this study, the protein orientation was varied in the range of the tilt angle from 0 to 180 degree, and the range of the twist angle from 0 to 360. The angle step size in calculation for both the tilt and twist angle is 10 degrees. In this study, the PDB structure of mAb and BsAb that were used as the input parameters for calculating SFG spectra were provided by Sanofi, as shown in Figure 5.2. Different chains are rendered in different colors for better visualization in Figure 5.2.

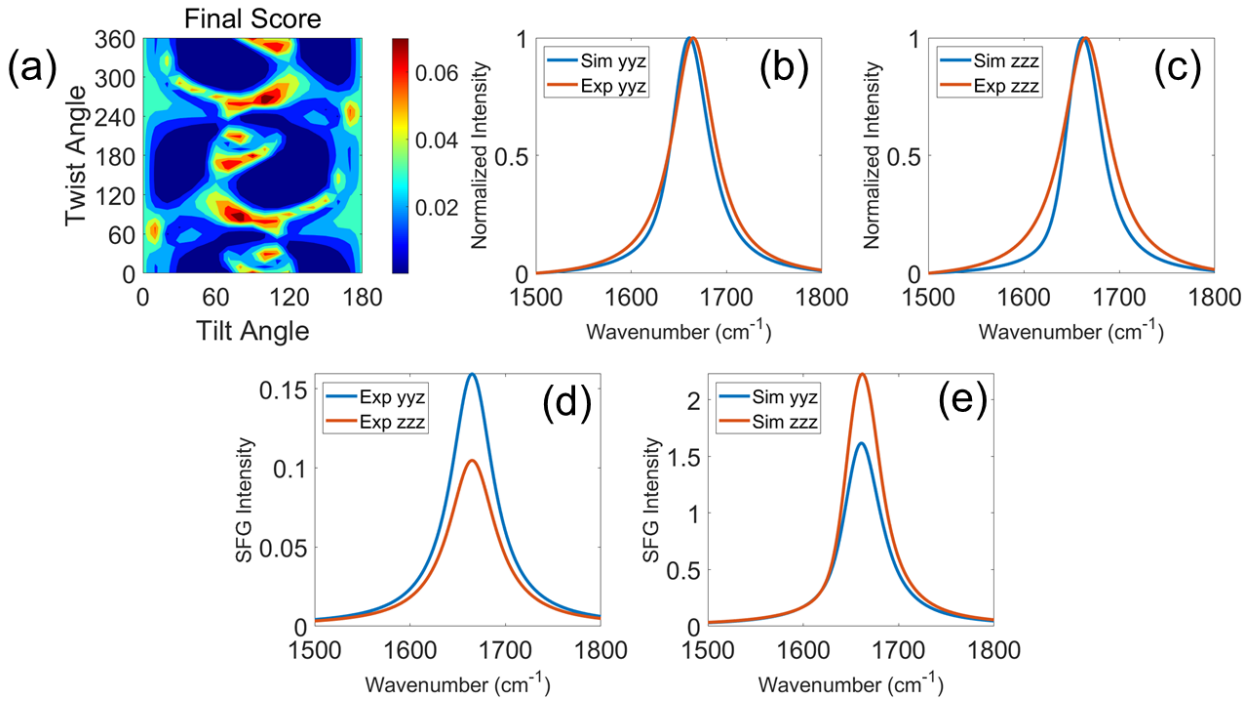


Figure 5.5 Matching qualities between the experimental data and calculated spectra of BsAb on silicone oil without PS80: (a) Heat map showing the matching quality between the reconstructed resonant SFG spectra of BsAb and the calculated spectra. The blue spectra in (b) and (c) show the calculated SFG yyz (b) and zzz (c) spectra of BsAb with the best matching quality with the reconstructed resonant SFG spectra (shown in red). The SFG spectra shown in (d) are replotted fitted experimentally collected SFG spectra. The spectra shown in (e) are calculated SFG yyz (blue) and zzz (red) spectra with the best matching quality. The matching qualities of the spectral features can be seen from (b) and (c), while the matching quality for the ssp/ppp intensity ratio can be seen from (d) and (e).

In this study, to find the most probable antibody orientation, the calculated SFG spectra and the reconstructed resonant spectra from experimental data are normalized in intensity (with the highest signal in the spectrum) to make the spectral feature comparison for ssp or ppp spectrum. The details of the Hamiltonian matching process have been discussed in Chapter 2 and will not be repeated here. The most likely antibody orientation can be determined by an overall heat map which combines the heat maps for ssp spectrum, ppp spectrum, and ssp/ppp signal strength ratio.

First, we studied the BsAb adsorption onto silicone oil without PS80 in the protein solution. Figure 5.4(a) shows the fitting results of experimental data collected from the interfaces between BsAb solution and silicone oil. The fitted spectra contain nonresonant contribution, which needs to be removed to compare the experimental data to the calculated spectra. The reconstructed SFG resonant experimental spectra are shown in red in Figures 5.5(b) and 5.5(c). With the Hamiltonian method we described above and the BsAb solution structure, we can calculate SFG spectra of BsAb as a function of orientation, and compare the calculated spectra to the fitted experimental spectra to generate the matching heat map. Figure 5.5 shows the overall heat map with the three comparison standards (Figure 5.5(a)), and the comparison between the calculated and reconstructed experimental spectra of BsAb on silicone oil without PS80 with the highest matching score (Figures 5.5(b) and 5.5(c)). The matching qualities for the spectral features and intensity ratios of BsAb on silicone oil without PS80 are poor. Especially the ssp/ppp intensity ratios of the simulated and observed spectra do not match at all (comparing Figures 5.5(d) and 5.5(e)). The calculated zzz spectrum has a higher intensity than that of calculated yyz spectrum. Oppositely, the experimentally collected yyz spectrum is more intense than the zzz spectrum. As we mentioned above, the simulated SFG spectra were calculated based on the BsAb solution structure provided by Sanofi. The vast differences between the calculated and experimental SFG spectra for the

orientation with the highest matching score show that the antibody structure used for calculation may not be reasonable, indicating that the molecular structure of BsAb on silicone oil likely is not the same as that in solution. This may be because of the strong interaction between BsAb and silicone oil, which led to substantial BsAb structural change on silicone oil. To obtain better matching quality between the calculated and observed SFG spectra, a different BsAb structure should be used for spectral calculation using the Hamiltonian method. We believe that it is necessary to perform molecular dynamics (MD) simulation to obtain more reasonable structural models of BsAb on silicone oil by taking the antibody-silicone oil interaction into account. Since BsAb conformation likely changed due to the surface interaction, all-atom simulation is not appropriate in this study because it is difficult to capture the protein conformational changes. Coarse-grain MD simulation can possibly provide more stabilized antibody structure on silicone oil to improve the matching result between the calculated and observed SFG spectra, which is beyond this study and should be performed in the future.

We then studied the adsorption of BsAb onto silicone oil with 0.002 wt% PS80 in the protein solution. As we presented above, at this low PS80 solution concentration, complete prevention of BsAb adsorption to silicone oil did not occur, thus SFG signals could be detected from BsAb adsorbed on silicone oil. The collected SFG spectra along with the fitting results from the silicone oil/BsAb solution (with 0.002 wt% PS80) are shown in Figure 5.4(b) presented above. The reconstructed resonant SFG spectra from experimental data are shown in red in Figures 5.6(b) and 5.6(c).

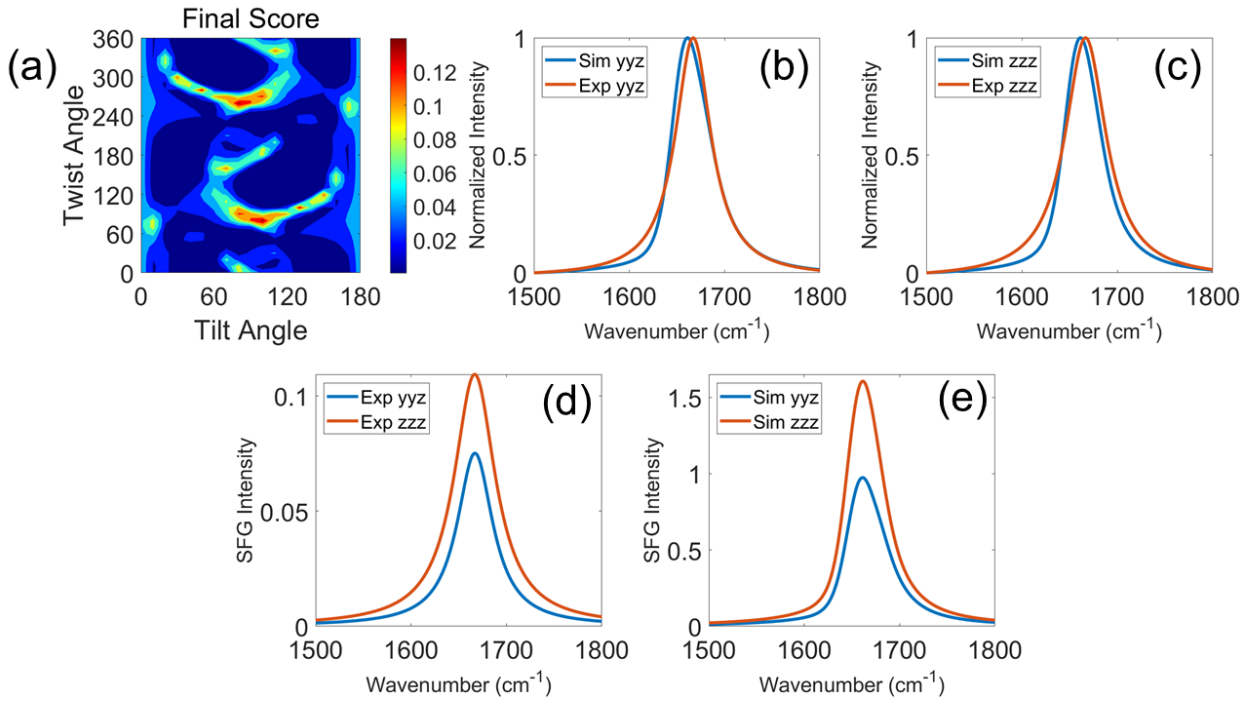


Figure 5.6 Matching qualities between the experimental data and calculated spectra of BsAb on silicone oil with PS80: (a) Heat map showing the matching quality between the reconstructed resonant SFG spectra of BsAb and the calculated spectra. The blue spectra in (b) and (c) show the calculated SFG yyz (b) and zzz (c) spectra of BsAb with the best matching quality with the reconstructed resonant SFG spectra (shown in red). The SFG spectra shown in (d) are replotted fitted experimental spectra. The spectra shown in (e) are calculated SFG yyz (blue) and zzz (red) spectra with the best matching quality. The matching qualities of the spectral features can be seen from (b) and (c), while the matching quality for the ssp/ppp intensity ratio can be seen from (d) and (e).

Figure 5.6 shows the Hamiltonian analysis result of BsAb on silicone oil with 0.002 wt% PS80 in the solution based on the BsAb solution structure. Different from the matching results shown in Figure 5.5 above for BsAb without PS80, here the matching qualities between the simulated and experimentally measured SFG spectra are quite good. Both the ssp and ppp spectra have well matched spectral features (Figures 5.6(b) and 5.6(c)), along with similar ppp/ssp intensity ratios (Figures 5.6(d) and 5.6(e)). Apparently, the BsAb solution structure serves as a good model for the BsAb structure on silicone oil with the presence of small amount of PS80 in the solution, which can generate calculated SFG spectra well matched the experimental data. This shows that PS80 does interact with BsAb on silicone oil to preserve the BsAb structure. The deduced orientation of BsAb on silicone oil is shown in Figure 5.7, which is a "stand-up"

orientation. More detailed discussions on the adsorbed antibody orientation will be presented later, along with the quantitative analysis of the surface property of adsorbed BsAb molecules by calculating the solvent accessible surface area (SASA).

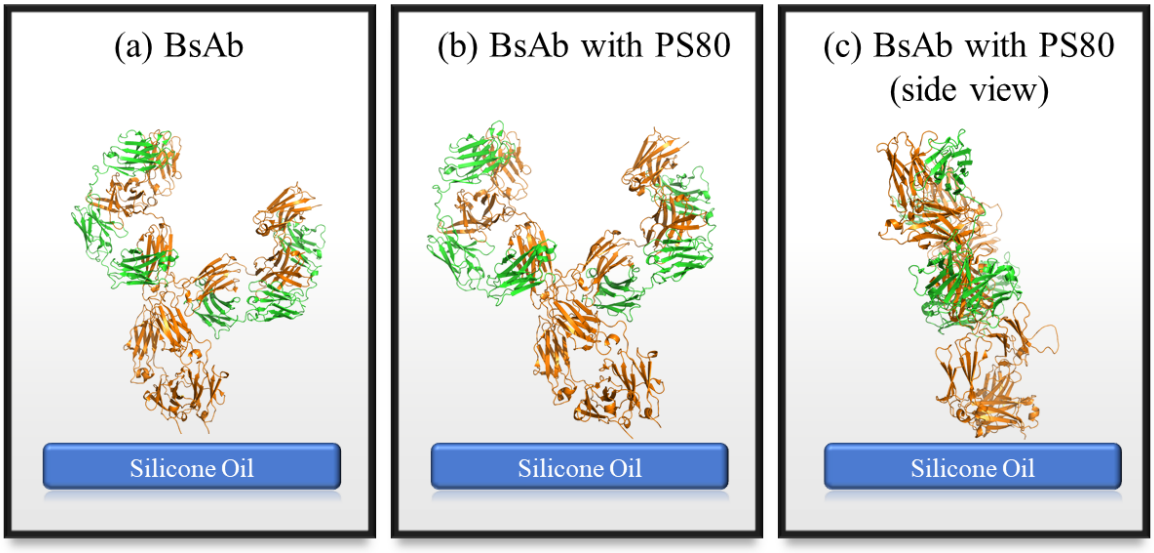


Figure 5.7 The deduced most likely orientations of BsAb on silicone oil (a) without PS80 in solution, (b) with 0.002 wt% PS80 in solution in "front view" and (c) with 0.002 wt% PS80 in solution in "side view".

5.3.4 Orientation analysis of mAb by Hamiltonian method

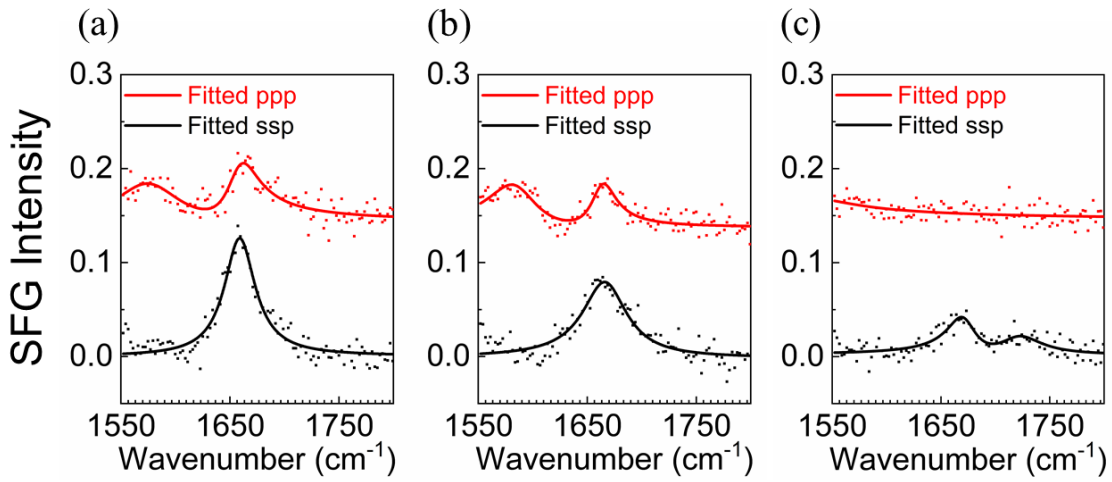


Figure 5.8 SFG spectra and fitting results of interfaces between solutions of (a) mAb, (b) mAb with 0.002% PS80, (c) mAb with 0.02% PS80 and silicone oil. Dots are experimental data, and lines are fitting results.

In addition to the adsorption of BsAb on silicone oil, we also studied adsorption of mAb on silicone oil. Figure 5.8 shows the SFG spectra collected from the silicone oil/mAb solution (without and with 0.002 wt% as well as 0.02 wt% PS80) interfaces along with the fitting results. The fitting parameters are presented in Table 5.2. As what we did above, the Hamiltonian method was also used to study adsorbed mAb structure on silicone oil from the antibody solution without and with 0.002 wt% PS80. We calculated the mAb SFG spectra as a function of orientation and compared these calculated spectra with experimentally measured data. We studied the mAb solution without PS80 first. Figure 5.9(a) shows the matching quality heat map. The reconstructed resonant experimental SFG spectra from the silicone oil/mAb solution (without PS80) interface are shown in red in Figures 5.9(b) and 5.9(c), which do not match the calculated spectra (with the highest matching score) well. Also similar to the BsAb case, the zzz/yyz intensity ratios of the calculated and experimental data do not match. The simulated SFG zzz spectrum has a similar intensity to the yyz spectrum. Oppositely, the collected zzz spectrum has a substantially lower intensity than the yyz spectrum. As we discussed above for BsAb, here we believe that the solution structure of mAb is not a good model for mAb structure on silicone oil. The interactions between the silicone oil and mAb caused the mAb structure to change on silicone oil.

We then studied the adsorption of mAb onto silicone oil from the mAb solution with 0.002 wt% PS80. Figure 5.10(a) shows that matching quality heat map. Figures 5.10(b) and 5.10(c) show that the calculated spectra match the spectral features of the experimental data very well. Figures 5.10(d) and 5.10(e) indicate that the ppp/ssp spectral intensity ratio of the simulated and experimentally matches with each other. Similar to the BsAb case presented above, here with the presence of 0.002 wt% PS80, the matching qualities are much better than those of the mAb without PS80. This shows that with the presence of PS80, the mAb solution structure can serve as a good

model for the mAb structure on silicone oil. The different behavior of mAb on silicone oil with and without PS80 demonstrates that PS80 interacts with mAb on silicone oil, similar to the BsAb case. The most likely orientation of the mAb adsorbed on silicone oil is shown in Figure 5.11, which is a "stand-up" orientation. More detailed discussions on adsorbed mAb orientation on silicone oil will be presented below.

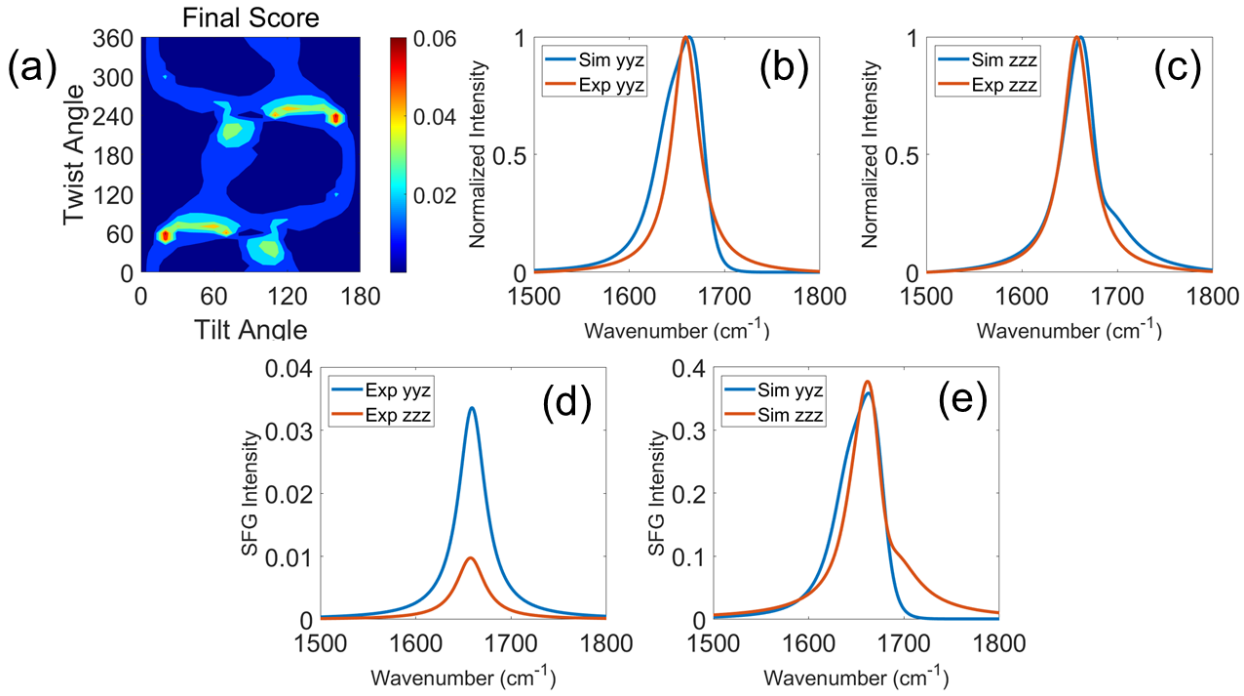


Figure 5.9 Matching qualities between the experimental data and calculated spectra of mAb on silicone oil without PS80: (a) Heat map showing the matching quality between the reconstructed resonant SFG spectra of mAb and the calculated SFG spectra. The blue spectra in (b) and (c) show the calculated SFG yyz (b) and zzz (c) spectra of mAb with the best matching quality with the reconstructed resonant SFG spectra (shown in red). The SFG spectra shown in (d) are replotted fitted experimental spectra. The spectra shown in (e) are calculated SFG yyz (blue) and zzz (red) spectra with the best matching quality. The matching qualities of the spectral features can be seen from (b) and (c), while the matching quality for the ssp/ppp intensity ratio can be seen from (d) and (e).

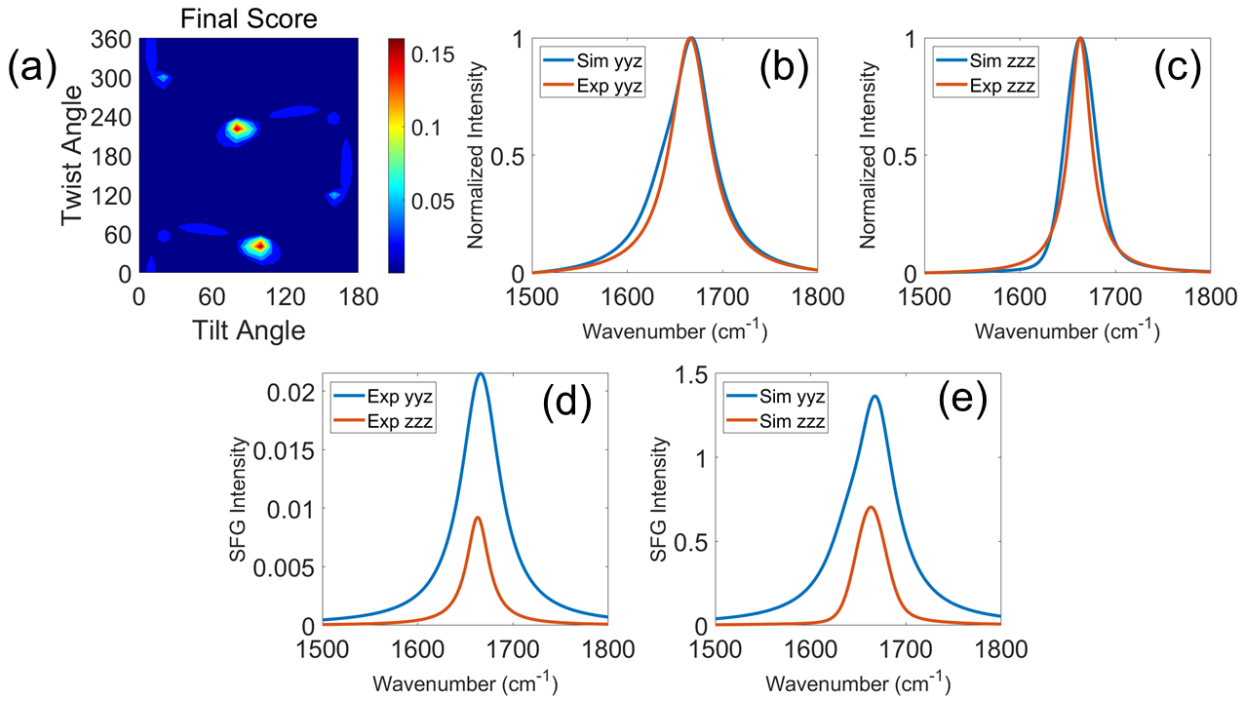


Figure 5.10 Matching qualities between the experimental data and calculated spectra of mAb on silicone oil with PS80: (a) Heat map showing the matching quality between the reconstructed resonant SFG spectra of mAb and the calculated SFG spectra. The blue spectra in (b) and (c) show the calculated SFG yyz (b) and zzz (c) spectra of mAb with the best matching quality with the reconstructed resonant SFG spectra (shown in red). The SFG spectra shown in (d) are replotted fitted experimental spectra. The spectra shown in (e) are calculated SFG yyz (blue) and zzz (red) spectra with the best matching quality. The matching qualities of the spectral features can be seen from (b) and (c), while the matching quality for the ssp/ppp intensity ratio can be seen from (d) and (e).

When the concentration of PS80 was increased to 0.02% in mAb solution (as shown in Figure 5.8(c)), the SFG ppp amide I signal was not detected, thus we could not deduce the adsorbed mAb orientation. The SFG ssp amide I signal could still be obserevd from adsorbed mAb under this condition, indicating that the mAb adsorption is not completely prevented by 0.02% PS80 in the mixture. This result shows that mAb requires a higher concentration of PS80 to prevent the adsorption onto silicone oil than BsAb, suggesting the interaction between mAb and silicone oil may be stronger.

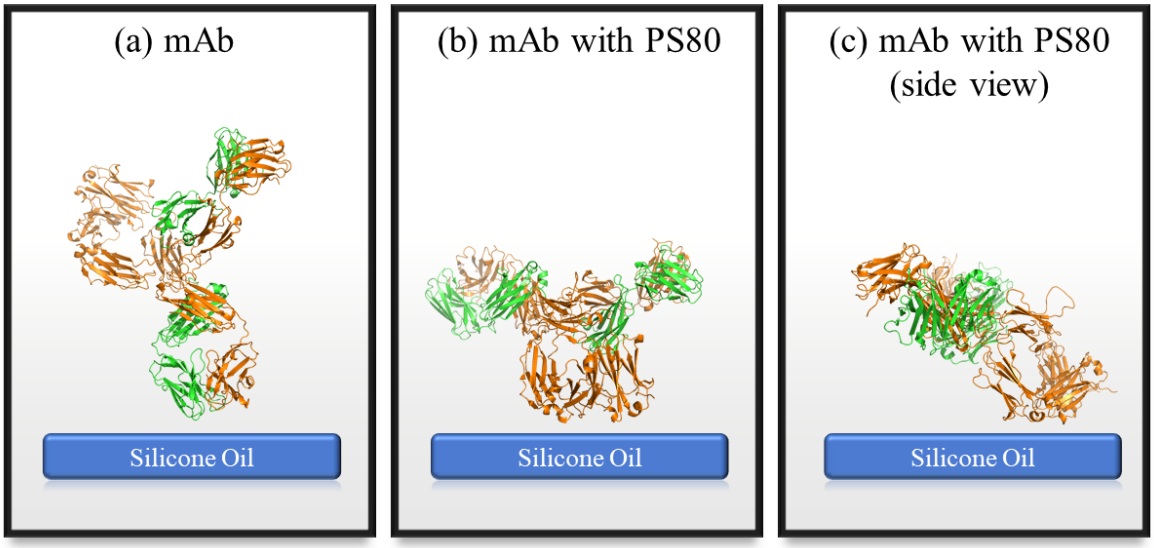


Figure 5.11 The deduced most likely orientations of mAb on silicone oil in contact with mAb solution (a) without PS80, (b) with 0.002 wt% PS80 in "front view" and (c) with 0.002 wt% PS80 viewed from a different angle in "side view".

Since the silicone oil surface is relatively hydrophobic, the adsorption of antibody to silicone oil is possibly mainly driven by the hydrophobic interaction. For a large protein such as an antibody, in aqueous solution the outer surface is mostly hydrophilic, and the inner core is generally more hydrophobic. The hydrophobic interaction between silicone oil and antibody may tend to expose the hydrophobic inner part of the antibody and denature the protein. Therefore, the structure of the adsorbed antibody in solution is different from that on the silicone oil, as we observed from adsorbed mAb and BsAb at the silicone oil/antibody solution (without PS80) interfaces. When a surfactant such as PS80 is present in the solution, the surfactant molecules can surround an antibody molecule and suppress the strong hydrophobic interaction between silicone oil and the inner core of the adsorbed antibody, therefore the adsorbed antibody on silicone oil could still maintain the molecular structure in solution without major conformational changes.

That is to say, the adsorbed mAb or BsAb is not antibody molecule alone, but antibody complexed with PS80 instead.

5.3.5 Solvent Accessible Surface Analysis of Adsorbed Antibody Structure

We refer the antibody orientation with the highest matching score as the most likely orientation of the antibody on silicone oil. The deduced orientations of adsorbed BsAb and mAb on silicone oil without and with 0.002 wt% PS80 in solution were plotted in Figure 5.7 and Figure 5.11 above, respectively. It is worth mentioning that the orientations shown in Figure 5.7(a) and 5.11(a) for BsAb and mAb without PS80 in solution were deduced from the best matching scores between the reconstructed experimentally collected and calculated SFG spectra, but overall the matching qualities for these two cases are quite low, as discussed above. This is due to the likely conformational changes of the antibodies adsorbed on silicone oil. The deduced orientations in both cases shown in Figures 5.7(a) and 5.11(a) only have one Fab fragment adsorbed to the silicone oil, which may not be mechanically stable. This further demonstrates that the deduced orientations are not reliable, again showing that likely the protein structures used for spectral calculation were not correct.

Figures 5.7(b), 5.7(c), 5.11(b), and 5.11(c) show the likely orientations of the adsorbed BsAb and mAb molecules on silicone oil surface with 0.002 wt% PS80 in antibody solution, deduced by the highest matching scores. Since the regular SFG experiment does not provide the absolute molecular orientation information, the silicone oil films (blue bars) in Figure 5.7 and Figure 5.11 can either be placed on the top of or at the bottom of the protein molecules, therefore the antibody adsorption domain on silicone oil is unclear. To identify the most likely protein orientation from the two opposite possible orientations for each case and to further understand the antibody adsorption mechanism at the molecular level, the solvent accessible surface areas

(SASAs) of the Fab and the Fc regions of adsorbed antibodies were calculated by VMD. Due to the hydrophobicity of the silicone oil surface, the main driving force of the antibody adsorption onto the silicone oil surface can be the hydrophobic interaction between the hydrophobic amino acid residues and the silicone oil surface. Since the absolute SASA value is proportional to the number of amino acids, the hydrophobic SASA result was normalized by dividing the hydrophobic SASA by the total SASA, i.e., the percentage of the hydrophobic SASA within the total SASA of the antibody domain.

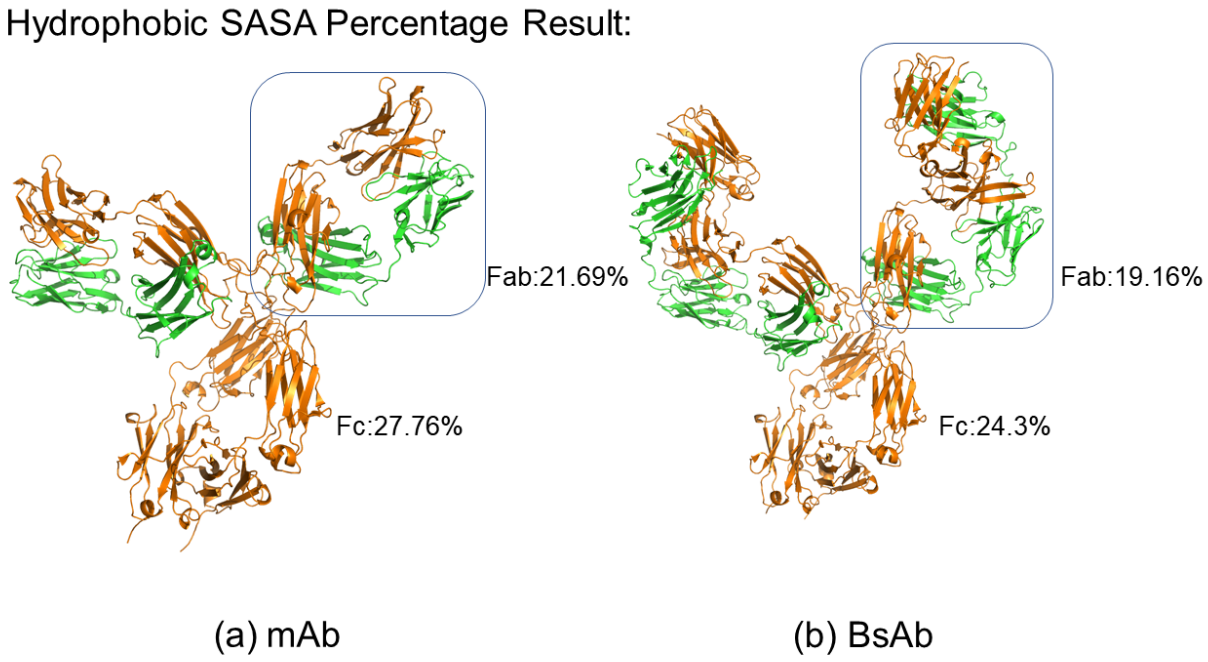


Figure 5.12 Hydrophobic SASA percentage calculation result of Fab and Fc fragments of (a) mAb and (b) BsAb.

	Hydrophobic SASA Value (Å^2)	Total SASA Value (Å^2)	Hydrophobic SASA percentage (%)
mAb, Fab	4224.75	19476.46	21.69
mAb, Fc	6263.23	22561.50	27.76
BsAb, Fab	5612.79	29293.46	19.16
BsAb, Fc	8940.10	36821.40	24.30

Table 5.3 Hydrophobic SASA calculation results of the Fab and Fc fragments in mAb and BsAb. The results are calculated by VMD with "-restrict" option, thus the amino acids that are buried inside the protein are excluded in the calculation.

The calculated hydrophobic SASA percentage results of the Fab and the Fc fragments of mAb and BsAb are shown in Figure 5.12, with the quantitative values listed in Table 5.3. The hydrophobic SASA percentages of Fab and Fc in mAb are 21.67% and 27.76%, respectively, while for BsAb, they are 19.16% and 24.30%, respectively. For the mAb protein molecule, the Fc fragment with a higher hydrophobic SASA percentage is more hydrophobic than the Fab fragment, thus it is likely that the Fc fragments of mAb are attached to the silicone oil surface (with a "stand-up" orientation) rather than the Fab fragments, as shown in Figures 5.11(b) and 5.11(c). In the case of BsAb, the Fc fragment with a higher hydrophobic SASA percentage is also more hydrophobic than the Fab fragment, so the main adsorption site of BsAb should also be a Fc fragment. By comparing the hydrophobic SASA percentages of Fc fragments SASA of mAb and BsAb, we can see that the Fc fragment of mAb (27.76%) is more hydrophobic than the Fc fragment of BsAb (24.30%). This difference in the major adsorption sites may lead to the different adsorption prevention concentration of PS80 for mAb and BsAb. As mentioned above, no significant protein SFG amide I signal could be detected from the silicone oil/BsAb solution (with 0.02 wt% PS80) interface (shown in Figure 5.4), while the SFG amide I peak in ssp could be observed from the silicone oil/mAb solution (with 0.02 wt% PS80) interface (shown in Figure 5.8). We believe that the prevention of adsorption of antibodies (onto silicone oil) with higher hydrophobic adsorption sites on the protein surface would require a higher concentration of PS80 in the solution. We believe that the deduced orientations of mAb and BsAb on silicone oil shown in Figures 5.7 and 5.11 are both reasonable, which can be explained by the protein-surface hydrophobic interaction and SASA calculation.

Besides the hydrophobic interaction, the charge interaction between antibody and silicone oil might also play a role. To quantify the charge interaction, the SASA values of positively

charged and negatively charged amino acids are calculated, as shown in Table 5.4. Since the silicone oil surface is slightly negatively charged,[33-34] more positive amino acids on the antibody surface can possibly induce stronger interaction during the antibody adsorption. Here, we use the ratio of positive SASA and negative SASA to describe the strength of charge interaction between antibody and silicone oil surface.

	Positive SASA (Å^2)	Negative SASA (Å^2)	Ratio of +/-
mAb, Fab	3853.59	2403.79	1.603
mAb, Fc	4898.85	3457.07	1.417
BsAb, Fab	5128.60	3558.73	1.441
BsAb, Fc	6789.60	5274.70	1.287

Table 5.4 Positive and negative SASA calculation result of the Fab and Fc fragments in mAb and BsAb.

The ratio of positive/negative SASA of the Fab and the Fc fragments in mAb are 1.603 and 1.417, respectively, while for BsAb are 1.441 and 1.287. We can clearly see that the Fab and Fc fragments of both mAb and BsAb are positively charged, and Fab fragments are more positively charged than Fc fragments in both mAb and BsAb. By comparing the ratios of the positive/negative SASA of Fab fragments of mAb and BsAb, we can see that the Fab fragments of mAb (1.603) are more positively charged than the Fab fragments of BsAb (1.441). This difference in the Fab fragments may lead to the different orientation of adsorbed mAb and BsAb. For mAb antibody molecules, after the Fc fragment was adsorbed onto the surface, the Fab fragments were more likely to get closer to the surface due to a stronger charge interaction, thus the adsorbed mAb antibody molecules tend to tilt more toward the surface. In the case of BsAb, the adsorbed BsAb antibody molecules tend to stand up freely since the charge interaction between the Fab fragments and the surface is weaker. We believe that the adsorption of antibodies is affected by the hydrophobic interaction and charge interaction. The hydrophobic interaction determines the major adsorption site of antibody molecules and adsorption stability (i.e. a higher concentration of PS80

is required to prevent the adsorption), while the charge interaction will affect the adsorbed orientation of antibodies.

As we presented above, we refer the PS80 concentration at which no SFG signal was observed from interfacial antibody as the adsorption prevention concentration of PS80. We believe that at this PS80 concentration in antibody solution, no protein can be adsorbed to the silicone oil surface, leading to the absence of SFG signal. The absence of SFG signal can also be caused by randomly oriented antibody at interface or complete denaturation of antibody structure at interface. From our SFG study results reported above, we know that with the presence of PS80, both adsorbed mAb and BsAb more likely adopt their solution structures. The adsorbed proteins with PS80 exhibited less conformational changes compared to the cases without PS80. Therefore we believe that PS80 helps to retain the native antibody structure on silicone oil surface rather than denature the adsorbed protein structure, thus the absence of SFG antibody signal is unlikely due to the complete denaturation of interfacial antibodies. The protein orientation study presented above demonstrated that both mAb and BsAb adopt well defined and preferred orientations on silicone oil with the presence of PS80. It is unlikely that more PS80 in the solution could lead to complete random orientation of antibodies on silicone oil. We therefore believe that in this study the absence of SFG signal from the antibody molecules on silicone oil is due to the lack of protein adsorption on silicone oil.

It is worth mentioning that the above SASA analysis on silicone oil – antibody interactions did not consider the effect of PS80 on the adsorbed antibodies. The real situation could be more complicated and may be able to be understood further by computer simulations of proteins and PS80 at the silicone oil/solution interfaces. This is beyond the scope of this thesis and should be researched in the future.

5.4 Summary

This chapter applied the developed Hamiltonian SFG spectral calculation method and SFG technique to investigate molecular adsorption of antibody molecules on silicone oil surface, and the effect of surfactant PS80 on such protein adsorption behavior. The SFG data on antibody adsorption shows that the adsorption behaviors of different antibodies onto silicone oil can be different, due to different interaction strengths of antibody with silicone oil. Because of such different interactions, different antibodies may require different minimum concentrations of PS80 in the antibody solution to fully prevent the antibody from adsorption onto the silicone oil surface. By using the Hamiltonian method and the protein solution structures, the orientations of BsAb and mAb adsorbed onto silicone oil with 0.002 wt% PS80 in antibody solution were successfully deduced. The adsorbed mAb and BsAb adopt a stand-up orientation. The solvent accessible surface area (SASA) analysis was conducted to quantify the hydrophobicity and positive charges of the Fab and Fc fragments of the antibodies, and the result shows that the hydrophobic and charge interaction between the antibody and silicone oil both affects the adsorption site of the antibodies thus influences the final orientation. Moreover, likely only hydrophobic interactions are related to the minimum concentration of PS80 for preventing antibody from adsorption.

Good matching qualities of the simulated and observed SFG spectra of the antibodies adsorbed on silicone oil with the presence of PS80 indicate that the model using antibody solution structures to calculate SFG spectra is reasonable. Therefore, under this condition no substantial conformation changes occurred after mAb and BsAb adsorbed to silicone oil, due to the surfactant PS80 protection. Differently, without PS80, no good matching can be found between the calculated and observed SFG spectra, showing that the protein solution structures used for spectra calculation are not correct. This indicates that substantial conformational changes of adsorbed antibodies on

silicone oil happened without the presence of PS80. Such antibody structural changes may lead to protein aggregation and consequently to lose the protein function.

This is the first time that the molecular structure of adsorbed antibody on silicone oil at liquid/liquid interface was successfully elucidated in situ in real time. Our studies show that surfactant can prevent antibody from adsorption to silicone oil when the concentration reaches a certain level. Below this level even though the surfactant molecules in antibody solution cannot completely prevent antibody from adsorption to silicone oil, they can prevent antibody structural changes on silicone oil, minimizing the loss of functions of antibody drugs. This knowledge is extremely important for optimizing the antibody drug formulation to prevent the loss of antibody drug function caused by silicone oil interaction.

5.5 References

1. Sedykh, S. E.; Prinz, V. V.; Buneva, V. N.; Nevinsky, G. A., Bispecific antibodies: design, therapy, perspectives. *Drug design, development and therapy* **2018,** *12*, 195.

2. Sharun, K.; Tiwari, R.; Iqbal Yatoo, M.; Patel, S. K.; Natesan, S.; Dhama, J.; Malik, Y. S.; Harapan, H.; Singh, R. K.; Dhama, K., Antibody-based immunotherapeutics and use of convalescent plasma to counter COVID-19: advances and prospects. *Expert opinion on biological therapy* **2020,** *20* (9), 1033-1046.

3. Ning, L.; Abagna, H. B.; Jiang, Q.; Liu, S.; Huang, J., Development and application of therapeutic antibodies against COVID-19. *International journal of biological sciences* **2021,** *17* (6), 1486.

4. Esmaeilzadeh, A.; Rostami, S.; Yeganeh, P. M.; Tahmasebi, S.; Ahmadi, M., Recent advances in antibody‐based immunotherapy strategies for COVID‐19. *Journal of Cellular Biochemistry* **2021,** *122* (10), 1389-1412.

5. Brych, S. R.; Gokarn, Y. R.; Hultgen, H.; Stevenson, R. J.; Rajan, R.; Matsumura, M., Characterization of antibody aggregation: role of buried, unpaired cysteines in particle formation. *Journal of pharmaceutical sciences* **2010,** *99* (2), 764-781.

6. Arakawa, T.; Alton, N. K.; Hsu, Y.-R., Preparation and characterization of recombinant DNA-derived human interferon-gamma. *Journal of Biological Chemistry* **1985,** *260* (27), 14435-14439.

7. Schellekens, H., Bioequivalence and the immunogenicity of biopharmaceuticals. *Nature reviews Drug discovery* **2002,** *1* (6), 457-462.

8. Rosenberg, A. S., Effects of protein aggregates: an immunologic perspective. *The AAPS journal* **2006,** *8* (3), E501-E507.

9. Jenkins, N.; Murphy, L.; Tyther, R., Post-translational modifications of recombinant proteins: significance for biopharmaceuticals. *Molecular biotechnology* **2008,** *39* (2), 113-118.

10. Perera, H. G.; Lu, T.; Fu, L.; Zhang, J.; Chen, Z., Probing the Interfacial Interactions of Monoclonal and Bispecific Antibodies at the Silicone Oil–Aqueous Solution Interface by Using Sum Frequency Generation Vibrational Spectroscopy. *Langmuir* **2019,** *35* (44), 14339-14347.

11. Hamm, P.; Zanni, M., *Concepts and methods of 2D infrared spectroscopy*. Cambridge University Press: 2011.

12. Ding, B.; Laaser, J. E.; Liu, Y.; Wang, P.; Zanni, M. T.; Chen, Z., Site-specific orientation of an α-helical peptide ovispirin-1 from isotope-labeled SFG spectroscopy. *The Journal of Physical Chemistry B* **2013,** *117* (47), 14625-14634.

13. Ding, B.; Panahi, A.; Ho, J.-J.; Laaser, J. E.; Brooks III, C. L.; Zanni, M. T.; Chen, Z., Probing site-specific structural information of peptides at model membrane interface in situ. *Journal of the American Chemical Society* **2015,** *137* (32), 10190-10198.

14. Guo, W.; Zou, X.; Jiang, H.; Koebke, K. J.; Hoarau, M.; Crisci, R.; Lu, T.; Wei, T.; Marsh, E. N. G.; Chen, Z., Molecular Structure of the Surface-Immobilized Super Uranyl Binding Protein. *The Journal of Physical Chemistry B* **2021,** *125* (28), 7706-7716.

15. Li, Y.; Pan, D.; Nashine, V.; Deshmukh, S.; Vig, B.; Chen, Z., Understanding Protein-Interface Interactions of a Fusion Protein at Silicone Oil-Water Interface Probed by Sum Frequency Generation Vibrational Spectroscopy. *Journal of pharmaceutical sciences* **2018,** *107* (2), 682-689.

16. Lu, X.; Zhang, C.; Ulrich, N.; Xiao, M.; Ma, Y.-H.; Chen, Z., Studying polymer surfaces and interfaces with sum frequency generation vibrational spectroscopy. *Analytical chemistry* **2016,** *89* (1), 466-489.

17. Shen, Y., Surface properties probed by second-harmonic and sum-frequency generation. *Nature* **1989,** *337* (6207), 519.

18. Zhang, X.; Myers, J. N.; Huang, H.; Shobha, H.; Chen, Z.; Grill, A., SFG analysis of the molecular structures at the surfaces and buried interfaces of PECVD ultralow-dielectric constant pSiCOH. *Journal of Applied Physics* **2016,** *119* (8), 084101.

19. Myers, J. N.; Zhang, X.; Bielefeld, J.; Lin, Q.; Chen, Z., Nondestructive in situ characterization of molecular structures at the surface and buried interface of silicon-supported low-k dielectric films. *The Journal of Physical Chemistry B* **2015,** *119* (4), 1736-1746.

20. Lu, X.; Xue, G.; Wang, X.; Han, J.; Han, X.; Hankett, J.; Li, D.; Chen, Z., Directly probing molecular ordering at the buried polymer/metal interface 2: Using P-polarized input beams. *Macromolecules* **2012,** *45* (15), 6087-6094.

21. Lu, X.; Li, D.; Kristalyn, C. B.; Han, J.; Shephard, N.; Rhodes, S.; Xue, G.; Chen, Z., Directly probing molecular ordering at the buried polymer/metal interface. *Macromolecules* **2009,** *42* (22), 9052-9057.

22. Wang, J.; Even, M. A.; Chen, X.; Schmaier, A. H.; Waite, J. H.; Chen, Z., Detection of amide I signals of interfacial proteins in situ using SFG. *Journal of the American Chemical Society* **2003,** *125* (33), 9914-9915.

23. Wang, J.; Chen, X.; Clarke, M. L.; Chen, Z., Detection of chiral sum frequency generation vibrational spectra of proteins and peptides at interfaces in situ. *Proceedings of the National Academy of Sciences* **2005,** *102* (14), 4978-4983.

24. Xiao, M.; Wei, S.; Chen, J.; Tian, J.; Brooks III, C. L.; Marsh, E. N. G.; Chen, Z., Molecular Mechanisms of Interactions between Monolayered Transition Metal Dichalcogenides and Biological Molecules. *Journal of the American Chemical Society* **2019,** *141* (25), 9980-9988.

25. Boughton, A. P.; Yang, P.; Tesmer, V. M.; Ding, B.; Tesmer, J. J.; Chen, Z., Heterotrimeric G protein β1γ2 subunits change orientation upon complex formation with G protein-coupled receptor kinase 2 (GRK2) on a model membrane. *Proceedings of the National Academy of Sciences* **2011,** *108* (37), E667-E673.

26. Ding, B.; Jasensky, J.; Li, Y.; Chen, Z., Engineering and characterization of peptides and proteins at surfaces and interfaces: a case study in surface-sensitive vibrational spectroscopy. *Accounts of chemical research* **2016,** *49* (6), 1149-1157.

27. Nguyen, K. T.; Le Clair, S. V.; Ye, S.; Chen, Z., Orientation determination of protein helical secondary structures using linear and nonlinear vibrational spectroscopy. *The Journal of Physical Chemistry B* **2009,** *113* (36), 12169-12180.

28. Wang, J.; Clarke, M. L.; Chen, X.; Even, M. A.; Johnson, W. C.; Chen, Z., Molecular studies on protein conformations at polymer/liquid interfaces using sum frequency generation vibrational spectroscopy. *Surface Science* **2005,** *587* (1-2), 1-11.

29. Wei, S.; Zou, X.; Tian, J.; Huang, H.; Guo, W.; Chen, Z., Control of protein conformation and orientation on graphene. *Journal of the American Chemical Society* **2019,** *141* (51), 20335-20343.

30. Ye, S.; Nguyen, K. T.; Le Clair, S. V.; Chen, Z., In situ molecular level studies on membrane related peptides and proteins in real time using sum frequency generation vibrational spectroscopy. *Journal of structural biology* **2009,** *168* (1), 61-77.

31. Zou, X.; Wei, S.; Badieyan, S.; Schroeder, M.; Jasensky, J.; Brooks III, C. L.; Marsh, E. N. G.; Chen, Z., Investigating the effect of two-point surface attachment on enzyme stability and activity. *Journal of the American Chemical Society* **2018,** *140* (48), 16560-16569.

32. Zou, X.; Wei, S.; Jasensky, J.; Xiao, M.; Wang, Q.; Brooks III, C. L.; Chen, Z., Molecular interactions between graphene and biological molecules. *Journal of the American Chemical Society* **2017,** *139* (5), 1928-1936.

33. Kirby, B. J.; Hasselbrink Jr, E. F., Zeta potential of microfluidic substrates: 2. Data for polymers. *Electrophoresis* **2004,** *25* (2), 203-213.

34. Ludwig, D. B.; Carpenter, J. F.; Hamel, J. B.; Randolph, T. W., Protein adsorption and excipient effects on kinetic stability of silicone oil emulsions. *Journal of pharmaceutical sciences* **2010,** *99* (4), 1721-1733.

Chapter 6 Probing the Molecular Behavior of Barnacle Cement Peptide during the Fouling Process on Polystyrene using SFG and Molecular Dynamics Simulation

6.1 Introduction

Biofouling is defined as the undesired formation and growth of biofilms, which can occur in various situations and hinder the corresponding applications, such as the medical implant, water-process pipelines, and ship hulls.[1] Barnacle fouling has drawn extensive attention in terms of biofouling research since barnacle shows extremely high adhesion strength under sea environment and possesses outstanding degradation resistance.[2] Barnacle fouling on ship hulls can greatly increase frictional resistance and fuel consumption of the ship, which increases the operational expense and negatively impacts the environment.[3] Therefore, to remove and/or prevent the undesired barnacle fouling efficiently, it is necessary to understand the barnacle's adsorption and adhesion process on surfaces. In the barnacle adhesive, proteins compose 92% of the total biomacromolecule components,[4-5] which marks the importance of investigating the protein components responsible for the barnacle adhesion.

Research has found that the patterns in adhesive protein sequences determine the noncovalent interactions among proteins and lead to assemble into fibrous materials with β-sheet structure.[6-8] So et al. investigated the correlation between the protein sequence and the formation of adhesive fibers by synthesizing short peptides based on the barnacle cement peptides (BCP) and found that the central protein sequence with the charged segment shows rapid polymerization and forms significant fibril network.[9] The structures of BCP were characterized using common analytical tools, such as circular dichroism (CD), atomic force microscope (AFM), and ATR-

FTIR.[6-9] In this study, CD was used for probing the secondary structures of BCP in solution. Unfortunately, the BCP solution structure might be different from the BCP interfacial structure on surfaces due to peptide – surface interactions. AFM was used to probe morphology of the fibril network, not detailed molecular structure. So et al. applied ATR-FTIR investigate the dried BCP materials on CaF_2 substrate and successfully detected a peak attributed to the β-sheet structure.[9] The research results published by So and his colleagues provided important knowledge on BCP interactions and deposition, which are related to barnacle adhesion. To further understand the interfacial adsorption and aggregation mechanism of BCP, SFG was used to study BCP interfacial behavior in situ in real time.

As presented in previous chapters, SFG is a surface-sensitive tool that selectively probes the interfacial molecules, including proteins and peptides, at the buried solid/liquid interface in situ in real time.[10-19] SFG can provide detailed information about the orientation of adsorbed proteins/peptides. Using the Hamiltonian analysis method, as we discussed in the above chapters, the conformation of adsorbed protein can also be deduced by comparing the matching quality between the calculated SFG spectra with the reconstructed experimental data.

In this study, we applied SFG and Hamiltonian analysis method combined with molecular dynamics (MD) simulation to investigate the adsorption behavior of BCP on a model fouling surface, polystyrene (PS). Two BCP peptides were used in this study: (1) BCP2C, which contains one simple segment and one charged segment with strong fibril formation property (2) BCP1, which contains one simple segment and does not lead to fibril formation. Since the crystal structures are not available for BCP2C and BCP1, the I-TASSER server was used to predict the solution structures based on the peptide sequences, and the stabilized solution structures were obtained through MD simulations (using the predicted structures as initial structures for

simulations). The stabilized BCP2C and BCP1 structures were then combined with the PS surface in the simulation system to investigate the adsorption behaviors of BCP2C and BCP1 on the PS surface. The final structures of BCP2C and BCP1 after the ~ 1-μs MD simulation clearly showed that BCP2C formed significant β-sheet structures while BCP1 did not. These structures were then used in the Hamiltonian analysis, and the results suggested that the BCP2C structure with β-sheet segment has a much higher matching quality with SFG experimental data, confirming the existence of β-sheet structure in BCP2C on PS surface.

The SFG and CD experiments reported in this chapter were conducted by Ralph Crisci, a PhD candidate on our research group. The BCP structure prediction, MD simulation, and Hamiltonian analysis were performed by the author of this thesis.

6.2 Experimental Details

BCP2C and BCP1 were purchased from Biomatick (Wilmington, DE) and used as received. 1.0 mg/ml BCP2C or BCP1 solution was prepared in DI water (18 MΩ·cm) for adsorption studies.

Standard PS (Mw = 5000 g/mol) was purchased from Millipore Sigma (Burlington, MA). PS was dissolved in toluene (Sigma-Aldrich, St. Louis, MO) to make 1.0 wt% PS solution. Then the solution was spin-cast on a CaF_2 prism with 2000 rpm for 30 s. The PS film on CaF_2 was annealed at 120 ℃ overnight and then used for SFG experiments after cooled down to room temperature.

Details of SFG instrumentation and theories have already been discussed in previous chapters and will not be repeated here. In this study, a commercial picosecond SFG system, EKSPLA PL 2250 SFG (Vilnius, Lithuanian), was used. The 532 nm visible beam and the frequency-tunable IR beam were overlapped on the sample surface in time and space to generate

the sum frequency signal. The polymer samples were prepared on right angle CaF_2 prisms to implement the near total reflection geometry. The SFG spectra of adsorbed BCP were collected in ssp (s-polarized SFG signal, s-polarized visible beam, and p-polarized input IR beam) and ppp polarization combinations. All the SFG spectra presented here are averaged by three scans. The resolution of the SFG spectrometer is about 5 cm^{-1}.

6.3 Barnacle Cement Peptide Structure Prediction and MD Simulation

The crystal structures of BCP1 and BCP2C are not available in the Protein Data Bank; thus, I-TASSER server[20] was used to predict the barnacle cement peptide structure based on the sequences of BCP1 and BCP2C. The peptide sequences and the details of the structure prediction will be presented below in the results and discussions section below. The predicted structures were further used in the MD simulation.

The MD simulation software used in this study was Gromacs (2019.6).[21-23] The CHARMM36 (Feb 2021) force field[24] was used for assigning the simulation parameters for all the atoms. The simulation was run on the Stampede2 – TACC server. The MD simulation was performed with the guidance and help from Dr. Tao Wei at Howard University.

An amorphous PS surface (6.97200 × 6.92070 nm^2) was constructed with 78 polystyrene chains. Each chain consists of 20 monomers. The PS surface was initially relaxed in vacuum with a series of simulations of 30 ns for a total of 270 ns, which were carried out using a stepwise heating/annealing protocol starting from 298.15 K, reaching 700 K, and then recovering to 298.15 K. Then the surface was exposed to water solution for further relaxation for 150 ns. After that, the hydrated PS surface was assembled with the peptides, leaving an initial gap of at least 2.0 nm between the PS surface and the peptides with water molecules (Figure 6.1). Chloride counter ions were added to neutralize the system.

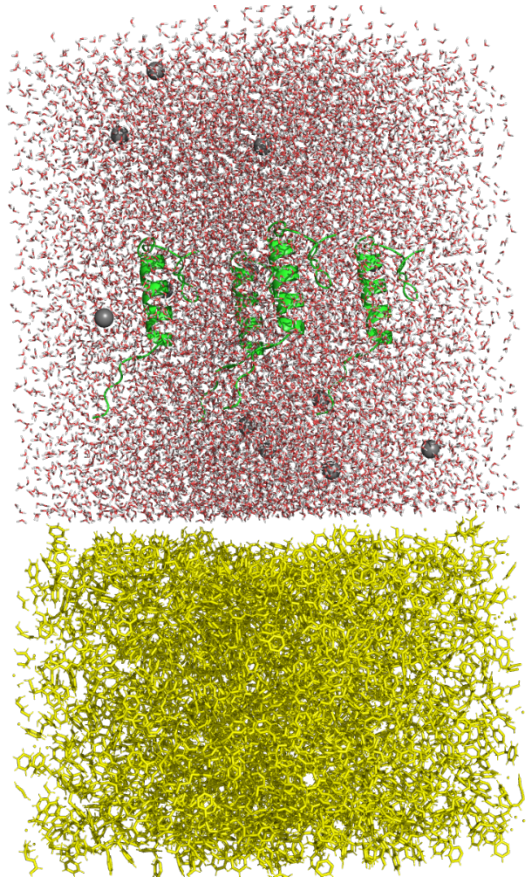


Figure 6.1 The initial configuration of combined simulation system between BCP2C (green) with water and polystyrene (yellow). The chloride counter ions are shown in balls with grey color.

6.4 Results and Discussions

6.4.1 SFG Results of BCP2C on PS

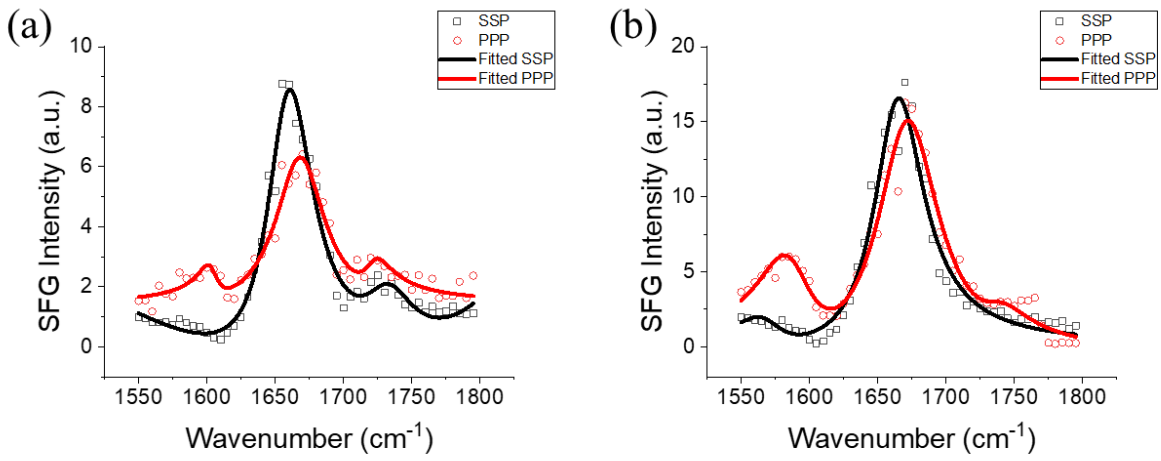


Figure 6.2 SFG spectra collected from the BCP2C/PS interface after (a) 1-hour and (b) 48-hour adsorption. The experimental data and fitted curves are denoted by open points and solid lines, respectively.

The 1.0 mg/mL BCP2C solution was placed into contact with PS surface on CaF_2 prism, and then ssp and ppp SFG spectra were collected after contacting for 1 hour and 48 hours. The adsorption of BCP2C was confirmed by the significant ~1660 cm^{-1} peak as shown in Figure 6.2, which can be attributed to the amide I stretch mode from the peptide backbone. By comparing Figure 6.2a and 6.2b, we can see that the SFG signal intensity became stronger after 48-hour adsorption, perhaps indicating that more BCP2C molecules were adsorbed onto the PS surface. The amide I signal ssp/ppp ratio was also changed after 48 hours, which might be due to the (1) orientation change or (2) secondary structure change of BCP2C. Details of the BCP2C structure at the molecular level will be discussed in the MD simulation section and the Hamiltonian analysis section below. The SFG spectra were fitted, and the fitting parameters are shown in Table 6.1.

	BCP2C 1h		BCP2C 48h	
	ssp	ppp	ssp	ppp
Offset	-0.1358	1.412	-0.02538	-0.5279
NR	6.639	0.04116	0.1627	-0.1013
A1	48.45	47.69	88.95	42.76
x01	1659	1668	1664	1588
w1	20.79	21.92	22.25	24.58
A2	13.72	6.437	20.55	104.33

x02	1732	1721	1568	1671
w2	22.66	12.15	21.34	27.76
A3	--	5.436	--	21.61
x03	--	1604	--	1738
w3	--	8.723	--	27.14

Table 6.1 Fitting parameters of the SFG spectra of BCP2C on PS shown in Figure 6.2.

6.4.2 I-TASSER Prediction and CD Results of BCP Solutions

BCP1: QTGYTRGGAAVSSTGATQGAGS

BCP2C: AVGNSGVSGSGVSIGDSGFRQKTQT NSEAGSKGTKRA

Simple Charged

Figure 6.3 Amino acid sequences of BCP1 and BCP2C. BCP1 only has one simple segment, and BCP2C has one simple segment and one charged segment.[9]

The sequences of BCP1 and BCP2C are shown in Figure 6.3. BCP1 only contains one simple section, and BCP2C has one simple and one charged section.[9] These sequences of BCP1 and BCP2C were used for the peptide structure prediction on I-TASSER server (Yang Zhang Lab, University of Michigan). The prediction result of BCP2C structure is shown as below in Figure 6.4.

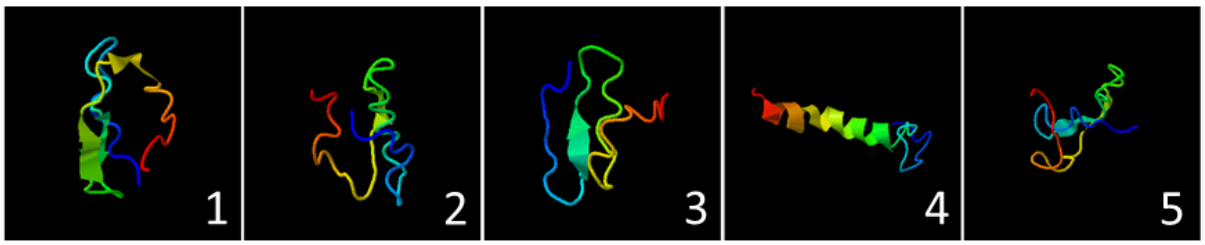


Figure 6.4 Top 5 final models predicted by I-TASSER using BCP2C sequence.

The top 5 final models predicted by I-TASSER are ranked by C-score, which is calculated based on the significance of threading template alignments and the convergence parameters of the structure assembly simulations.[20] Although the first model has a better quality in most cases due to the highest C-score, other models could be better. Therefore, more experimental evidence is

needed to verify the reliability of each candidate model. In this study, we conducted CD experiments on the BCP2C solution to determine which predicted model to use since CD can provide important information about the secondary structures of proteins/peptides in the solution, while the five predicted peptide models have varied secondary structures. The CD spectrum of a 1.0 mg/mL BCP2C solution is shown in Figure 6.5.

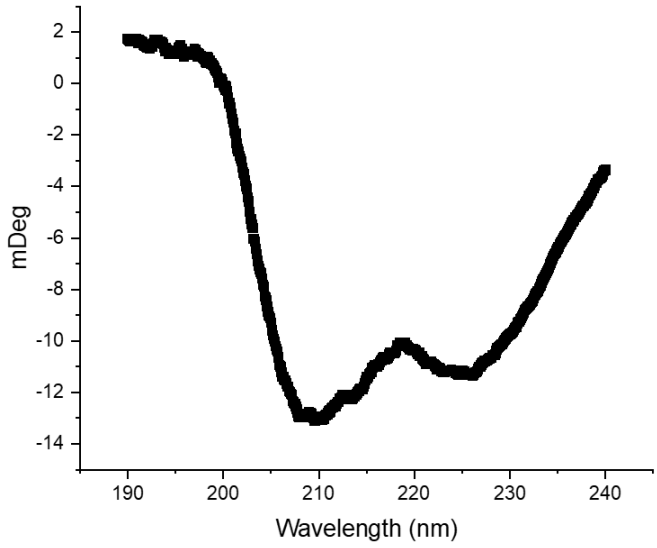


Figure 6.5 CD spectrum of a 1.0 mg/ml BCP2C solution.

As shown in Figure 6.5, the CD spectrum of the BCP2C solution shows two clear negative peaks at 210 and 225 nm, which corresponds to the α-helical signature response.[25] Among the top 5 models, as shown in Figure 6.4, Model 4 shows a clear α-helical structure. Thus, we believe that Model 4 represents the most probable molecular structure of BCP2C in the solution, and this structure was used as the initial structure file of BCP2C for the MD simulation in the next steps.

The Model 4 structure was then further stabilized in solution by conducting an all-atom molecular dynamic simulation. The initial structure was put into a 7.2 × 7.2 × 7.2 nm^3 simulation box and then solvated by water molecules. Chloride anions were added as the counterions. First, the peptide structure was fixed, and the solvent was relaxed for 10 ns. After stabilizing the water

molecules, the peptide was relaxed at 30K, 100K, 200K, and 298.15K consecutively. The MD simulation time at each temperature was at least 10 ns. This process was summarized in a flow chart, as shown in Figure 6.6. After the relaxation in water, the α-helical segment in the BCP2C is still clearly observable, indicating that this model is a reasonable structure to use in this study.

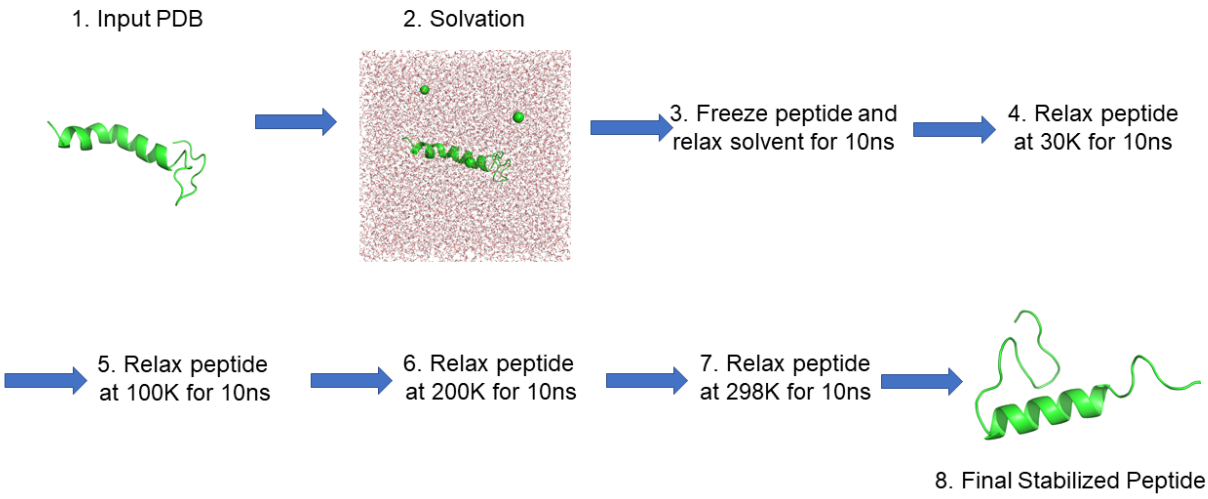


Figure 6.6 Flow chart showing the process of relaxing the predicted BCP2C structure in solution.

6.4.3 MD Simulation of BCP2C on PS Surface

The stabilized BCP2C structure in solution was further used in the MD simulation of BCP2C adsorption onto a PS surface. The details of this process have already been discussed in Section 6.3 above and shown in Figure 6.1. Here, four identical BCP2C peptides were put into the simulation box to investigate the interaction between the BCP2C peptides, e.g. entanglement or aggregation. Initially, the BCP2C peptides and the PS surface were fixed, while the water molecules were being stabilized, similarly to what was done as mentioned above (at different temperatures of 30K-100K-200K-298.15K). After the water molecules were stabilized and filled the entire simulation box, the peptides were kept frozen while the PS surface was relaxed for 10 ns. Then the entire system (including the peptides) was relaxed starting from 30K, and then increased the temperature to 100K, 200K, and 298.15K step by step. The peptides did not move

much under low temperatures at 30K and 100K but started to approach the PS surface slowly at 200K, and quickly adsorbed onto the PS surface at 298.15K. Several representative snapshots of the adsorption process in this MD simulation are shown in Figure 6.7.

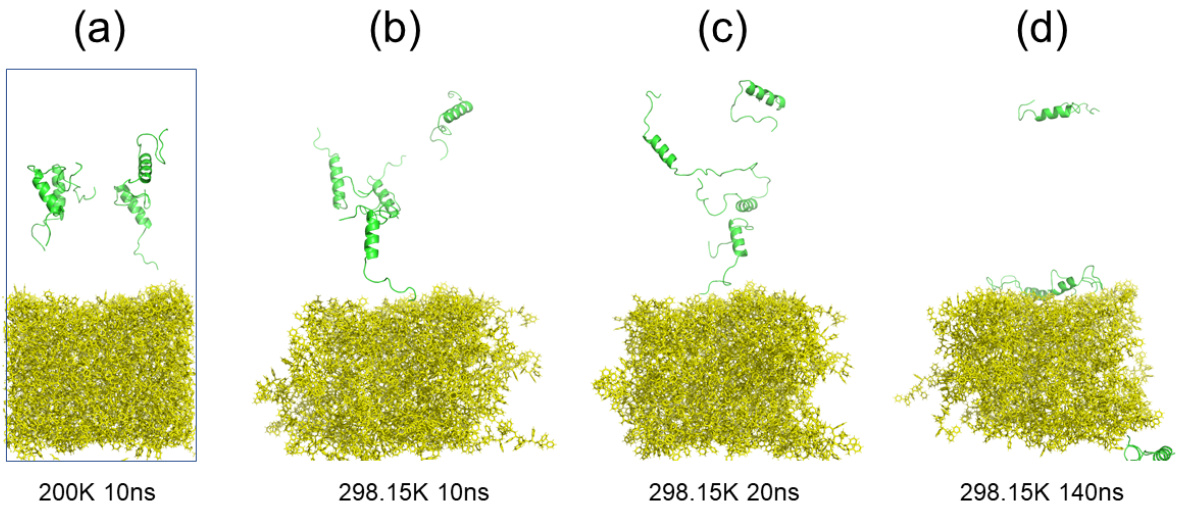


Figure 6.7 Snapshots of MD simulation box showing the adsorption of BCP2C (green) onto the PS surface (yellow) at (a) T=200 K after 10 ns, (b) T=298.15 K after 10 ns, (c) T=298.15 K after 20 ns, and (d) T=298.15 K after 140 ns. The periodic boundary is shown as blue rectangle in (a). Molecules in (b)(c)(d) are corrected by the periodic boundary for better visualization.

It is worth noting that the simulation box is corrected by periodic boundary correction (denoted by the blue rectangle in Figure 6.7), therefore the peptides (green in Figure 6.7) that stay on the top of the box are attached to the bottom of the PS surface (yellow in Figure 6.7). According to this MD simulation result, the BCP2C peptides completely lie down on the PS surface after around 140 ns. This simulation was further extended to 1 μs. The next section will discuss more details and the corresponding Hamiltonian analysis.

6.4.4 Hamiltonian Analysis of BCP2C after 1 μs MD Simulation

The BCP2C structures from the MD simulation result were used as the input structures for the Hamiltonian method to calculate SFG spectra to compare to experimental SFG data. The details of the Hamiltonian method have already been discussed in Chapter 2 and will not be repeated here.

The flow chart in Figure 6.8 shows the process of the Hamiltonian analysis method used in this study.

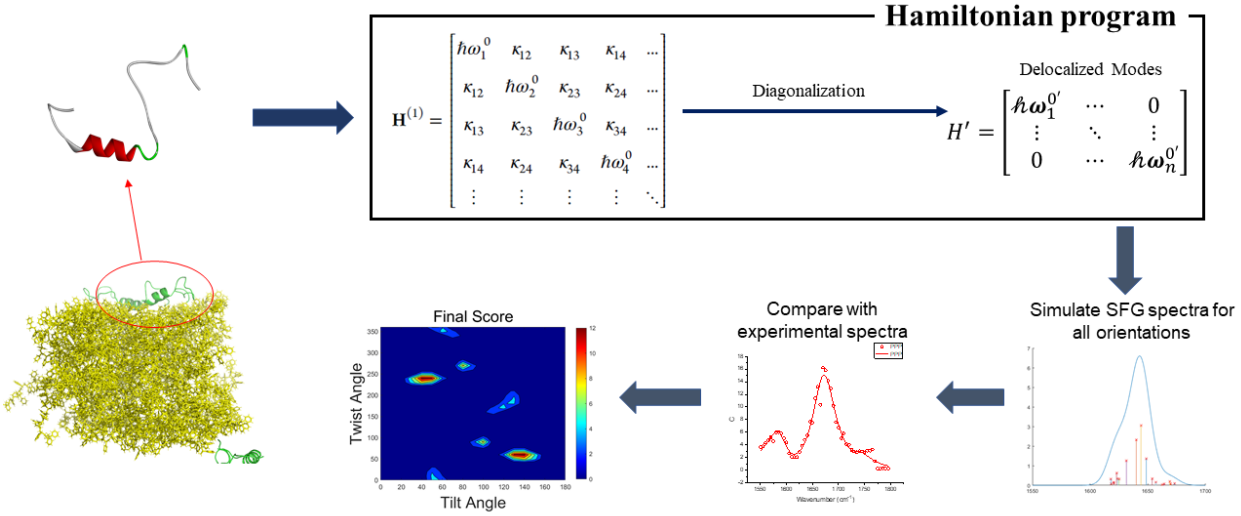


Figure 6.8 Flow chart showing the Hamiltonian analysis method used to deduce the orientation of adsorbed peptide on PS. The input structure was extracted from the MD simulation result.

Figure 6.9 shows the BCP2C peptides and the PS surface before the simulations and at the simulation time of 969 ns. The blue lines denote the periodic boundary correction box. Segments of the peptides were rendered by different colors according to secondary structures, e.g. α-helix: purple, random coil: white, β-sheet: yellow. From Figure 6.9, we can see that all the BCP2C peptides lied down on the PS surface, and three BCP2C peptides still maintained substantial α-helical segments while the fourth peptide completely lost the secondary structure and adopted a random coil conformation. One BCP2C shows a β-sheet section. These four final structures are also shown in Figure 6.10 for a closer look.

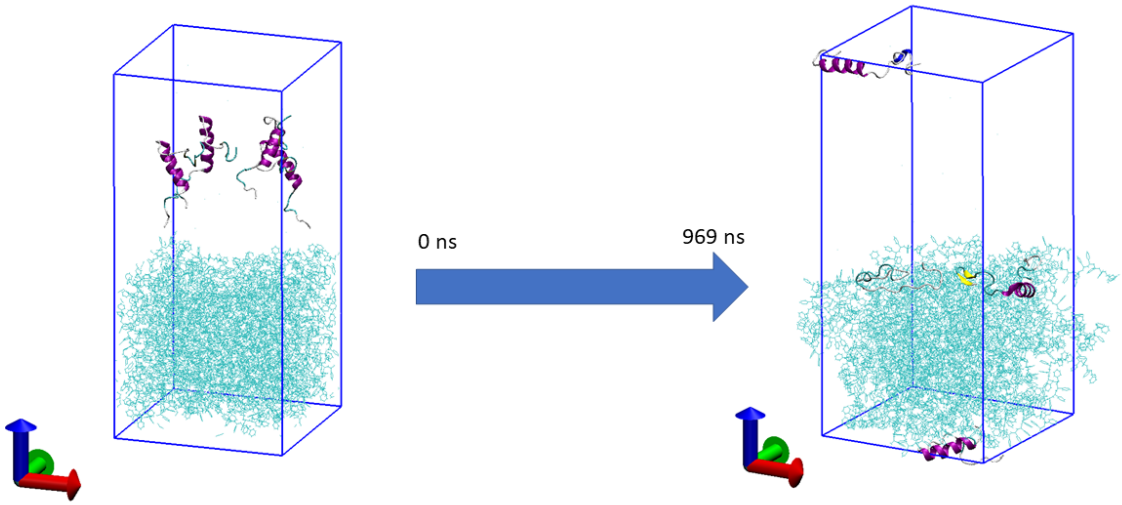


Figure 6.9 The initial simulatiuon system with four peptides and the PS layer (left) as well as the structures of the four BCP2C peptides at simulation time of 969 ns while interacting with the PS layer (right). Peptides are rendered in different colors based on the secondary structure. At the beginning of the simulation at 298.15K (left), four BCP2C peptides were not attached to the PS surface and only showed α-helical structure. After 969 ns, all the BCP2C molecules lied down on the PS surface, and β-sheet structure formation was observed.

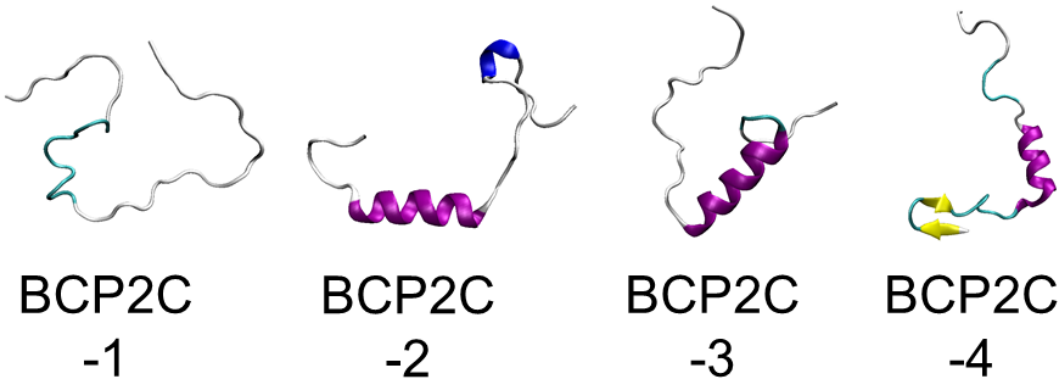


Figure 6.10 Closer look of the structures of the four BCP2C peptides at the simulation time of 969 ns.

All the four structures of BCP2C on the PS surface after the MD simulation (shown in Figure 6.10) are used to calculate the SFG spectra and compared with the experimental data (shown in Figure 6.2). As mentioned in Chapter 2 and Chapter 4, the absolute matching scores, which indicate the matching quality between the calculated and experimental SFG data, can be used as a standard to determine which conformation is the most likely conformation of the peptide. The highest matching scores of all the four BCP2C final structures extracted from the 969-ns

simulation are listed in Table 6.2. We can see that the structure with a β-sheet segment, BCP2C-4, has the highest matching score between the calculated SFG spectra and the reconstructed experimental data after one-hour adsorption of BCP2C on PS. This is consistent with the previous reported conclusion that the formation of β-sheet structure in BCP2C is the key to the peptide aggregation and fibril formation.[9]

It is surprising to find that BCP2C-1 has an excellent matching quality in the case of 48-hour-adsorption, and it is even better than BCP2C-4. We believe that the BCP2C on PS after 48 h may heavily aggregate, and the 1 μs MD simulation could not capture the structural change on such a long-time scale. More coarse-grain simulation is required in the future to understand the aggregation process of BCP2C and interpret the SFG data of BCP2C on PS after 48 h. Here, we focus on analyzing the SFG spectra collected from BCP2C after 1-hour adsorption onto the PS surface.

Adsorption Time in Experiment	Highest Matching Scores of Different BCP2C Final Structures			
	BCP2C-1	BCP2C-2	BCP2C-3	BCP2C-4
BCP2C 1h	0.2730	0.2427	0.3348	**0.9599**
BCP2C 48h	**2.4654**	0.1962	0.4219	**1.8216**

Table 6.2 Highest matching scores of different BCP2C final structures with the reconstructed SFG spectra collected from adsorbed BCP2C on PS after 1 h and 48 h.

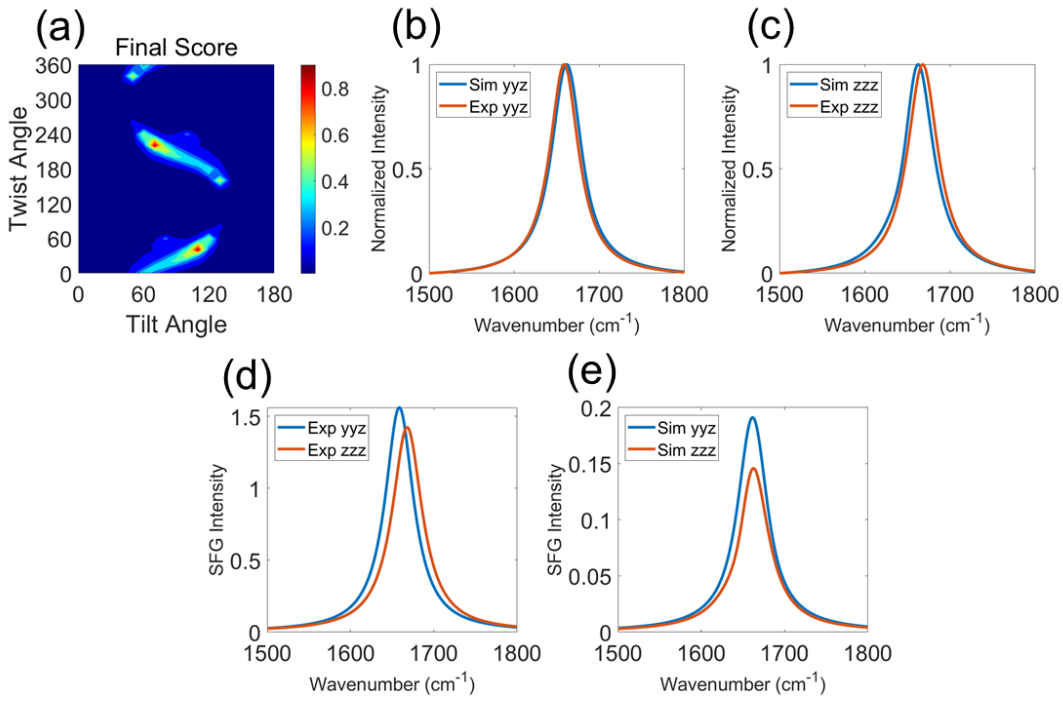


Figure 6.11 (a) The final matching score heat map showing the matching quality between the reconstructed resonant SFG experimental spectra (adsorption time = 1 h) and the calculated orientation dependent SFG spectra based on the **BCP2C-4** structure. The blue spectra in (b) and (c) show the calculated SFG yyz (b) and zzz (c) spectra of adsorbed BCP2C after one-hour adsorption with the highest matching score with the reconstructed experimental resonant SFG spectra (shown in orange). The unnormalized SFG spectra of (d) experimental data and (e) calculated spectra are plotted for evaluating the matching quality of the ssp and ppp intensity ratio.

The heatmap of the matching scores and the comparison between calculated and experimental yyz and zzz spectra are shown in Figure 6.11. Two possible orientations deduced from the heatmap in Figure 6.11(a) are plotted in Figure 6.12. Since the normal SFG experiment cannot resolve the absolute orientation of molecules, these two orientations which point to the opposite directions could not be distinguished by SFG. Here, we believe that Figure 6.12(b) is more reasonable because the peptide has a larger contact area which supports the peptide structure on the surface better. However, neither of these two orientations is close to the lie-down orientation that is shown in Figure 6.9, and the deduced orientation from Hamiltonian analysis shows a "side-on" orientation of BCP2C on the PS surface. It can be explained by the difference in surface coverage between the MD simulation box and the real system in SFG experiments. Only four peptides were put in the MD simulation box in this study, which made it possible for all peptides

completely lie down on PS surface. In the real system, due to the peptide/PS interaction, there might be more BCP2C peptides densely adsorbed on PS surface; thus, the adsorbed peptide tends to tilt up due to the crowded surface.

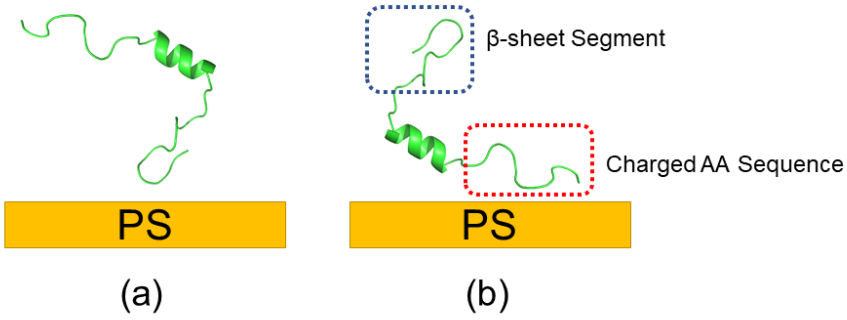


Figure 6.12 Two most probable orientations of BCP2C on PS after one-hour adsorption.

As mentioned in Section 6.4.2 Figure 6.3, the BCP2C peptide sequence contains one simple segment and one charged segment. The charged segment and β-sheet segment are denoted by a red rectangle and blue rectangle, respectively, as shown in Figure 6.12b. It is worth mentioning that the charged segment is not responsible for the formation of β-sheet structure of BCP2C. This result indicates that the strong fibril formation of BCP2C is not only resulted from the charged segment but also affected by the simple segment.

6.4.5 Secondary Structure Evolution Plot of BCP2C during the MD Simulation

To further understand the interaction between the BCP2C and PS surface, the secondary structure change during the MD simulation was calculated and plotted in Figure 6.13. Four BCP2C peptides are plotted together for a better comparison. In Figure 6.13, α-helix and β-sheet are shown in blue and red colors, respectively. The significant β-sheet formation was observed during t = 480 to 840 ns from three BCP2C peptides. However, due to the strong interaction between BCP2C and PS, and the small peptide size, the secondary structure (especially β-sheet) is not stable in a long timescale. The β-sheet structure showed an "on-and-off" manner. Only the last configurations at

969 ns of the four peptides were used as the input structures in the Hamiltonian analysis mentioned above. Here, we believe that even after more than 900 ns, the BCP2C peptides on PS are still in transition states and not fully stabilized.

In the future, to better capture the BCP2C peptide conformations and orientations on the PS surface, two approaches could be adopted. One possible approach is to conduct coarse-grain MD simulations (instead of all-atom MD simulations), which can extend the simulation to a much longer timescale. The other approach is to conduct a statistical analysis of the BCP2C structures during the all-atom MD simulation. For example, extract more BCP2C structures at different timesteps from the all-atom MD simulation, conduct the Hamiltonian analysis, compare the absolute matching scores, and locate the best conformations/orientations representing the adsorbed structure of BCP2C on PS. The secondary structure evolution plot of BCP2C/PS proves that the BCP2C can form β-sheet structure on PS surface, which is believed to be the key step in the barnacle peptide interfacial aggregation. The Hamiltonian result also shows that the BCP2C peptide with β-sheet segment has higher matching quality with the reconstructed experimental SFG spectra, further confirming the β-sheet formation of BCP2C on PS surface. Possibly in reality when β-sheet structure formation of adsorbed BCP2C starts, peptide aggregation occurs. Unfortunately this could not be observed by the all-atom MD simulation because aggregation takes more peptides while only limited peptides can be used in the all-atom simulation. Therefore the conformation changes after the formation of β-sheet of adsorbed BCP2C on PS may not happen in reality, but only exists in simulations. In the future, it is necessary to extract all the peptide structures with β-sheet formation in the MD simulations to perform Hamiltonian analysis to compare to other peptide structures to select the highest matching scores. We hope that the

structures with the highest matching scores should contain β-sheet structure. The above proposed study is beyond the research scope of this thesis.

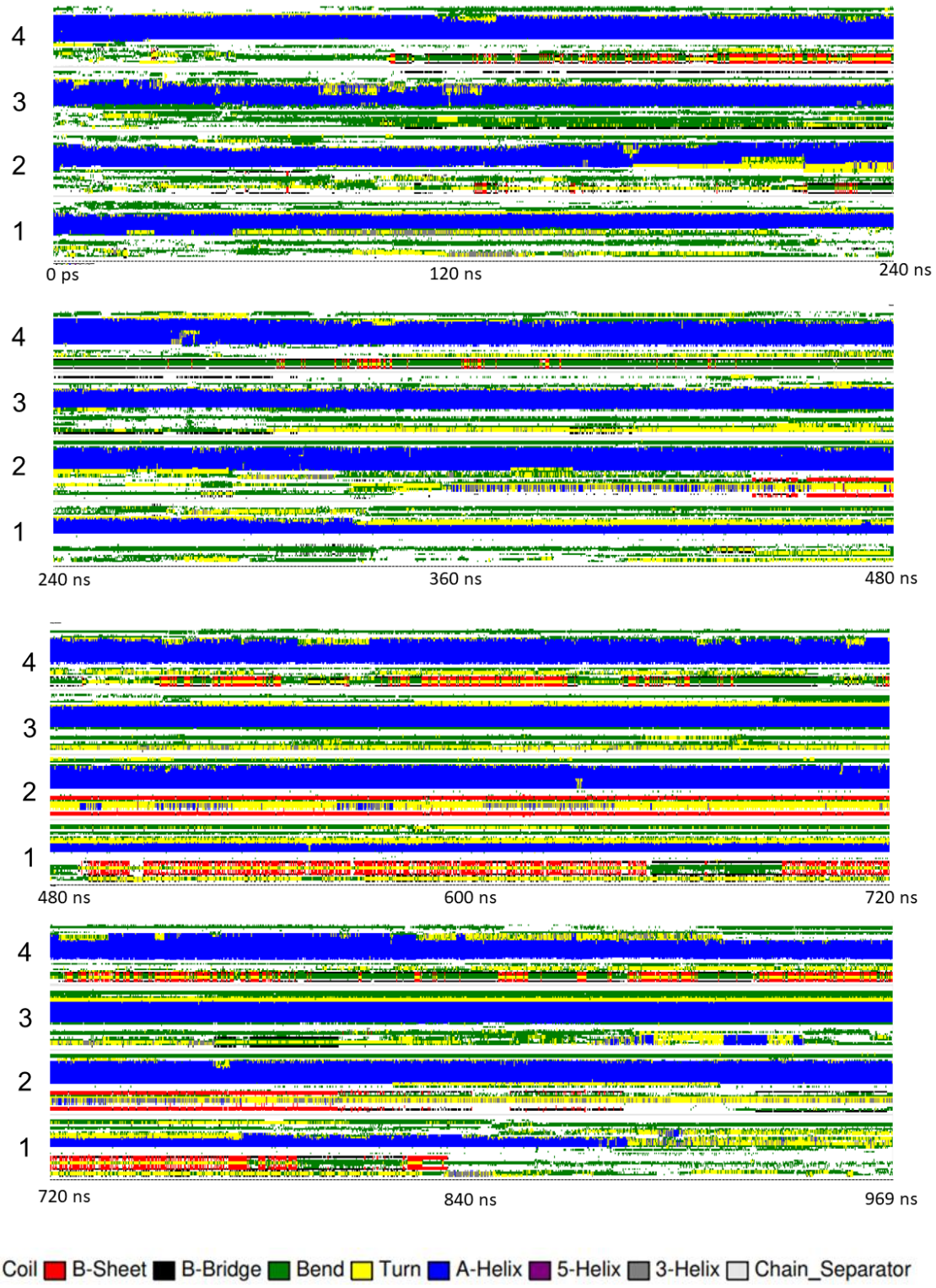


Figure 6.13 Secondary structure evolution plot of BCP2C/PS system during the simulation from 0 to 969 ns. The results of the four BCP2C peptides are plotted together. Different colors represent different secondary structures. Significant β-sheet formation was observed during 480 to 840 ns for BCP2C-1, BCP2C-2, and BCP2C-4.

6.4.6 SFG Results of BCP1

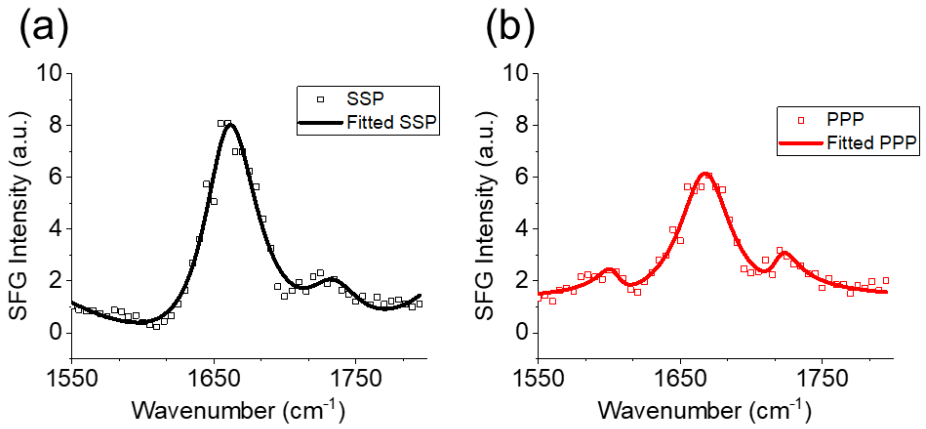


Figure 6.14 (a) Ssp and (b) ppp SFG spectra collected from the BCP1/PS interface after 1-hour adsorption.

After a BCP1 solution was placed into contact with PS surface for 1 h, SFG spectra were collected from the BCP1/PS interface as shown in Figure 6.14. The peak at ~1660 cm^{-1} can be assigned to the amide I stretch mode of the BCP1 peptide backbone, which confirms the adsorption of BCP1 on the PS surface. SFG spectra were collected in ssp and ppp polarization combinations, and the fitted results are plotted in Figure 6.14. The fitting parameters using the Lorentzian function are shown in Table 6.3 and will be used to reconstruct the resonant SFG spectra in the Hamiltonian analysis method.

	BCP1 on PS	
	ssp	ppp
Offset	-0.3047	1.271
NR	8.846	0.05529
A1	53.10	48.03
x01	1660	1667
w1	23.70	22.13
A2	15.50	5.514
x02	1734	1603
w2	24.64	9.802
A3	--	7.042
x03	--	1720
w3	--	11.01

Table 6.3 Fitting parameters of the SFG spectra of BCP1 on PS shown in Figure 6.14.

6.4.7 Structure Prediction and MD Simulation of BCP1

Similar to BCP2C, the crystal structure of BCP1 is not available in the Protein Data Bank. Thus the initial structure of BCP1 in solution was predicted by I-TASSER based on the sequence of BCP1 and then further stabilized by conducting an MD simulation on BCP1 in solution. These same steps as those used to study BCP2C have been discussed in previous sections and will not be repeated here. The top 5 final predicted models are shown in Figure 6.15. All structures adopt mainly random-coil conformation, and no significant secondary structure is present, which is consistent with the expectation.[9] Here, the first model, BCP1-1, was used as the structure for MD simulation because of the highest C-score.

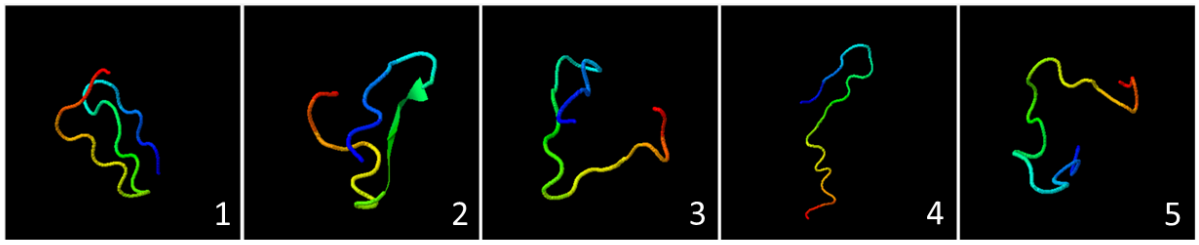


Figure 6.15 Top 5 final models predicted by I-TASSER using BCP1 sequence.

The BCP1-1 structure was then put into a simulation box, solvated by water molecules, and stabilized by running an MD simulation. This process is shown in Figure 6.6. After the stable solution structure of BCP1 was obtained, we placed four stabilized BCP1 peptides into the same simulation box, solvated the box with water molecules, and combined them with the PS surface. After the water molecules and PS surface were relaxed for at least 10 ns, the BCP1 peptides were unfixed. This process is the same as that used to study BCP2C, the details of which were presented in Section 6.4.3 above.

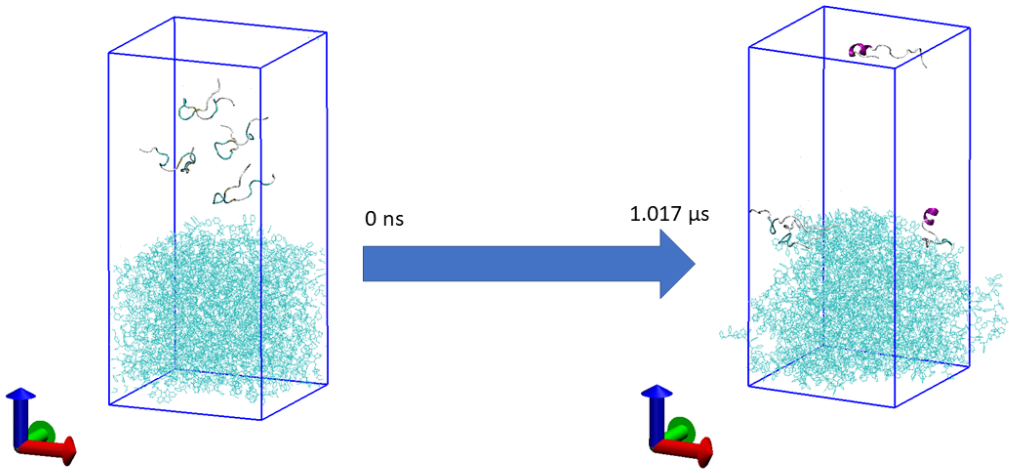


Figure 6.16 The initial simulatiuon configuration of four peptides and the PS layer (left) as well as the structures of the foiur peptides and the PS layer at the end of the simulation (right). Peptides are rendered in different colors based on the secondary structures.

The initial simulation configuration of the four BCP1 peptides and the PS layer as well as the structures of the peptides and the PS layer at the end of simulation are shown in Figure 6.16. The periodic boundary is depicted by blue lines. After the simulation of 1.017 μs, all the four BCP1 peptides lay down on the PS surface, while two of them formed short α-helical segments. For a closer look, the final structures of the four BCP1 peptides on the PS surface were extracted and displayed in Figure 6.17, which will be used as the input structures for the Hamiltonian analysis below.

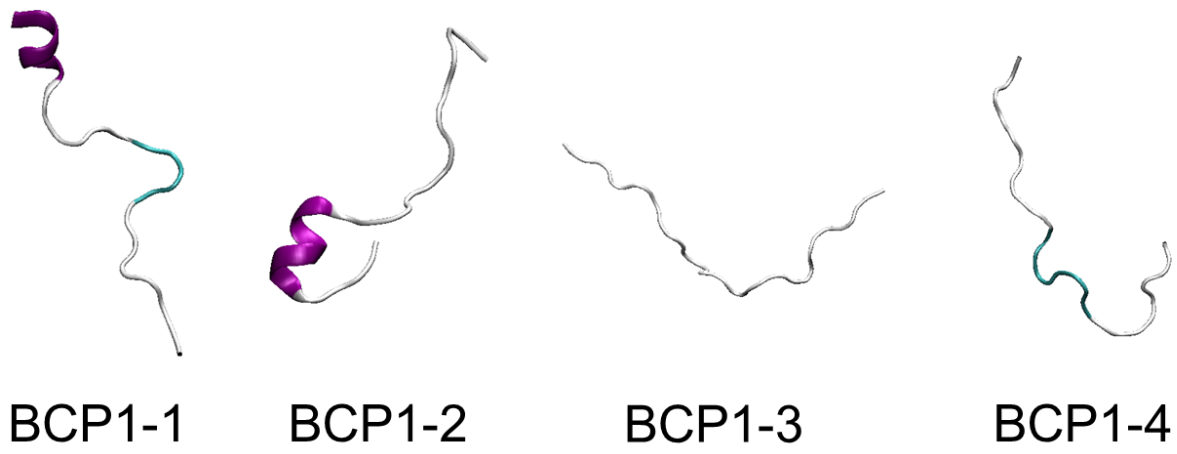


Figure 6.17 The extracted structures of four BCP1 peptides on the PS from the MD simulation at the end of the simulatiuon with t = 1.017 μs.

6.4.8 Hamiltonian Analysis of BCP1 on PS

The extracted final structures of BCP1 peptides on the PS surface from MD simulation were used as the input structures in the Hamiltonian method. The input structures were rotated to calculate the SFG spectra, which were used to match with the reconstructed experimentally collected SFG spectra. The highest matching scores among all the orientations of each BCP1 structure are shown in Table 6.4. Here, the BCP1-2 shows the highest matching quality with the reconstructed experimental SFG spectra, indicating that the BCP1-2 is the most likely conformation of adsorbed BCP1 on the PS surface. The matching score heat map and matching qualities of BCP1-2 are shown in Figure 6.18.

Adsorption Time in Experiment	Highest Matching Scores of Different BCP1Final Structures			
	BCP1-1	BCP1-2	BCP1-3	BCP1-4
BCP1 1h	0.9752	**1.265**	0.2698	0.6978

Table 6.4 Highest matching scores between the calculated and reconstructed experimental SFG spectra obtained based on the four final BCP1 simulation structures and the spectra collected after 1 h adsorption.

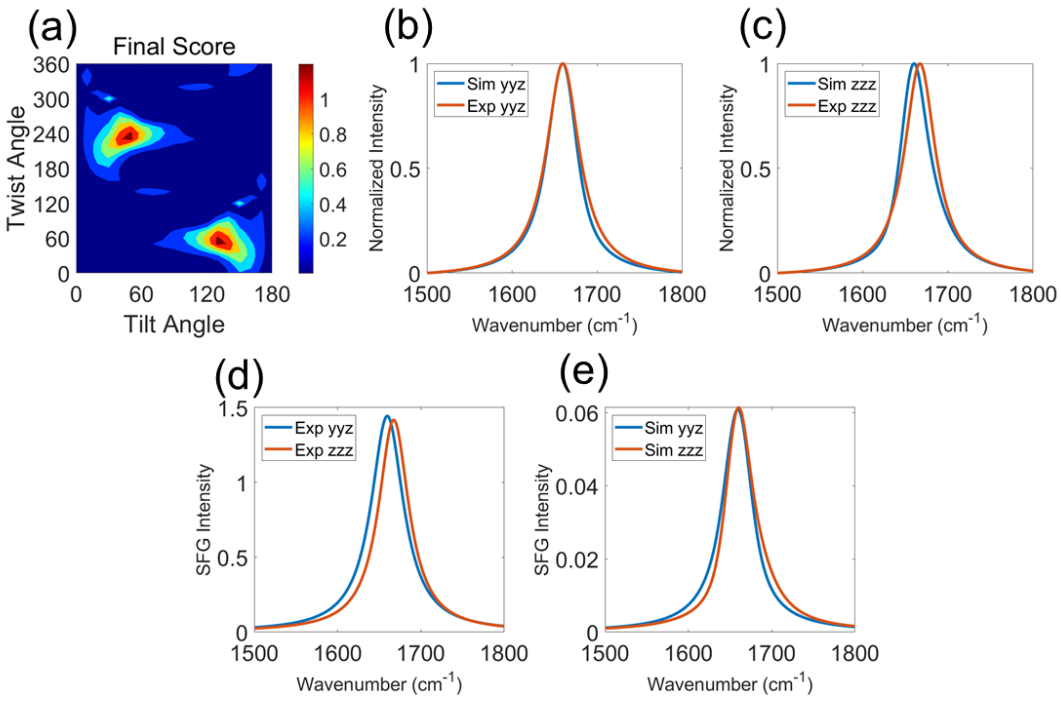


Figure 6.18 (a) The final matching score heat map showing the matching quality between the reconstructed resonant SFG experimental spectra (adsorption time = 1 h) and the calculated orientation dependent SFG spectra based on the **BCP1-2** structure. The blue spectra in (b) and (c) show the calculated SFG yyz (b) and zzz (c) spectra of adsorbed BCP2C after one-hour adsorption with the highest matching score with the reconstructed experimental resonant SFG spectra (shown in orange). The unnormalized SFG spectra of (d) experimental data and (e) calculated spectra are plotted for evaluating the matching quality of the ssp and ppp intensity ratio.

From the heat map, as shown in Figure 6.18a, we can see that two orientations have the highest matching score, which correspond to the two most likely orientations of adsorbed BCP1 on PS. Figure 6.19 displays these two orientations. Here, we believe that the orientation as shown in Figure 6.19a is not reasonable since only one amino acid is attached to the PS surface, which is not a stable pose of a peptide on a surface in solution. The more proper orientation in Figure 6.19b shows that the α-helical segment of BCP1 is attached to the PS surface and the entire peptide tilts on the surface. This is not consistent with the orientation directly obtained from the MD simulation. As what we observed in BCP2C study presented above, this is possibly due to the crowded surface covered by more BCP1 peptides in the real system detected by SFG experiment. In the current MD simulation box, each of the four BCP1 peptides can have enough space to lie down, while in the

SFG experiment, perhaps there are more BCP1 peptides adsorbed on the PS surface; thus, the adsorbed BCP1 peptides cannot lie down but tilt on the surface.

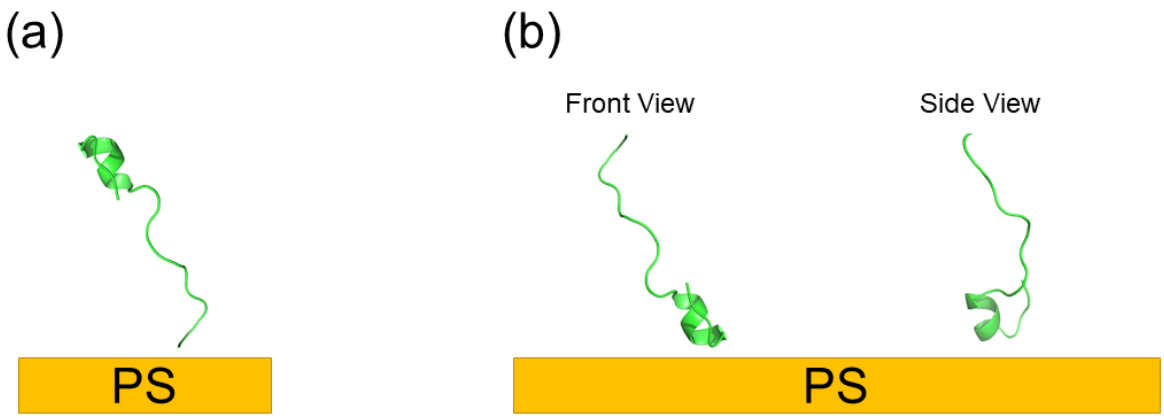


Figure 6.19 Two possible orientations of BCP1 on PS: (a) Tilt = 50, Twist = 230 degree, (b) Front and side view of Tilt = 130, Twist = 50 degree.s

6.4.9 Secondary Structure Evolution Plot of BCP1 during the MD Simulation

The secondary structure evolution plot of BCP1 is shown in Figure 6.20. No significant β-sheet structure is formed during the MD simulation, which is different from the BCP2C as shown in Figure 6.13. This β-sheet structure formation on the PS surface can explain the results reported previously on why BCP2C shows stronger fibril formation than BCP1.[9]

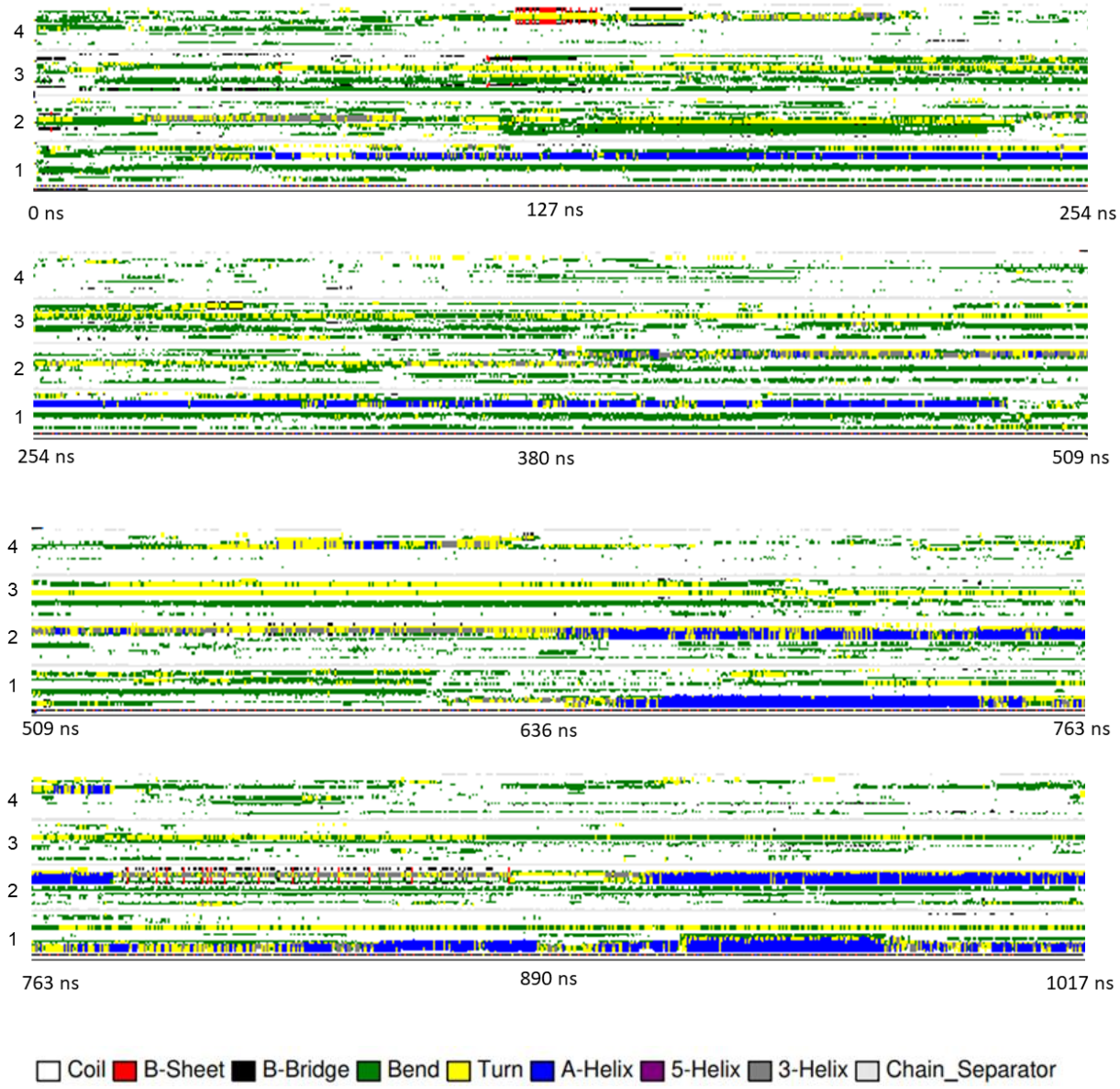


Figure 6.20 Secondary structure evolution plot of BCP1/PS system during the simulation from 0 to 1017 ns. Different colors represent different secondary structures.

However, as we presented in Section 6.4.4 and Figure 6.12, the charged segment of BCP2C is not involved in the β-sheet segment, which indicates that the simple segment is also important for the β-sheet formation and affects the aggregation process of barnacle cement peptide. From Figure 6.20, we can see that BCP1 can form a short α-helix segment, which can remain stable for more than 100 ns. In the Hamiltonian analysis shown in Table 6.4, the BCP1 structures with a

short α-helix segment have much higher matching qualities than the random-coiled BCP1 structure, suggesting that the adsorbed BCP1 on PS mainly formed the α-helix segment as observed in SFG experiments.

6.5 Conclusion

This chapter applied the Hamiltonian analysis method, SFG technique, and MD simulation to investigate the adsorption behaviors of two barnacle cement peptides, BCP1 and BCP2C, on the PS surface. The SFG spectra collected from the peptide solution/PS interface showed that both BCP1 and BCP2C were adsorbed onto the PS surface. I-TASSER server was used to predict the 3D structure of BCP1 and BCP2C in solution according to the peptide sequences. The predicted BCP2C structure was further confirmed by the CD spectrum, which shows the signature peaks of α-helix. The predicted structures were then used in the MD simulation. The peptides were combined with a PS layer to conduct the full-atom MD simulation to monitor the adsorption behavior of peptides onto a PS surface. The simulation result after ~ 1 μs shows that BCP2C can form significant β-sheet structures on PS with an "on-and-off" manner over a long timescale due to the strong interaction between BCP2C and PS, while BCP1 does not form significant β-sheet structure. This is consistent with the previous publication which reported that BCP2C can form β-sheet structure and lead to strong fibril network formation, while BCP1 cannot. The Hamiltonian analysis method used the final simulation structures of BCP2C and BCP1 to calculate the SFG spectra. The matching score heat maps show that the SFG spectra calculated with the BCP2C structures with β-sheet segment have higher matching qualities with the reconstructed experimental SFG spectra, indicating that likely β-sheet structure is formed in adsorbed BCP2C at the BCP2C solution/PS interface, observed in the SFG experiment. Similar methods were applied

to analyze the BCP1 simulation result and SFG data. The results showed that BCP1 formed a short α-helix segment on the PS surface.

The orientations of BCP1 and BCP2C were deduced using the simulated molecular structures of BCP1 and BCP2C on PS using the Hamiltonian analysis method and SFG data. Both BCP1 and BCP2C tend to tilt on the PS surface, which differ from the MD simulation results where all peptides tend to lie down on the PS surface. This is likely due to the surface coverage difference between the MD simulations and SFG adsorption experiments. In the MD simulations, only four peptides of BCP2C or BCP1 were placed in the simulation box, thus there was enough space for each peptide to lie down on the PS surface. However, in SFG adsorption experiments, 1 mg/mL peptide solution was placed into contact with the surface, and peptides were adsorbed onto the PS surface until it was saturated, so the adsorbed peptides tended to tilt up because of the crowded surface.

This is the first time that the formation of β-sheet structure of adsorbed barnacle cement peptide on PS surface was successfully confirmed by experiments in situ in real time using SFG. This study shows that the adsorbed BCP2C can form significant β-sheet structures while the adsorbed BCP1 cannot on the PS surface. However, the charged segment in BCP2C does not directly participate in the formation of β-sheet structure, suggesting that the simple segment of barnacle cement peptide may also play an essential role in the β-sheet formation. This knowledge is extremely important for understanding the aggregation mechanism of barnacle cement peptides on surface as well as the marine fouling mechanisms of barnacles.

In the study, we only used the final simulation structures of the peptides for Hamiltonian analysis and spectra matching. In the future, statistical analysis with more simulated structures

along the simulation trajectory will be used for SFG data analysis, which will be discussed further in the next chapter below.

6.6 References

1. Flemming, H.-C., Biofouling in water systems–cases, causes and countermeasures. *Applied microbiology and biotechnology* **2002,** *59* (6), 629-640.

2. Wang, Y.; Pu, J.; An, B.; Lu, T. K.; Zhong, C., Emerging paradigms for synthetic design of functional amyloids. *Journal of molecular biology* **2018,** *430* (20), 3720-3734.

3. Demirel, Y. K.; Uzun, D.; Zhang, Y.; Fang, H.-C.; Day, A. H.; Turan, O., Effect of barnacle fouling on ship resistance and powering. *Biofouling* **2017,** *33* (10), 819-834.

4. Khandeparker, L.; Anil, A. C., Underwater adhesion: the barnacle way. *International Journal of Adhesion and Adhesives* **2007,** *27* (2), 165-172.

5. Li, X.; Li, S.; Huang, X.; Chen, Y.; Cheng, J.; Zhan, A., Protein-mediated bioadhesion in marine organisms: A review. *Marine Environmental Research* **2021,** *170*, 105409.

6. Nakano, M.; Shen, J.-R.; Kamino, K., Self-assembling peptide inspired by a barnacle underwater adhesive protein. *Biomacromolecules* **2007,** *8* (6), 1830-1835.

7. Nakano, M.; Kamino, K., Amyloid-like conformation and interaction for the self-assembly in barnacle underwater cement. *Biochemistry* **2015,** *54* (3), 826-835.

8. So, C. R.; Liu, J.; Fears, K. P.; Leary, D. H.; Golden, J. P.; Wahl, K. J., Self-assembly of protein nanofibrils orchestrates calcite step movement through selective nonchiral interactions. *ACS nano* **2015,** *9* (6), 5782-5791.

9. So, C. R.; Yates, E. A.; Estrella, L. A.; Fears, K. P.; Schenck, A. M.; Yip, C. M.; Wahl, K. J., Molecular recognition of structures is key in the polymerization of patterned barnacle adhesive sequences. *ACS nano* **2019,** *13* (5), 5172-5183.

10. Wang, J.; Even, M. A.; Chen, X.; Schmaier, A. H.; Waite, J. H.; Chen, Z., Detection of amide I signals of interfacial proteins in situ using SFG. *Journal of the American Chemical Society* **2003,** *125* (33), 9914-9915.

11. Wang, J.; Chen, X.; Clarke, M. L.; Chen, Z., Detection of chiral sum frequency generation vibrational spectra of proteins and peptides at interfaces in situ. *Proceedings of the National Academy of Sciences* **2005,** *102* (14), 4978-4983.

12. Clarke, M. L.; Chen, Z., Polymer surface reorientation after protein adsorption. *Langmuir* **2006,** *22* (21), 8627-8630.

13. Wang, J.; Lee, S.-H.; Chen, Z., Quantifying the ordering of adsorbed proteins in situ. *The Journal of Physical Chemistry B* **2008,** *112* (7), 2281-2290.

14. Nguyen, K. T.; King, J. T.; Chen, Z., Orientation determination of interfacial β-sheet structures in situ. *The Journal of Physical Chemistry B* **2010,** *114* (25), 8291-8300.

15. Liu, Y.; Jasensky, J.; Chen, Z., Molecular interactions of proteins and peptides at interfaces studied by sum frequency generation vibrational spectroscopy. *Langmuir* **2012,** *28* (4), 2113-2121.

16. Li, Y.; Pan, D.; Nashine, V.; Deshmukh, S.; Vig, B.; Chen, Z., Understanding Protein-Interface Interactions of a Fusion Protein at Silicone Oil-Water Interface Probed by Sum Frequency Generation Vibrational Spectroscopy. *Journal of pharmaceutical sciences* **2018,** *107* (2), 682-689.

17. Wei, S.; Zou, X.; Tian, J.; Huang, H.; Guo, W.; Chen, Z., Control of protein conformation and orientation on graphene. *Journal of the American Chemical Society* **2019,** *141* (51), 20335-20343.

18. Guo, W.; Zou, X.; Jiang, H.; Koebke, K. J.; Hoarau, M.; Crisci, R.; Lu, T.; Wei, T.; Marsh, E. N. G.; Chen, Z., Molecular Structure of the Surface-Immobilized Super Uranyl Binding Protein. *The Journal of Physical Chemistry B* **2021,** *125* (28), 7706-7716.

19. Lu, T.; Guo, W.; Datar, P. M.; Xin, Y.; Marsh, E. N. G.; Chen, Z., Probing protein aggregation at buried interfaces: distinguishing between adsorbed protein monomers, dimers, and a monomer–dimer mixture in situ. *Chemical Science* **2022,** *13* (4), 975-984.

20. Yang, J.; Yan, R.; Roy, A.; Xu, D.; Poisson, J.; Zhang, Y., The I-TASSER Suite: protein structure and function prediction. *Nature methods* **2015,** *12* (1), 7-8.

21. Pronk, S.; Páll, S.; Schulz, R.; Larsson, P.; Bjelkmar, P.; Apostolov, R.; Shirts, M. R.; Smith, J. C.; Kasson, P. M.; Van Der Spoel, D., GROMACS 4.5: a high-throughput and highly parallel open source molecular simulation toolkit. *Bioinformatics* **2013,** *29* (7), 845-854.

22. Abraham, M. J.; Murtola, T.; Schulz, R.; Páll, S.; Smith, J. C.; Hess, B.; Lindahl, E., GROMACS: High performance molecular simulations through multi-level parallelism from laptops to supercomputers. *SoftwareX* **2015,** *1*, 19-25.

23. Páll, S.; Abraham, M. J.; Kutzner, C.; Hess, B.; Lindahl, E., Solving software challenges for exascale. Springer International Publishing Switzerland: 2015; Vol. 8750, pp 3-27.

24. Huang, J.; MacKerell Jr, A. D., CHARMM36 all-atom additive protein force field: Validation based on comparison to NMR data. *Journal of computational chemistry* **2013,** *34* (25), 2135-2145.

25. Greenfield, N. J., Using circular dichroism spectra to estimate protein secondary structure. *Nature protocols* **2006,** *1* (6), 2876-2890.

Chapter 7 Summary and Outlook

Protein adsorption has drawn extensive research attention since it can happen in various scenarios and is strongly related to many important biological research fields and practical applications. Sum frequency generation (SFG) vibrational spectroscopy, a unique intrinsic surface-sensitive tool, has been used for deducing the orientations of various interfacial proteins/peptides in various interfacial systems. However, great challenges remain in developing/using SFG data analysis method to effectively obtain insightful structural information for complicated protein structures. Here, my dissertation aimed to develop/apply an SFG data analysis method called the Hamiltonian analysis method to elucidate the molecular structural information, including orientation and conformation, of interfacial proteins/peptides.

Chapter 1 of this thesis briefly introduced significance of protein adsorption and previous SFG research on interfacial proteins/peptides. The contents and results of the research presented in each of the following chapters were described.

In Chapter 2, the development of the Hamiltonian analysis method was introduced. The Hamiltonian analysis method can calculate SFG spectra based on an input protein structure at a given orientation. This method was previously published but lacked the capability of deducing the orientation of proteins/peptides by matching the calculated spectra with experimental data. In this study, the MATLAB scripts of the original Hamiltonian method were adopted and developed into a new software package that can calculate the SFG spectra in different polarization combinations, modify the SFG spectra by considering Fresnel coefficients, generate heat maps by matching the calculated SFG spectra with the reconstructed resonant spectra from SFG experiments, and output

the most probable protein orientations and corresponding matching scores. Since the matching quality is highly relevant to the accuracy of input protein structure, the final matching scores could be used to evaluate protein conformation as well. This new version of the Hamiltonian analysis method was used in this thesis to investigate the orientations and conformations of several proteins and peptides at the solid/liquid interface.

In Chapter 3, we studied the adsorption behavior of bovine serum albumin (BSA) onto silicone oil surface and differentiated the BSA dimer and monomer adsorption. Our Hamiltonian analysis results indicated that the BSA dimers dominated the silicone oil surface. The crystal structure of BSA (pdb: 4f5s) used in this study is a BSA dimer structure, and one of the monomers in pdb:4f5s was used as the input structure for the BSA monomer orientation analysis. The calculated SFG spectra using BSA monomer and dimer structures were matched with the reconstructed experimental SFG spectra separately. We found that the BSA dimer structure has a much higher matching quality with the experiment data, especially the 1625 cm^{-1} peak in ppp. The adsorbed BSA dimer was further confirmed by treating the surface with dithiothreitol (DTT), and the SFG data showed no 1625 cm^{-1} peak in ppp. The circular dichroism spectra collected from the BSA on silicone oil before and after DTT treatment implied no significant secondary structure change, indicating the change in SFG spectra is due to the reaction between BSA dimer and DTT. The SFG spectra collected from the BSA after DTT treatment were analyzed by the Hamiltonian method, and it was found that the silicone oil was covered by a mixture of BSA dimer and monomer, which is consistent with the expectation that BSA dimers are not completely reacted with DTT under mild reaction conditions. The combination of the SFG experiment and Hamiltonian analysis method can be used to elucidate the aggregation (or dimer formation) and

orientation of adsorbed BSA on silicone oil surface and monitor the interfacial chemical reaction between BSA and DTT.

In Chapter 4, we studied the fibrinogen's orientation and conformation change during the adsorption process on silicone oil. A femtosecond SFG system with a broad-band IR pulse was applied in this study, which allowed fast data acquisition during the protein adsorption process. The ssp and ppp SFG spectra collected from the adsorbed fibrinogen on silicone oil were analyzed by the Hamiltonian method. The fibrinogen crystal structure (pdb:3ghg) was used, and the angle between the two coiled coils in the original crystal structure was slightly varied to bend the entire fibrinogen molecule for SFG data analysis. During the first 900 s of the adsorption, the SFG signal contributed from the adsorbed fibrinogen was weak, and no reasonable fitting could be generated. Thus, the detailed orientation and conformation of fibrinogen could only be obtained after 900 s. The matching quality scores between the calculated SFG spectra using the Hamiltonian analysis and the SFG experimental data showed that the adsorbed fibrinogen tends to bend more on the surface and tilt more (or stand up more) when more adsorbed fibrinogen molecules cover the surface over time. We further calculated the relative surface coverage using the Hamiltonian method to compare the effective $\chi^{(2)}$ values at different adsorption time steps. The trend in the coverage percentage plot shows that the amount of adsorbed fibrinogen molecules gradually increased and approached the equilibrium. This study provides insight into molecular structure change during the adsorption process of proteins onto a surface and shows that SFG with the Hamiltonian method will be a valuable tool for quantifying the surface coverage of interfacial biomolecules over the adsorption process.

In Chapter 5, interactions between silicone oil and two commercial antibody products, mAb and BsAb, from Sanofi were investigated. Our previous study showed that a highly

concentrated PS80 solution in the antibody solution can completely remove and prevent the adsorption of both antibodies. Here, the possible lowest effective PS80 concentration, which represents the lowest PS80 concentration that no antibody signal could be observed in SFG, was found for BsAb to be 0.02 wt%. The time-dependent SFG studies and analysis showed that 0.002 wt% PS80 could accelerate the adsorption rate of BsAb and cause slow desorption of BsAb on silicone oil. We then used the molecular structures of mAb and BsAb provided by Sanofi for Hamiltonian analysis. The calculated SFG spectra based on the provided mAb and BsAb structures showed much worse matching qualities with the experimental SFG data when PS80 surfactant was not present in the solution compared to the case where the antibody solutions contain PS80. Likely without PS80, adsorbed antibodies cannot adopt native structure and may form aggregates, therefore the calculated SFG spectra based on the antibody native structures cannot match the experimental data. The above results also indicate that diluted PS80 in an antibody solution can stabilize the native structure of adsorbed antibody on silicone oil surface. This is an important finding to show that even the low PS 80 concentration could not completely prevent adsorption of antibody onto silicone oil, PS80 molecules could prevent aggregation of adsorbed antibody molecules on silicone oil.

In Chapter 6, we investigated the fouling behaviors of two barnacle cement peptides, BCP1 and BCP2C, on the polystyrene (PS) surface. The molecular structures of BCP1 and BCP2C were predicted by I-TASSER, and their solution structures were obtained by running all-atom MD simulations. We also built an amorphous PS layer and combined it with the peptides in a simulation box to investigate the adsorption behaviors of BCP1 and BCP2C onto PS using MD simulation. The simulation results showed that both BCP1 and BCP2C were adsorbed onto the PS surface in less than 100 ns. Furthermore, the secondary structure evolution plot showed that BCP2C could

form significant β-sheet structures on the PS surface, while BCP1 mostly adopted random coil conformation. After the MD simulation, the molecule structures of BCP1 and BCP2C were extracted and used in the Hamiltonian analysis. The Hamiltonian analysis results suggested that the BCP2C structures with β-sheet segments have higher matching scores than other structures, which confirmed the formation of β-sheet structures of BCP2C on the PS surface. The charged segment in the BCP2C sequence is believed to be the key to the β-sheet formation in a previous study, but we found that in the MD simulation result, the β-sheet structure was formed by the simple segment rather than the charged segment, which means that the simple segment in barnacle cement peptide also plays a role in the aggregation mechanism. BCP1 did not show β-sheet formation on the PS surface, which is well correlated to the published results.

To summarize, for the first time, this thesis research developed a systematic data analysis methodology to deduce interfacial protein structure based on SFG experimental data. This methodology involves protein structural prediction using protein sequence, MD simulations of protein structures in solution and on polymer surface, SFG spectra calculation using Hamiltonian analysis based on protein structure, SFG spectra matching between calculated and reconstructed experimental data, interfacial protein structure plotting etc. This developed methodology was successfully applied to investigate adsorbed protein structures including conformations and orientations. Many important questions regarding protein adsorption such as adsorbed protein conformation and orientation, adsorbed protein aggregation, time-dependent protein adsorption amount and related structural changes could be answered. The developed method is generally applicable which can be widely applied to study adsorption behavior of many different proteins, adding an important technique to the toolbox for protein studies.

In the future, this thesis research can be extended in many directions, examples of which are listed below:

First, for the SFG spectra calculation using the Hamiltonian analysis method, extra corrections could be added to the transition dipole model to more accurately calculate the coupling effects between various local amide I stretches of peptide units. The local mode frequency may need to be varied slightly depending on each peptide unit.

Second, the current spectra matching based on the assumption that all the interfacial proteins adopt the same orientation (delta distribution). In the future, more complicated orientation distribution functions can be implemented into the Hamiltonian method for spectra matching. For example, a Gaussian orientation distribution function can be used to study protein orientation on a polymer surface. Also, more possible conformations of the protein at interface can be deduced by using more simulated structures (e.g., all the structures in the last 100 ns simulation for BCP2C and BCP1) instead of only using the last simulation structure. According to the matching scores, many possible conformations can be deduced, and statistical analysis should be performed to find common characters of such conformations, providing more accurate results than that obtained from the delta distribution assumption.

Third, the developed method can be used to study protein aggregation at interfaces. The "trial" aggregated protein structure can be used for Hamiltonian analysis and spectra matching. For example, the protein/peptide orientation and conformation change during the formation of amyloid may be able to be elucidated by SFG, which is critical to understanding the aggregation mechanism of amyloids.

Fourth, other simulation methods, such as coarse-grain and discontinued MD, can simulate large proteins and provide structural changes which cannot be found when using all-atom MD

simulations. These simulation methods can provide more accurate protein solution structures and interfacial structures. The interfacial structure can then be used to combine with the SFG technique and Hamiltonian method to deduce interfacial conformations and orientations of these larger proteins, providing better understanding of protein-protein or protein-surface interactions at the molecular level.

Fifth, experimentally, phase-sensitive SFG can be introduced to deduce the absolute orientation of interfacial proteins and peptides. In this dissertation, only regular SFG experiments were conducted, which could not distinguish two most likely orientations with two opposite absolute orientations and requires further analysis to determine which one of the two orientations is more reasonable. The phase-sensitive SFG study can provide phase information with measuring imaginary SFG signal. The spectra calculation on the SFG imaginary signal is achievable by modifying the current Hamiltonian method.

Sixth, this method can be applied to study other important proteins, such as other blood proteins besides fibrinogen and albumin: globulin, immunoglobulin, and prothrombin. The adsorption behaviors of these blood proteins on the medical implant surface can help us better understand the protein-implant interactions and benefit the rational design of medical implant materials. Other adhesive proteins, such as mussel adhesive proteins (MAP), laminin, and lectin, can also be investigated using this method since the adsorption and aggregations of these adhesive proteins mainly occur at the solid/liquid interface. Beyond the protein adsorption phenomenon, one can also investigate the drug effect on membrane proteins or the enzyme interaction with target molecules/proteins by deducing the conformation variations of proteins during these processes.

It is worth re-iterating that the developed systematic SFG approach in this thesis is widely applicable. Therefore it can be used to study interfacial protein structure of many different proteins

adsorbed at interfaces. Furthermore, it can be applied to study interfacial proteins beyond those physically adsorbed on the surface, such as membrane proteins, chemically immobilized proteins, etc.